REPAIR, EVALUATION, MAINTENANCE, AND
REHABILITATION RESEARCH PROGRAM

TECHNICAL REPORT REMR-CS-29

METHODS OF EVALUATING THE STABILITY AND SAFETY OF GRAVITY EARTH RETAINING STRUCTURES FOUNDED ON ROCK

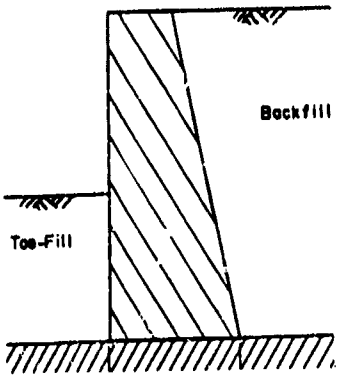

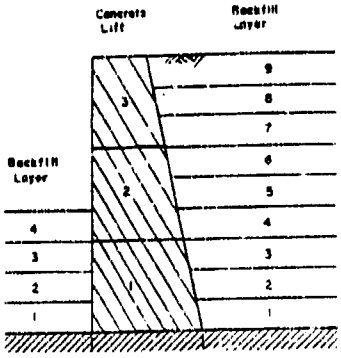

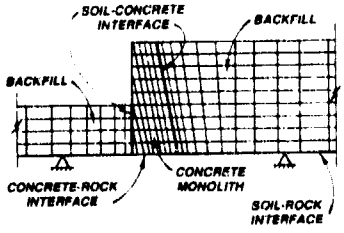

by

R. M. Ebeling

Information Technology Laboratory

DEPARTMENT OF THE ARMY
Waterways Experiment Station, Corps of Engineers
3909 Halls Ferry Road, Vicksburg, Mississippi 39180-6199

and

G. W. Clough, J. M. Duncan, T. L. Brandon

Virginia Polytechnic Institute
and State University
Blacksburg, Virginia 24061

March 1992
Final Report

Prepared for DEPARTMENT OF THE ARMY
US Army Corps of Engineers
Washington, DC 20314-1000

Under REMR Work Unit 32306 and
CWR&D Work Unit 31713
Contract No DACW39-86-K-0007

The following two letters used as part of the number designating technical reports of research published under the Repair, Evaluation, Maintenance, and Rehabilitation (REMR) Research Program identify the problem area under which the report was prepared

	Problem Area		Problem Area
CS	Concrete and Steel Structures	EM	Electrical and Mechanical
GT	Geotechnical	EI	Environmental Impacts
HY	Hydraulics	OM	Operations Management
CO	Coastal		

Destroy this report when no longer needed. Do not return it to the originator.

The findings in this report are not to be construed as an official Department of the Army position unless so designated by other authorized documents

The contents of this report are not to be used for advertising, publication, or promotional purposes. Citation of trade names does not constitute an official endorsement or approval of the use of such commercial products.

COVER PHOTOS.

TOP – Base case hypothetical structure used in the backfill placement analyses.

MIDDLE – Idealization of the base case structure for backfill placement analysis.

BOTTOM – Finite element mesh used to model a base case hypothetical structure with additional backfill beyond the toe.

REPORT DOCUMENTATION PAGE

Form Approved
OMB No. 0704-0188

1. AGENCY USE ONLY (Leave blank)	2. REPORT DATE	3. REPORT TYPE AND DATES COVERED
	March 1992	Final report

4. TITLE AND SUBTITLE
Methods of Evaluating the Stability and Safety of Gravity Earth Retaining Structures Founded on Rock

5. FUNDING NUMBERS
REMR Work Unit 32306
CWR&D Work Unit 31713
Contract No. DACW39-86-K-0007

6. AUTHOR(S)
R. M. Eberling, G. W. Clough,
J. M. Duncan, T. L. Brandon

7. PERFORMING ORGANIZATION NAME(S) AND ADDRESS(ES)
USAEWES, Information Technology Laboratory
3909 Halls Ferry Road, Vicksburg, MS 39180-6199
and Virginia Polytechnic Institute and State University
Blacksburg, VA 24061

8. PERFORMING ORGANIZATION REPORT NUMBER

9. SPONSORING/MONITORING AGENCY NAME(S) AND ADDRESS(ES)
US Army Corps of Engineers
Washington, DC 20314-1000

10. SPONSORING/MONITORING AGENCY REPORT NUMBER
Technical Report
REMR-CS-29

11. SUPPLEMENTARY NOTES This is a report of the Concrete and Steel Structures Problem Area of the Repair, Evaluation, Maintenance, and Rehabilitation (REMR) Research Program. Available from National Technical Information Service, 5285 Port Royal Road, Springfield, VA 22161.

12a. DISTRIBUTION/AVAILABILITY STATEMENT
Approved for public release; distribution unlimited.

12b. DISTRIBUTION CODE

13. ABSTRACT *(Maximum 200 words)*

The objective of this study was to investigate the accuracy of the procedures employed in the conventional equilibrium method of analysis of gravity earth retaining structures founded on rock, using the finite element method of analysis. This study was initiated when a number of existing large retaining structures at various navigation lock sites in the United States that showed no signs of instability or substandard performance failed to meet the criteria currently used for design of new structures.

The results of the following load analyses show that when the loss of contact along the base of a wall is modeled in the finite element analysis, the calculated values of effective base contact area and maximum contact pressure are somewhat larger than those calculated using conventional equilibrium analyses. The mobilized base friction angle values calculated using the two methods are in precise agreement.

(Continued)

14. SUBJECT TERMS			15. NUMBER OF PAGES
Analysis	Retaining walls	Stability	165
Earth pressures	Rock foundation		16. PRICE CODE
Finite element	Soil-structure interaction		

17. SECURITY CLASSIFICATION OF REPORT	18. SECURITY CLASSIFICATION OF THIS PAGE	19. SECURITY CLASSIFICATION OF ABSTRACT	20. LIMITATION OF ABSTRACT
UNCLASSIFIED	UNCLASSIFIED		

13. ABSTRACT (Continued).

Comparisons between the results of backfill placement analyses using the finite element method and the conventional equilibrium analyses indicate that conventional analyses are very conservative. The finite element analyses indicate that the backfill exerts downward shear loads on the backs of retaining walls. These shear forces have a very important stabilizing effect on the walls. Expressed in terms of a vertical shear stress coefficient ($K_v = \tau_{xy}/\sigma$), this shear loading ranged in value from 0.09 to 0.21, depending on the geometrical features and the values of the material parameters involved in the problem.

Another important factor not considered in the conventional equilibrium method is that the displacements of the wall have a significant influence on the distribution of both the stabilizing and destabilizing forces exerted on the wall. In general, as the wall moves away from the backfill, the lateral forces exerted on the wall by the backfill decrease, and the lateral forces exerted on the front of the wall by the toe fill increase.

PREFACE

The work described in this report was sponsored by Headquarters, US Army Corps of Engineers (HQUSACE), as part of the Concrete and Steel Structures Problem Area of the Repair, Evaluation, Maintenance, and Rehabilitation (REMR) Research Program and the Civil Works Research and Development (CWR&D) program on Structural Engineering. The work was performed under the REMR Work Unit 32306, "Stability of Existing Concrete Structures on Rock," for which Mr. William F. McCleese, Structures Laboratory (SL), US Army Engineer Waterways Experiment Station (WES), is Principal Investigator, and the CWR&D Work Unit 31713, "Soil-Structure Interaction Studies of Walls," for which Dr. Reed L. Mosher, Computer-Aided Engineering Division (CAED), Information Technology Laboratory (ITL), is Principal Investigator. Mr. Lucian G. Guthrie (CECW-ED) was the REMR Technical Monitor, and Mr. Donald R. Dressler (CECW-ED) was the CWR&D Technical Monitor for this work. Additional funding for this work was provided by the Computer-Aided Structural Engineering Project.

Mr. Jesse A. Pfeiffer, Jr., is the REMR Coordinator at the Directorate of Research and Development, HQUSACE; Mr. James E. Crews (CECW-OM) and Dr. Tony C. Liu (CECW-EG) serve as the REMR Overview Committee; Mr. McCleese is the REMR Program Manager; and Mr. James E. McDonald, SL, WES, is the Problem Area Leader.

The work was performed by Virginia Polytechnic Institute and State University (VPI&SU), under Contract No. DACW39-86-K-0007. The report was prepared by Dr. R. M. Ebeling, ITL, WES, Drs. G. W. Clough, J. M. Duncan, and T. L. Brandon, VPI&SU, under the direct supervision at WES of Dr. Mosher and under general supervision of the late Mr. Paul Senter, Chief, CAED, ITL, and Dr. N. Radhakrishnan, Director, ITL.

At the time of publication of this report, Director of WES was Dr. Robert W. Whalin. Commander and Deputy Director was COL Leonard G. Hassell, EN.

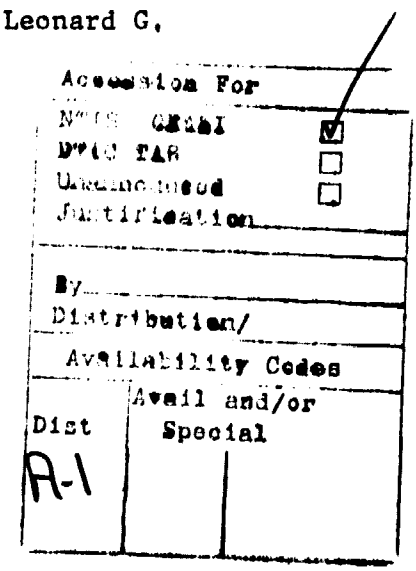

CONTENTS

CONTENTS (Continued)

LIST OF TABLES

LIST OF FIGURES

CONVERSION FACTORS, NON-SI TO SI (METRIC) UNITS OF MEASUREMENT

Non-SI units of measurement used in this report can be converted to SI (metric) units as follows:

Multiply	By	To Obtain
degrees (angle)	0.01745329	radians
feet	0.3048	metres
kips (force)	4.448222	kilonewtons
kip-feet	1355.818	newton metres
pounds (force)	4.448222	newtons
pounds (force) per square foot	47.88026	pascals
pounds (force) per square inch	0.006894757	megapascals
pounds (mass) per cubic foot	16.01846	kilograms per cubic metre
pounds (mass) per cubic inch	27.6799	grams per cubic centimetre

METHODS OF EVALUATING THE STABILITY AND SAFETY OF GRAVITY EARTH RETAINING STRUCTURES FOUNDED ON ROCK

PART I: INTRODUCTION

1. The US Army Corps of Engineers has responsibility for designing and maintaining a large number of gravity retaining walls at navigation lock structures and other facilities. The procedures currently used for designing new structures and for evaluating the safety of existing structures are the conventional equilibrium methods the same general method as those used for analysis of earth retaining structures. Because the conditions of equilibrium are insufficient for a complete analysis of all the aspects of soil-structure interaction involved in the stability and performance of these structures, these conventional equilibrium methods necessarily involve assumptions regarding the loading and resisting forces that act on the structures.

2. Although the conditions and assumptions employed in the conventional equilibrium methods are generally accepted as providing reasonable engineering procedures, and although there have been few reported failures of structures designed using these procedures, there is nevertheless some uncertainty concerning their accuracy. A number of existing structures that show no signs of instability or substandard performance have not met the criteria currently used for design of new structures, and the possibility exists that the combination of the criteria and the methods currently used are more conservative than necessary.

3. The research investigation described in this report was undertaken to study the behavior of gravity earth retaining structures using the finite element method of analysis and to compare the results of the finite element analysis with the results of conventional analyses. Specifically, the finite element method of analysis of earth retaining structures was used to study;

a. The progressive development of cracks at the interface between the base of the monoliths and their foundation.

b. The factors that control the extent of the area of contact between the base of the monoliths and their foundation.

c. The magnitude and distribution of stresses developed on the front, back, and along the base of the monoliths.

d. The factors that influence the movements of the monoliths and the effect of wall movements on the magnitude and orientation of resultant forces acting on the wall.

e. The development of shear forces acting on the front and back of the wall as a result of the placement of the soil fill against the wall.

4. The evaluation of the stability of earth retaining structures by the finite element method is well established. However, this analytical procedure has not been applied to walls that are loaded so heavily that gaps may develop between the base and the foundation, i.e., structures deemed to be in a condition of incipient instability. Preliminary evaluations of earth retaining monoliths for three locks under the jurisdiction of the Corps of Engineers were found to have this characteristic. The structures analyzed in this study were consistent with these monoliths.

5. This study was divided into two phases: The objective of this phase was to develop, through a series of preliminary analyses, analytical procedures for modeling separation of the base of a monolith from its foundation and apply this procedure to a limited number of earth retaining structures (as described in Part VI of this report). A number of procedures were evaluated based on their accuracy and computational efficiency. These analyses were performed using following loads, loads of predetermined magnitude and independent of the movement of the monolith. The accuracy of the analysis procedures was determined by comparing the results with the results of conventional equilibrium analysis.

6. Further into this first phase analyses was a literature study to compile information on the properties of rock masses, thereby providing a basis for selecting rock properties for use in finite element analyses (FEA).

7. In the second phase of study (Ebeling, Duncan, and Clough 1990), FEA's were performed to determine the effects of various geometrical and material parameters on the stability of the walls, extending the study described in Part VI of this report to other types of earth retaining structures. These analyses were performed using two types of loading; following loads and loads resulting from backfill placement. In the following load analyses, the earth and water loads are prescribed, as described previously. In the backfill placement analyses, loadings on the wall were generated automatically by simulating placement of the fill behind the wall. These backfill placement analyses are believed to be the most realistic that can be performed using the

finite element method. The magnitude of the forces acting on the monolith depends on the relative movement of the soil and the monolith and requires no assumptions with regard to the applied earth loads.

8. The stability of three earth retaining structures founded on rock were evaluated using both backfill placement analysis and conventional equilibrium method of analysis. The assumptions made with regard to applied loads and resisting forces in the conventional equilibrium analysis (CEA) were consistent with the assumptions used by the Corps of Engineers in equilibrium analysis. The degree of conservatism introduced by these assumptions was evaluated by comparing the results to those from backfill placement analyses.

9. This report is divided into seven parts and two appendixes. Part II reviews the CEA of gravity earth retaining monoliths. The safety of the wall against three modes of failure (sliding, overturning, and bearing capacity) is defined in terms of the forces acting on the wall and the dimensions of the wall.

10. In Part III the hypothetical structures used in the FEA are shown. The characteristics of the earth retaining structures at three existing Corps of Engineers locks are described using dimensionless ratios of forces acting on the walls and dimensions of the walls.

11. Part IV discusses the development of analytical procedures used in the FEA of retaining structures in a condition of incipient instability. The implementation of this procedure in a backfill placement analysis is also described.

12. The results from a series of parametric analyses of retaining walls are described in Parts V and VI. Part V discusses the results of the following load analyses used to determine the effects of various geometrical and material parameters on the stability of the wall. Part VI presents the results of the backfill placement analyses and makes comparisons between the results of the FEA and the results of CEA.

13. The findings of the studies to date are summarized in Part VII, and recommendations of topics for further study are given.

14. Appendix A shows cross sections through the concrete monoliths at the Emsworth, Montgomery, and Troy locks.

15. Theoretical considerations of the effect of the scale of a structure upon the computed results are explained in Appendix B.

PART II: CONVENTIONAL ANALYSES OF RETAINING WALL STABILITY

Forces Considered in Analyses

16. The conventional method of evaluating the stability of gravity retaining walls employs the requirements of equilibrium to ensure safety with regard to sliding, overturning, and bearing capacity. Figure 1 shows the different loads on gravity structures. The forces considered in these analyses are shown in Figure 1a:

a. The vertical force, F_v, includes the weight of the structure itself and the backfill contained within the enveloping rectangle, usually included in the free body considered in CEA.

b. The horizontal force, F_h, includes the loads due to earth pressure, water pressure, mooring forces, and vessel impact forces; F_h is the vector sum of all these forces.

c. The force U on the base of the structure is the uplift water pressure force. Consistent with the standard practice of the Corps of Engineers, the uplift water pressures on the base of the structures were assumed to vary linearly with distance across the base of the structure, from the hydrostatic value at the heel of the wall (zero if the backfill is drained effectively) to the full hydrostatic value at the toe of the wall.

d. The force N' is the effective normal force between the base of the wall and the rock beneath. Its magnitude is equal to the difference between F_v and U.

e. The force T is the shear force required for equilibrium of the wall and is equal to the net horizontal force, F_h.

Base Interface Friction Angle Evaluation

17. The safety of the wall against sliding can be determined by evaluating the mobilized angle of interface friction between the bottom of the wall and the foundation. In this report the base interface friction angle is called δ_b, and the value of δ_b required for horizontal equilibrium of the wall is called δ_{bm}, the subscript m signifying the mobilized value of δ_b. The value of δ_{bm} can be expressed as follows:

$$\delta_{bm} = \tan^{-1}\left(\frac{T}{N'}\right) \qquad (1)$$

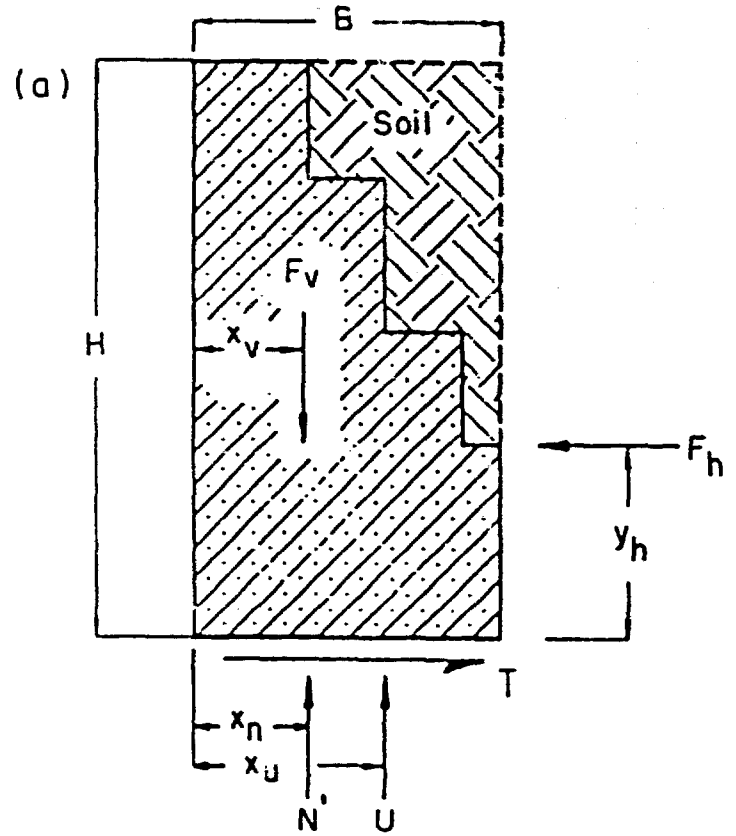

F_h = Net horizontal force due to all sources
F_v = Net vertical force due to all sources
U = Uplift force due to water pressure acting on base
N' = Net effective vertical force due to all sources
T = Not horizontal shear force due to all sources
B = Width of structure
H = Height of structure

a. Forces considered in conventional analyses

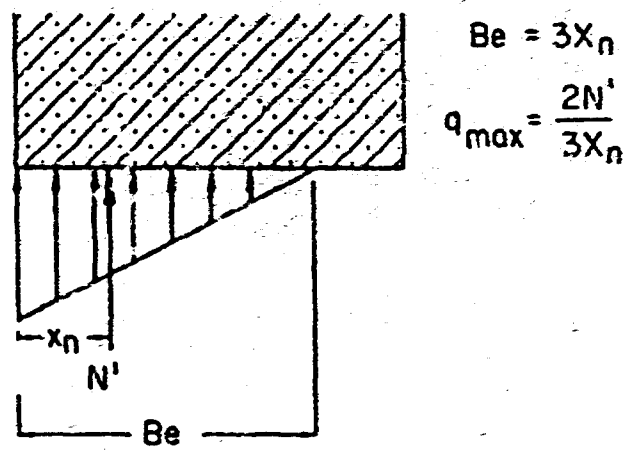

b. Linear base pressure distribution

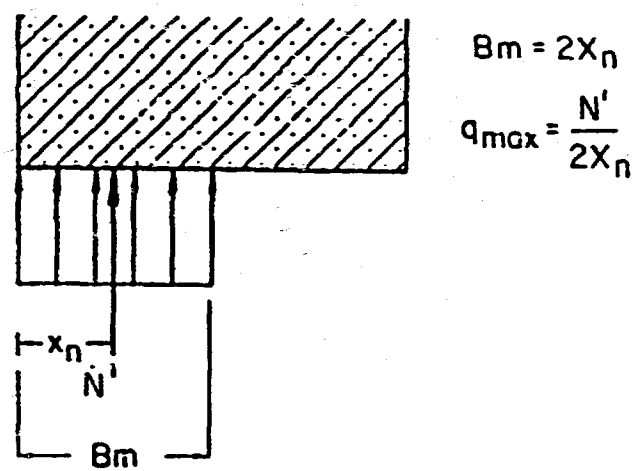

c. Uniform base pressure distribution

Figure 1. Loads on gravity structures

The factor of safety against sliding of the wall is equal to the ratio of the friction angle of the interface to the mobilized angle of interface friction:

$$F_s = \frac{\tan \delta_{bmax}}{\tan \delta_{bm}} \tag{2}$$

where δ_{bmax} is the maximum possible value of the base interface friction angle, a value that would cause sliding of the wall. For a wall to be safe with regard to sliding, the value of F_s should be greater than 1.0. A frequently used criterion of safety is that the factor of safety against sliding should be at least 1.5.

18. The safety of the wall against overturning can be expressed in terms of the position of the resultant N' that acts on the base of the wall. As the overturning moment due to F_h increases, N' moves to the left, and the distance x_n becomes smaller. The value of x_n can be expressed as:

$$x_n = \frac{F_v \cdot x_v - F_h \cdot Y_h - U \cdot x_u}{N'} \tag{3}$$

19. In the most basic terms, the wall is stable against overturning for any value of x_n greater than zero. However, to provide a margin of safety, it is required that x_n exceed some minimum value. Current Corps of Engineers criteria are that the value of x_n should equal or exceed 25 percent of the base width of the structure. The allowable value for x_n varies with the type of structure and the type of loading(s) used in the analysis (refer to Tables 4-1 through 4-3, Chapter 4 in EM 1110-2-2502 (Headquarters, Department of the Army, 1989)).

20. The overturning criterion is usually expressed in terms of the percentage of effective base contact area (B_e/B), where B_e is the width of the area of effective base contact and B is the base width. Assuming that the bearing pressure between the base of the structure and the underlying rock varies linearly from a maximum at the toe to zero at the inner edge of the area of effective base contact, as shown in Figure 1b, the value of B_e/B will be equal to three times the value of x_n/B . Thus, if the stress

distribution on the base is triangular, a value of x_n/B equal to 25 percent corresponds to a value of B_e/B equal to 75 percent.

21. An alternative assumption regarding base pressure distribution and contact area, suggested by Meyerhof (1953), is shown in Figure 1c. Meyerhof suggested that the width of effective base contact, denoted by B_m in Figure 1c, could be conservatively considered to be twice the distance from the edge to the resultant, corresponding to a uniform distribution of pressure across the area of contact. The logic behind this assumption is that the base would in fact be centrally loaded and the bearing pressure would be uniform if the base width was equal to B_m .

22. It may be seen that the assumption illustrated in Figure 1b corresponds to a larger area of effective base contact and a larger value of q_{max} (maximum base contact pressure) than the assumption illustrated in Figure 1c. Meyerhof's (1953) pressure distribution has been used widely for foundations on soil and is most appropriate for foundation materials that exhibit ductile mechanisms of failure. The assumption is less appropriate for brittle materials. The analyses described in subsequent sections of this report, that employ assumed linear elastic behavior of the structure and the underlying rock, result in distributions of bearing pressures on the base that correspond more closely to the distribution shown in Figure 1b than to the distribution suggested by Meyerhof.

23. The factor of safety against bearing capacity failure or crushing of the concrete or the rock at the toe can be expressed as

$$F_b = \frac{q_{ult}}{q_{max}} \tag{4}$$

where q_{ult} is the ultimate bearing capacity or compressive strength of the concrete or the rock at the toe, and q_{max} is the maximum bearing pressure at the toe. For brittle materials like unconfined concrete or unconfined hard rock, the ultimate bearing capacity is equal to the compressive strength of the material. For ductile foundation materials that undergo plastic failure, the ultimate bearing capacity is larger than the compressive strength of the material.

PART III: CHARACTERISTICS OF GRAVITY EARTH RETAINING STRUCTURES AND THEIR LOADING

24. To select an appropriate range of dimensions for the hypothetical structures to be analyzed in this research study, the characteristics of the monoliths at three Corps of Engineers locks (Emsworth, Montgomery, and Troy) were examined in detail. Data regarding these structures were obtained from reports by Pace (1976), Pace and Peatross (1977), and Pace, Campbell, and Wong (1981). Cross sections through many of the structures examined in these reports are contained in Appendix A. Some of the monoliths at these three locks do not retain earth backfills, and thus understandably have somewhat different characteristics from those that do retain earth. In selecting dimensions for study, more attention was paid to the characteristics of earth retaining monoliths.

Earth Retaining Monoliths at Three Existing Locks

25. Cross sections through all of the earth retaining monoliths at Emsworth, Montgomery, and Troy locks are shown in Figures 2 and 3. It may be seen that they have a wide variety of shapes and sizes, undoubtedly due to differences in the conditions of loading and foundation support at the locations where they were constructed. For purposes of examining the range of dimensions and loadings of these structures, a number of characteristics of each structure have been summarized in Table 1. They vary in height from 30 to 76 ft,* their base widths vary from 10 to 35 ft, and they are subjected to a very wide range of earth pressures and uplift water pressure forces.

Dimensionless Parameters for Geometry and Load

26. For purposes of characterizing the shapes of gravity retaining structures and the types of loadings to which they are subjected, it was

---

* A table of factors for converting non-SI units of measurement to SI (metric) units is on page 7.

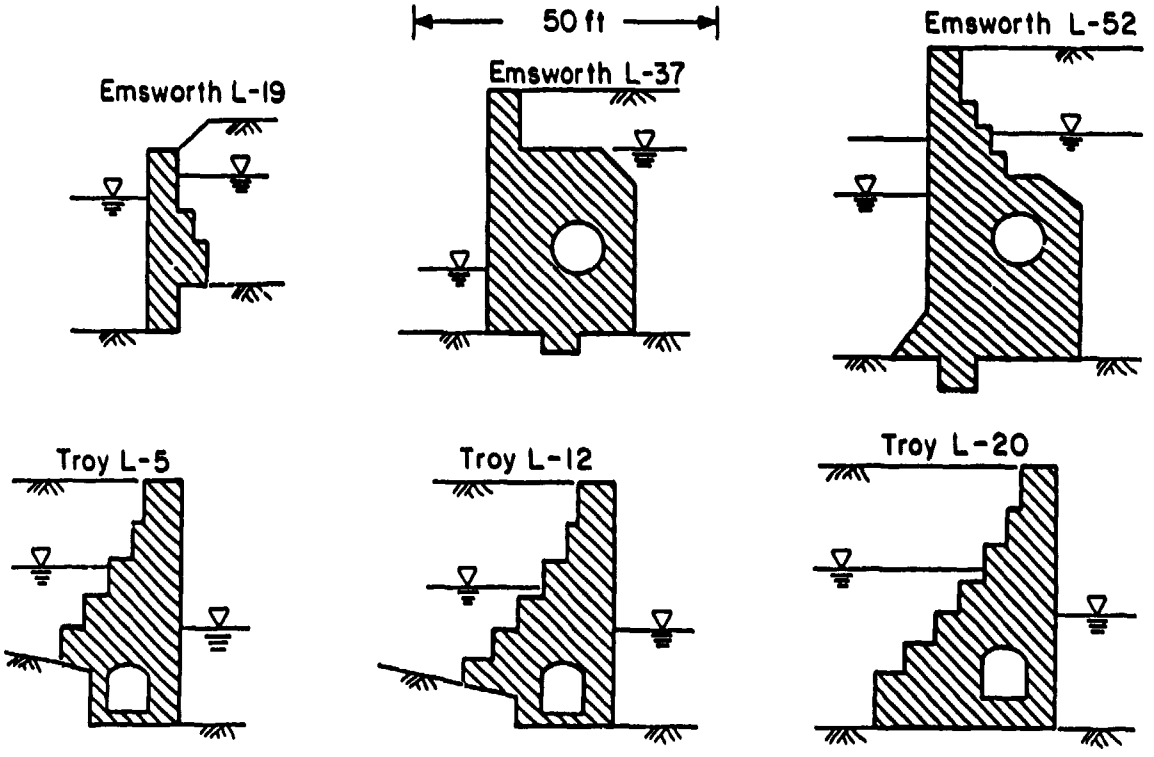

Figure 2. Sections through Emsworth and Troy earth retaining monoliths

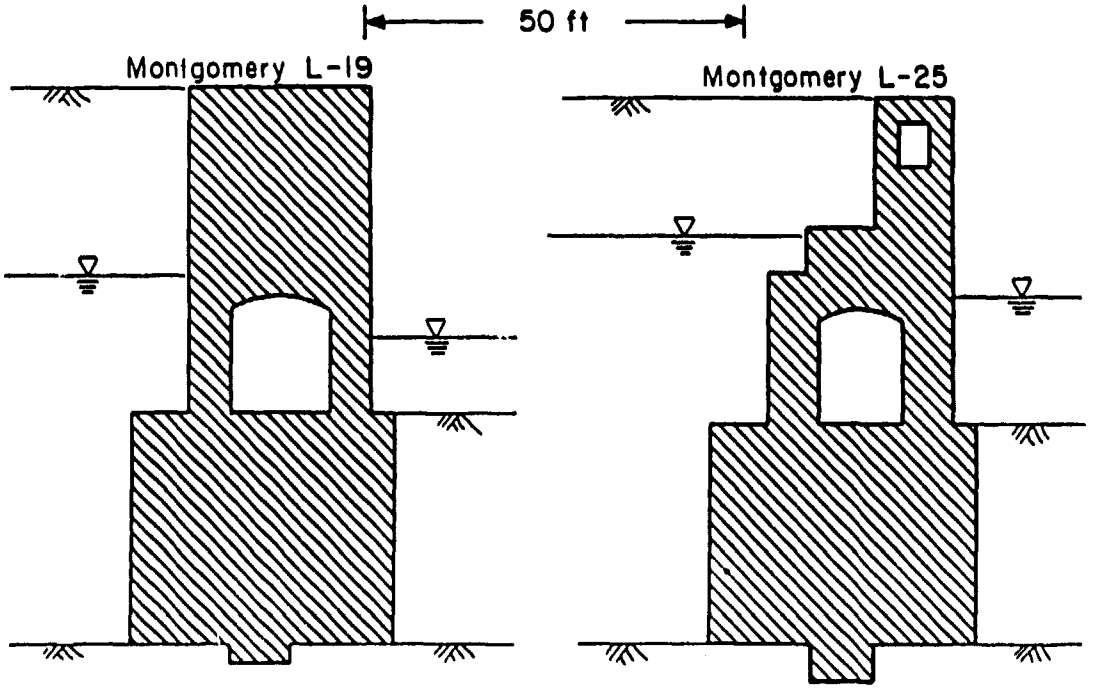

Figure 3. Sections through Montgomery earth retaining monoliths

Table 1

Dimensions and Forces on Earth Retaining Structures at Emsworth, Montgomery, and Troy Locks

Case No.	Lock, Station No., Loading*	Summary of Dimensions and Forces per Monolith							
		H ft	B ft	F_h kips	F_v kips	U kips	M_r k-ft	M_d k-ft	M_u k-ft
2	Emsworth L-19, H	30.0	10.0	18.8	38.5	13.0	176	327	61
3	Emsworth L-37, NC	38.9	23.7	48.3	127.1	27.3	1,470	660	351
4	Emsworth L-37, MC	38.9	23.7	58.2	122.2	20.3	1,398	728	321
5	Emsworth L-52, NC	51.0	31.7	76.2	177.9	56.7	2,914	1,607	885
6	Emsworth L-52, NC	51.0	31.7	78.3	177.9	56.7	2,914	1,673	885
7	Emsworth L-52, MC	51.0	31.7	105.6	166.9	36.7	2,823	1,947	728
20	Montgomery L-19, NC	71.0	35.0	130.7	335.2	104.7	6,090	3,764	1,888
21	Montgomery L-19, MC	71.0	35.0	178.6	321.6	61.9	5,934	4,634	1,444
22	Montgomery L-25, NC	76.0	35.0	129.9	333.5	104.7	6,048	3,725	1,888
23	Montgomery L-25, MC	76.0	35.0	180.9	321.1	57.1	5,890	4,510	1,332
34	Troy L-5, NC	40.0	20.0	33.2	100.5	22.7	931	584	221
35	Troy L-5, MC	40.0	20.0	62.4	97.7	17.9	914	760	220
36	Troy L-12, NC	40.0	25.0	38.3	126.3	29.3	1,492	626	365
37	Troy L-12, MC	40.0	25.0	62.4	123.9	25.1	1,485	760	383
38	Troy L-20, NC	43.0	30.0	57.6	174.3	42.4	2,589	828	670
39	Troy L-20, MC	43.0	30.0	73.4	172.4	27.9	2,597	963	558
		Summary of Statistics							
Maximum		76.00	35.00	180.9	335.2	104.7	6,090.0	4,634.0	1,888.0
Minimum		30.00	10.00	18.8	38.5	13.0	176.0	327.0	61.0
Average		48.74	26.30	83.3	182.3	44.0	2,854.0	1,755.9	762.4
Standard Deviation		15.32	7.97	47.3	91.2	27.4	1,967.2	1,463.5	567.4

* H = hawser pull, NC = normal condition, MC = maintenance condition.

to be useful to define a number of dimensionless ratios. The dimensionless variables used in this study are:

$$R_v = \frac{F_v}{B \cdot H \cdot \gamma_c} \qquad R_h = \frac{F_h}{B \cdot H \cdot \gamma_c}$$

$$R_u = \frac{U}{B \cdot H \cdot \gamma_c} \qquad R_{rm} = \frac{2 \cdot F_v \cdot x_v}{B^2 \cdot H \cdot \gamma_c}$$

$$R_{dm} = \frac{2 \cdot F_h \cdot y_h}{B^2 \cdot H \cdot \gamma_c} \qquad R_{um} = \frac{2 \cdot U \cdot x_u}{B^2 \cdot H \cdot \gamma_c}$$

$$\frac{B}{H} \qquad \frac{B_e}{B}$$

$$\delta_{bm}$$

where

F_v - vertical force

F_h - horizontal force

U - uplift force

x_v - moment arm of vertical force measured from the toe of the structure

x_u - moment arm of uplift force measured from the toe of the structure

y_h - moment arm of horizontal force measured from the toe of the structure

γ_c - unit weight of concrete = 150 lb/ft^3

H - nominal height of structure

B - nominal width of structure

δ_{bm} - mobilized base friction interface angle

M_r - Moment about toe of wall due to forces resisting overturning

M_d - Moment about toe of wall due to destabilizing forces

M_u - Moment about toe of wall due to uplift pressures acting across the base of the wall

The significance of the dimensionless parameters are described in the follcwing paragraphs.

R_v - weight index

27. The weight index is the ratio of the weight of the structure divided by the weight of a solid block of concrete filling the entire enveloping rectangle. The maximum value of R_v would be unity. Its value is smaller than unity if part of the rectangle is occupied by soil, air, or water, or if the structure contains holes, such as conduits, filled by air or water. Since the stability of a retaining wall is enhanced if its weight is increased (all other things being equal), the closer the value of R_v to unity the better. The value of R_v is almost always less than unity for real structures. Values of R_v and other dimensionless parameters are listed in Table 2 for each of the Corps of Engineers structures shown in Table 1. It may be seen that values of R_v for these structures vary from 0.69 to 0.92, and that the average value is 0.83.

28. The distribution of the values of R_v for all of the Corps of Engineers structures studied in this research project is shown in Figure 4. The values of R_v are shown on the horizontal axis, and the number of occurrences of each range of values is shown on the vertical axis. The range of values is the same for the structures that retain soil backfills as for all of the structures, including those that are not subjected to earth loadings. However, a somewhat larger fraction of the values of R_v for the earth retaining structures falls within the range from 0.8 to 0.925, indicating that the earth retaining monoliths are, on the average, slightly more massive than the structures that do no retain earth.

R_h - horizontal load index

29. The horizontal load index is the ratio of the net horizontal force acting on the structure to the weight of a solid block of concrete filling the entire area of the enveloping rectangle. The value of R_h is a measure of the severity of the horizontal loading on a structure. The values of R_h for the structures shown in Table 2 vary from a minimum of 0.26 to a maximum of 0.52, with an average of 0.38.

30. The distribution of the values of R_h for the structures is shown in Figure 5. For all of the structures, the range of values of R_h is quite wide. This indicates a considerable range of horizontal loadings on the

Table 2

Dimensionless Parameters for Earth Retaining Structures at Emsworth, Montgomery, and Troy Locks

Case No.	Lock, Station No., Loading*	Summary of Dimensionless Parameters per Monolith								
		R_v	R_h	R_u	R_{rm}	R_{dm}	R_{um}	B/H	$\tan(\delta_{bm})$	B_e/B %
2	Emsworth, L-19, H	0.856	0.418	0.289	0.78	1.45	0.27	0.33	0.737	0.0
3	Emsworth, L-37, NC, H	0.919	0.349	0.197	0.90	0.40	0.21	0.61	0.484	58.0
4	Emsworth, L-37, MC	0.884	0.421	0.147	0.85	0.44	0.20	0.61	0.571	43.0
5	Emsworth, L-52, NC, I	0.734	0.314	0.234	0.76	0.42	0.23	0.62	0.629	35.0
6	Emsworth, L-52, NC, H	0.734	0.323	0.234	0.76	0.44	0.23	0.62	0.646	29.0
7	Emsworth, L-52, MC	0.688	0.435	0.151	0.73	0.51	0.19	0.62	0.811	11.0
20	Montgomery, L-19, NC, H	0.899	0.351	0.281	0.93	0.58	0.29	0.49	0.567	16.3
21	Montgomery, L-19, MC	0.863	0.479	0.166	0.91	0.71	0.22	0.49	0.688	0.0
22	Montgomery, L-25, NC	0.836	0.326	0.262	0.87	0.53	0.27	0.46	0.568	16.4
23	Montgomery, L-25, MC	0.805	0.453	0.143	0.84	0.65	0.19	0.46	0.685	1.9
34	Troy L-5, NC	0.838	0.277	0.189	0.78	0.49	0.18	0.50	0.427	24.0
35	Troy L-5, MC	0.814	0.520	0.149	0.76	0.63	0.18	0.50	0.782	0.0
36	Troy L-12, NC	0.842	0.255	0.195	0.80	0.33	0.19	0.63	0.395	62.0
37	Troy L-12, MC	0.826	0.416	0.167	0.79	0.41	0.20	0.63	0.632	42.0
38	Troy L-20, NC	0.901	0.298	0.219	0.89	0.29	0.23	0.70	0.437	83.0
39	Troy L-20, MC	0.891	0.379	0.144	0.89	0.33	0.19	0.70	0.508	74.0
		Summary of Statistics								
Maximum		0.919	0.520	0.289	0.934	1.453	0.289	0.698	0.811	83.000
Minimum		0.688	0.255	0.143	0.734	0.285	0.183	0.333	0.395	0.000
Average		0.833	0.376	0.198	0.828	0.538	0.218	0.543	0.598	30.975
Standard deviation		0.064	0.074	0.048	0.063	0.264	0.033	0.110	0.122	26.382
Coefficient of variation		0.077	0.197	0.244	0.076	0.490	0.149	0.202	0.204	0.852

* H = hawser pull, NC = normal condition, MC = maintenance condition.

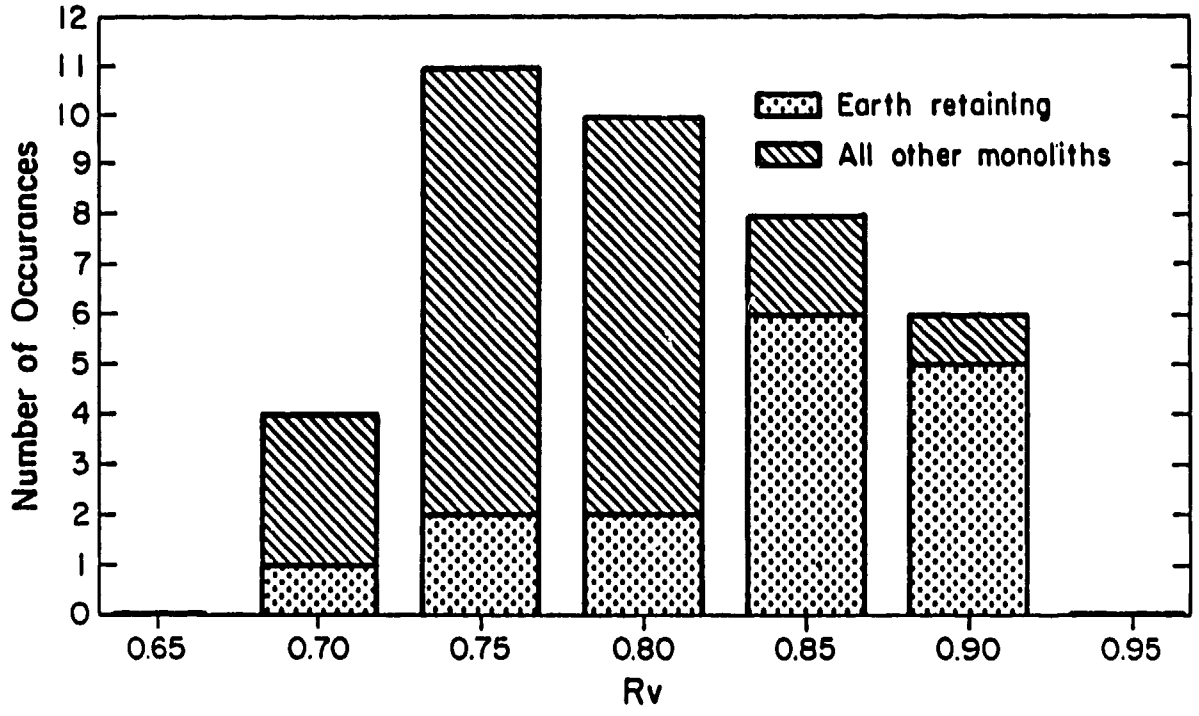

Figure 4. Distribution of dimensionless parameter R_v

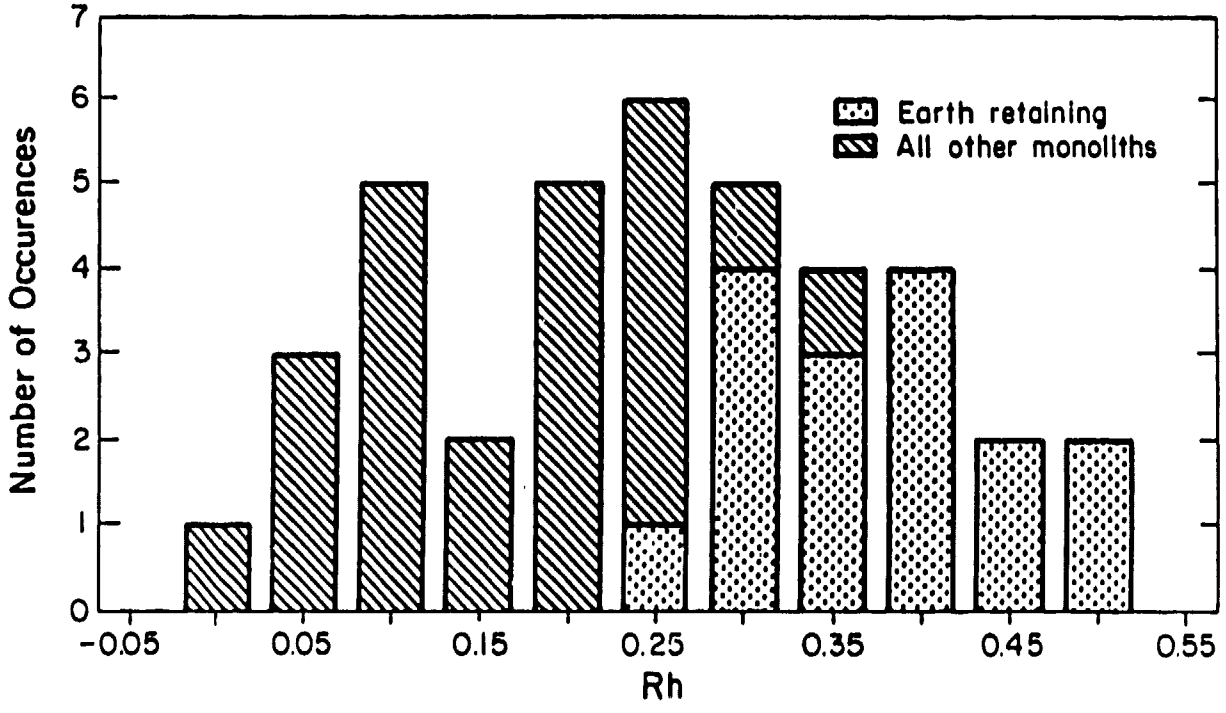

Figure 5. Distribution of dimensionless parameter R_h

structures, including some with very small horizontal loads. The distribution of values for the structures that retain earth backfills is concentrated in the upper range of values, indicating that these structures are usually subjected to high lateral loads.

R_u = Uplift force index

31. The uplift force index is the ratio of the uplift force acting on the base of the structure to the weight of a solid block of concrete filling the entire enveloping rectangle. The value of R_u is a measure of the severity of the uplift force acting on the base of the structure. The values of R_u for the structures shown in Table 2 vary from a minimum of 0.14 to a maximum of 0.29, with an average of 0.20. The distribution of the values of R_u for the structures is shown in Figure 6. There is little difference between the distributions of values for all structures and for those that retain earth backfills, as would be expected.

R_{rm} = resisting moment index

32. The resisting moment index is the ratio of the resisting moment of the structure (the product of the vertical force F_v multiplied by its moment arm around the toe of the wall) to the resisting moment of a solid block of concrete completely filling the enveloping rectangle. This ratio is a measure of the efficiency of the structure with respect to resistance to overturning. The values of R_{rm} for the structures shown in Table 2 vary from a minimum of 0.73 to a maximum of 0.93, with an average of 0.83.

33. Distributions of the values of R_{rm} are shown in Figure 7. The range of values for earth retaining structures is somewhat higher than for all structures, indicating that structures that retain earth are more likely to be broad and massive than are those that do not retain earth.

R_{dm} = driving moment index

34. The driving moment index is the ratio of the driving moment of the horizontal forces (the product of the horizontal force F_h multiplied by its moment arm around the toe of the wall) to the resisting moment of a solid block of concrete completely filling the enveloping rectangle. This ratio is a measure of the severity of the loading on the structure with respect to overturning moment. The values of R_{dm} for the structures shown in Table 2 vary from a minimum of 0.29 to a maximum of 1.45, with an average of 0.54.

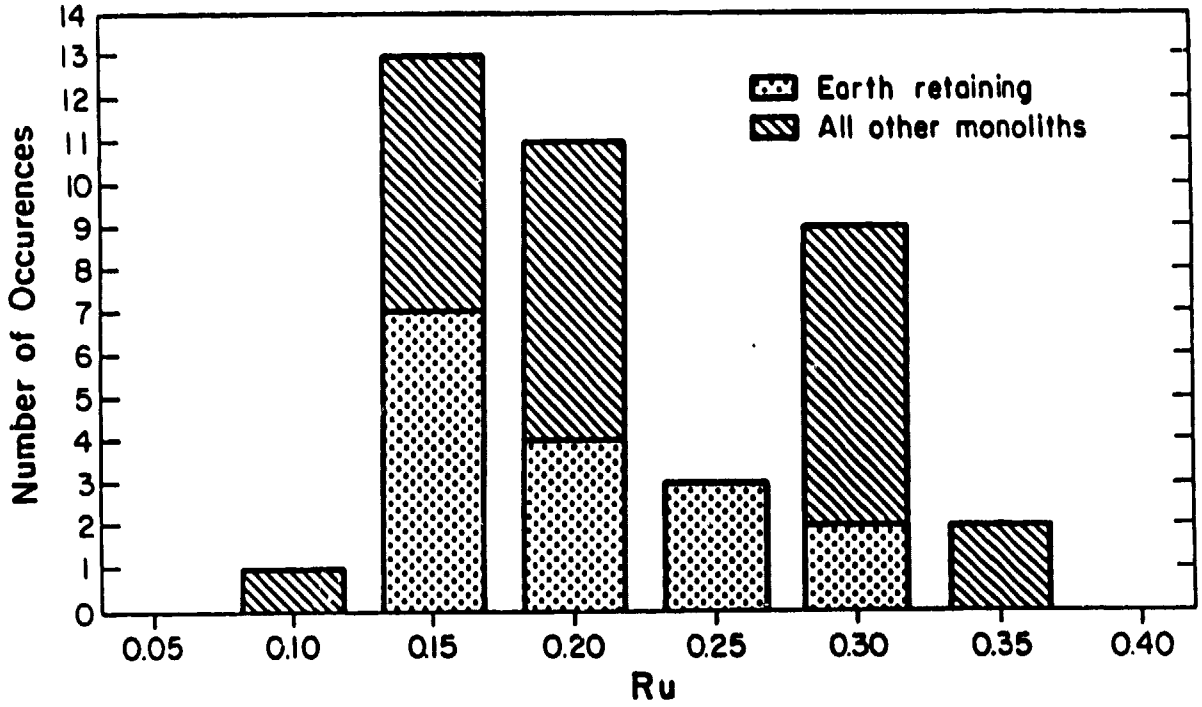

Figure 6. Distribution of dimensionless parameter R_u

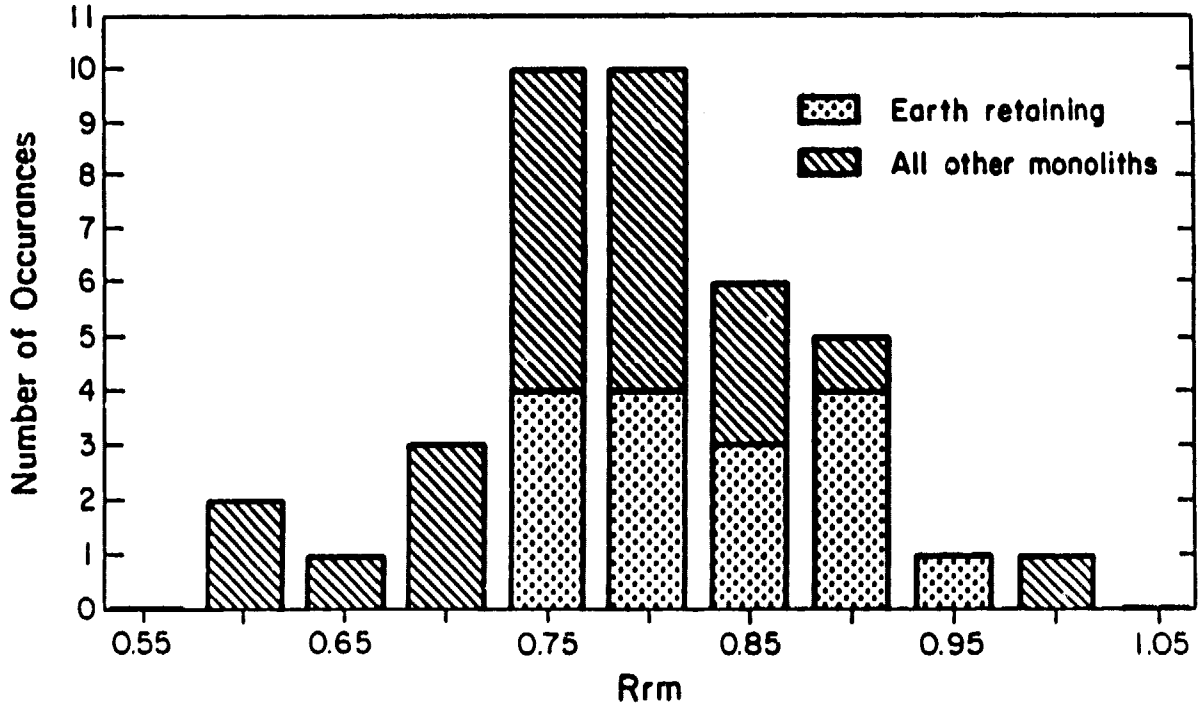

Figure 7. Distribution of dimensionless parameter R_{rm}

Excluding the extreme value of Emsworth L-19H, the next highest value is 0.71. The extreme value for Emsworth L-19H is due to the incorporation of a hawser pull load in the analysis. Distributions of the values of R_{dm} are shown in Figure 8. The range of values for the earth retaining structures is considerably narrower than for all structures, indicating a smaller range of driving or overturning moments on these structures.

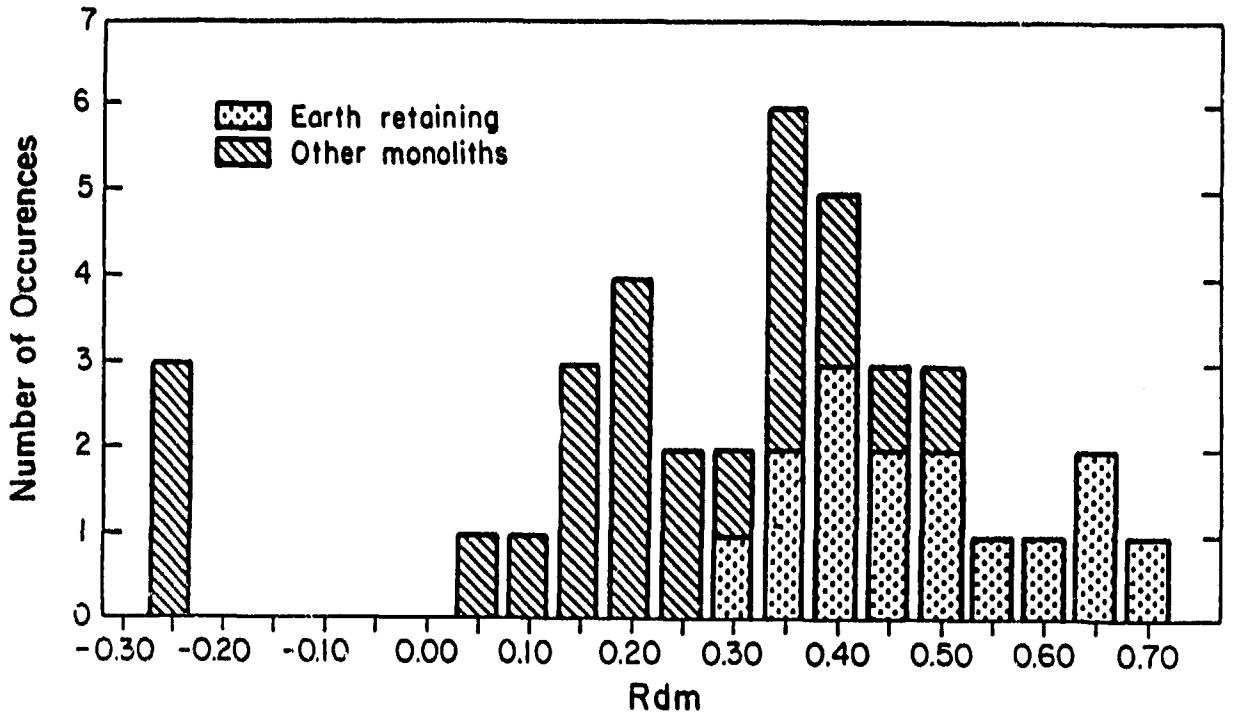

Figure 8. Distribution of dimensionless parameter R_{dm}

R_{um} - uplift moment index

35. The uplift moment index is the ratio of the overturning moment on the structure due to the uplift water pressure force (the product of the uplift force U multiplied by its moment arm around the toe of the wall) to the resisting moment of a solid block of concrete completely filling the enveloping rectangle. This ratio is a measure of the severity of the overturning moment to which the structure is subjected by the uplift water pressures. The values of R_{um} for the structures shown in Table 2 vary from a minimum of 0.18 to a maximum of 0.29, with an average of 0.22. Distributions of the values of R_{um} are shown in Figure 9. The values for the earth retaining structures cover nearly as wide a range as do the values for all structures,

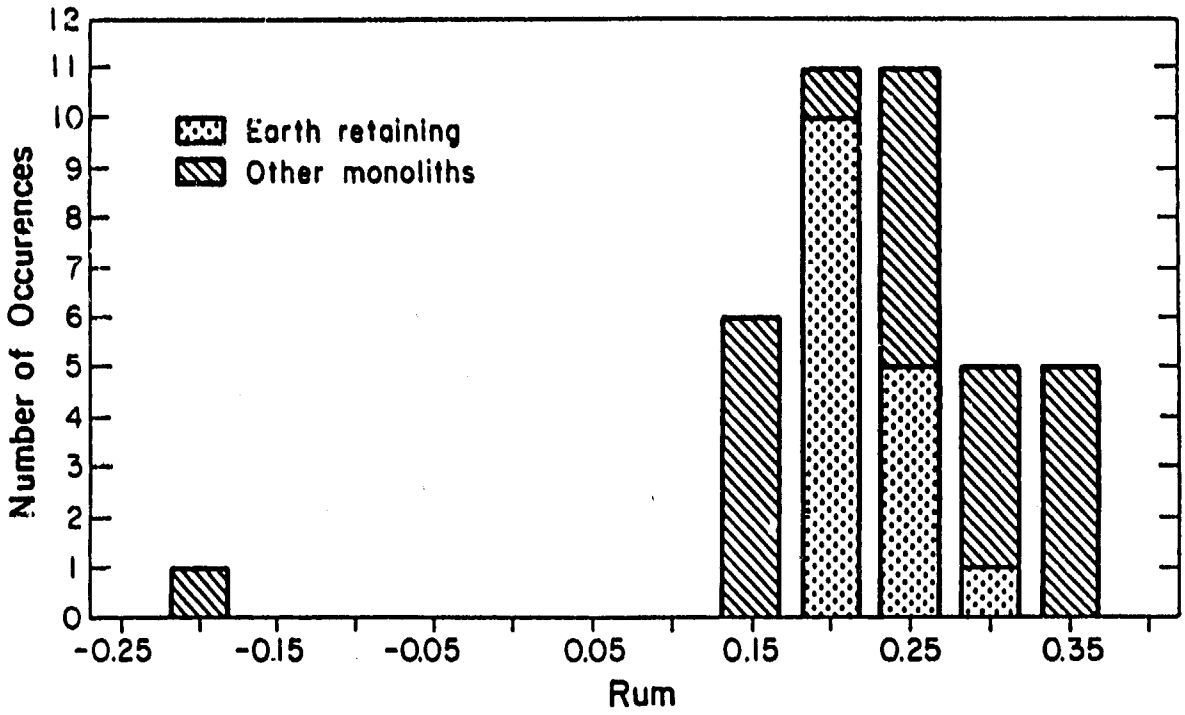

Figure 9. Distribution of dimensionless parameter R_{um}

indicating little effect of the type of structure on the value of R_{um} .

B/H = aspect ratio

36. This is the ratio of the base width to the height of the structure. It is a measure of the shape of the structure that is particularly significant with respect to the resistance of the structure to tipping under the influence of overturning moments. The values of B/H for the structures shown in Table 2 vary from a minimum of 0.33 to a maximum of 0.70, with an average of 0.54. Distributions of the values of B/H are shown in Figure 10. It may be seen that the base width-to-height ratios for the earth retaining structures are somewhat larger than the values for the other structures.

δ_{bm} = mobilized base friction angle

37. As explained in paragraph 17, δ_{bm} is the mobilized friction angle on the interface between the base of the structure and the underlying rock. It is a basic measure of the severity of the horizontal loading with respect to sliding. The values of $\tan(\delta_{bm})$ for the structures shown in Table 2 vary from a minimum of 0.4 to a maximum of 0.81, with an average of 0.6. Distributions of the values of $\tan(\delta_{bm})$ are shown in Figure 11. The range for

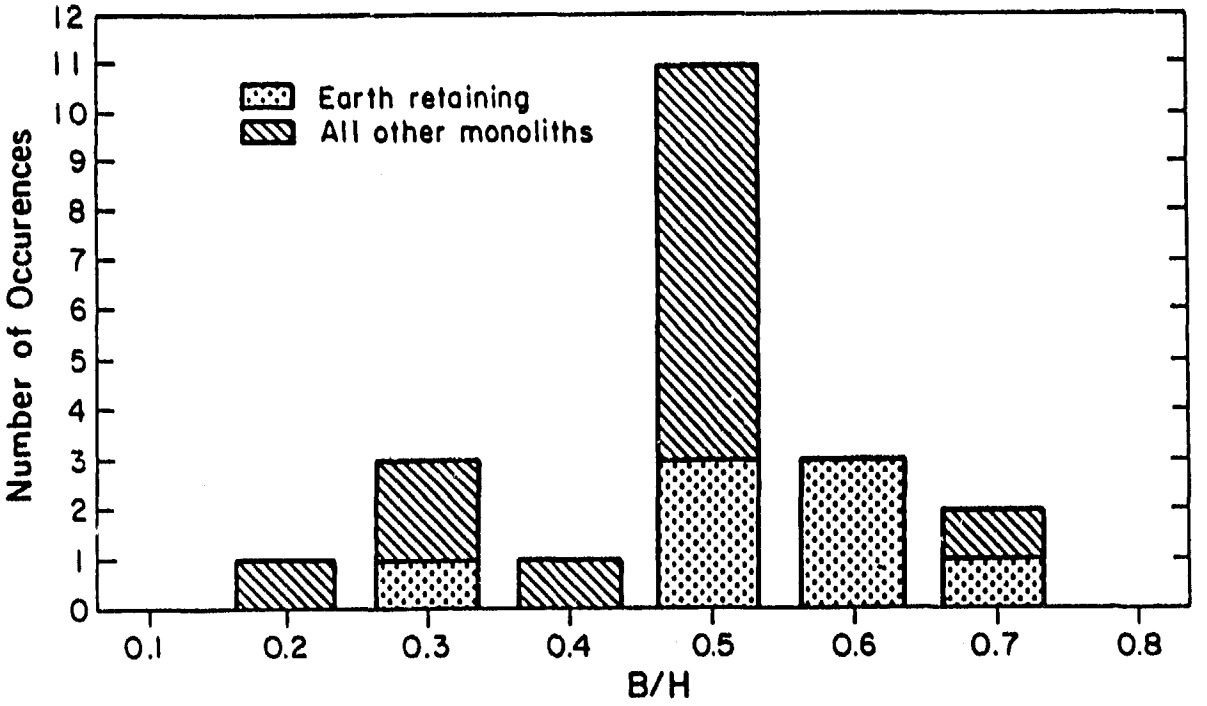

Figure 10. Distribution of dimensionless parameter B/H

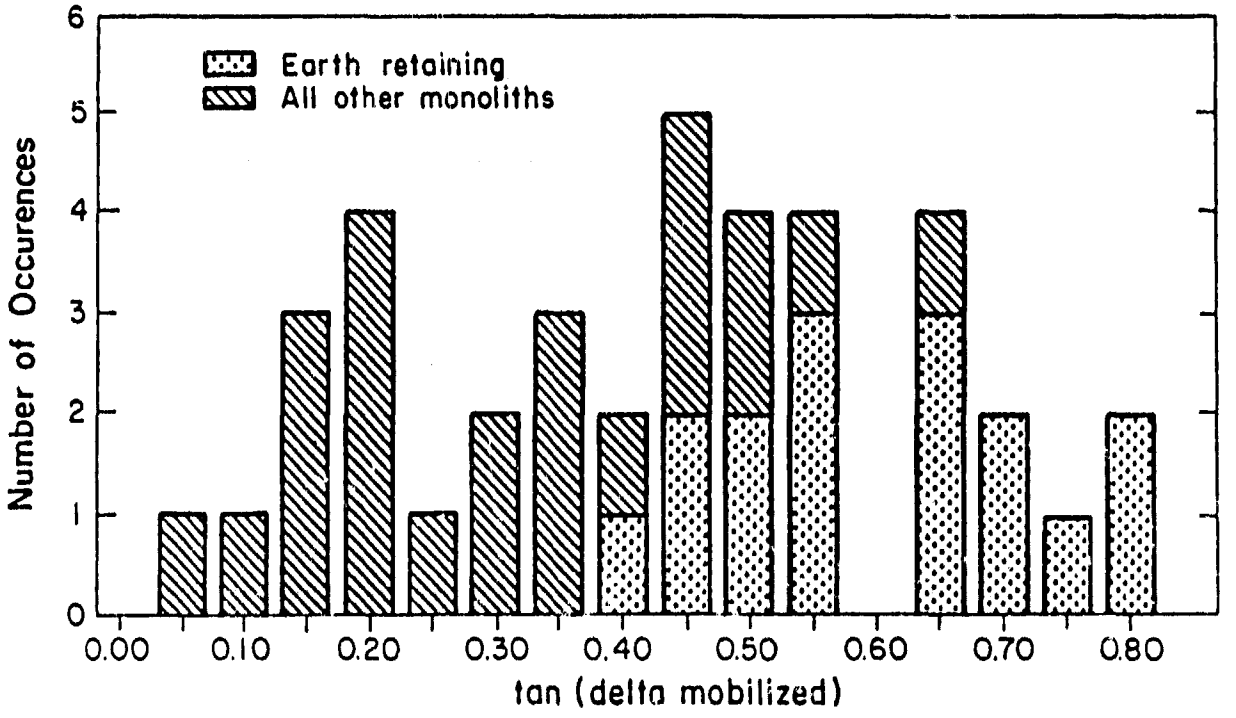

Figure 11. Distribution of $\tan(\delta_{bm})$

earth retaining structures is considerably narrower than for all structures combined, as would be expected.

B_e/B - fraction or percentage of effective base contact area

38. As discussed previously, B_e/B is the ratio of the effective base contact area to the full base area, and is usually expressed in percent. It is a measure of the safety of the structure with respect to overturning; the larger the value of B_e/B, the safer the structure with respect to overturning. The values of B_e/B for the structures shown in Table 2 vary from a minimum of zero to a maximum of 83 percent, with an average of 31 percent. Only 1 of the 16 structures listed in Table 2 meets the Corps of Engineers criterion with respect to having an effective base contact area of 75 percent or more.

39. Distributions of the values of B_e/B are shown in Figure 12, where the range of values for all structures is wider than the range for the earth retaining structures, and a considerable number of the structures that do not retain earth have B_e/B ratios that satisfy the criterion of 75 percent effective base contact.

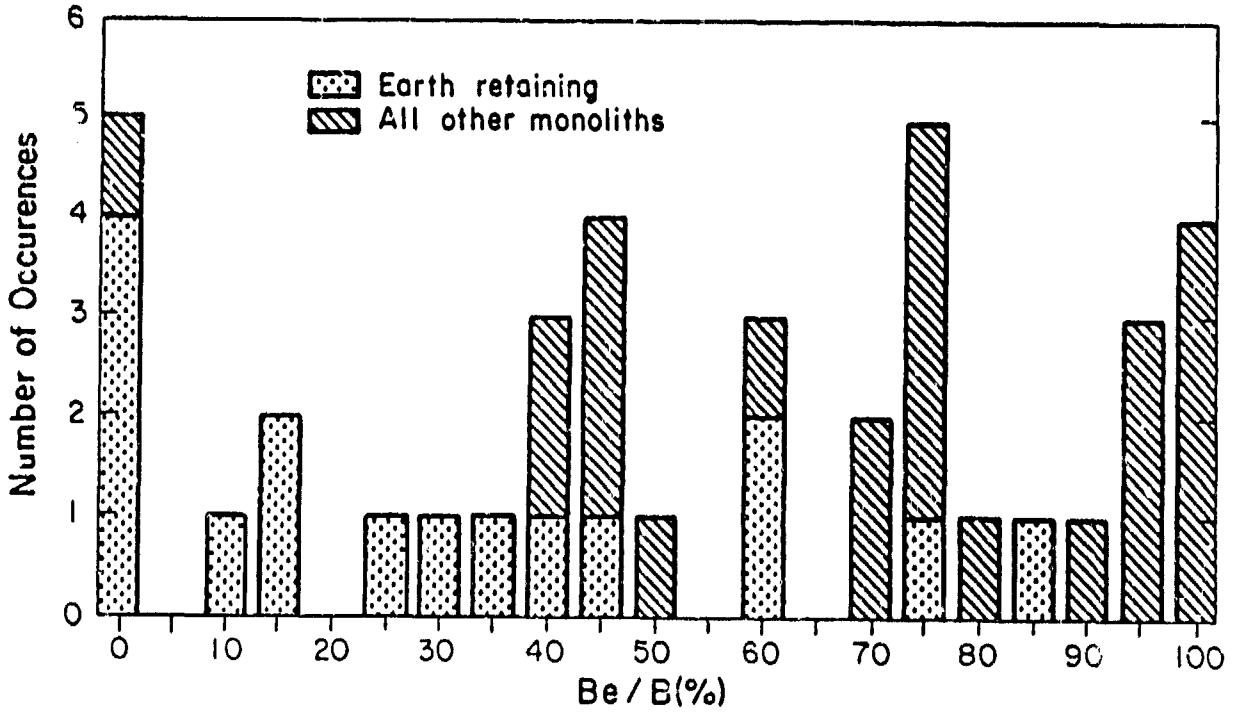

Figure 12. Distribution of B_e/B

Use of Dimensionless Parameters

40. The parameters discussed in the preceding paragraphs provide a convenient means of describing some of the important characteristics of gravity retaining walls. The values summarized in Table 2 and Figures 4 through 12 were used in selecting the characteristics of the hypothetical structures studied during this investigation and the ranges of loadings analyzed. Matching the characteristics of the real and the hypothetical structures in this way ensured that the hypothetical structures were, in fact, representative of actual Corps of Engineers structures and that they provided a suitable basis for research into the significance of the various factors that govern wall stability.

41. The safety of a wall with respect to sliding and overturning can be related directly to the dimensionless parameters. The value of δ_{bm} can be expressed as:

$$\delta_{bm} = \tan^{-1}\left(\frac{R_h}{R_v - R_u}\right) \tag{5}$$

The relationship expressed by Equation 5 is precise, as indicated by the variation of $\tan(\delta_{bm})$ with $(R_h/R_v - R_u)$ shown in Figure 13 for the monoliths at Emsworth, Montgomery, and Troy locks.

42. The effective base area ratio can be expressed in terms of the dimensionless parameters as follows:

$$B_e/B = \frac{3 \cdot (R_{rm} - R_{dm} - R_{um})}{2 \cdot (R_v - R_u)} \cdot 100\% \tag{6}$$

This relationship is also precise, as shown by the data plotted in Figure 14 for the Corps of Engineers lock structures.

43. Thus, the measures of stability used for design are determined completely by the characteristics of the structures with regard to the values of the dimensionless parameters that characterize its shape and mass, and the loadings to which it is subjected.

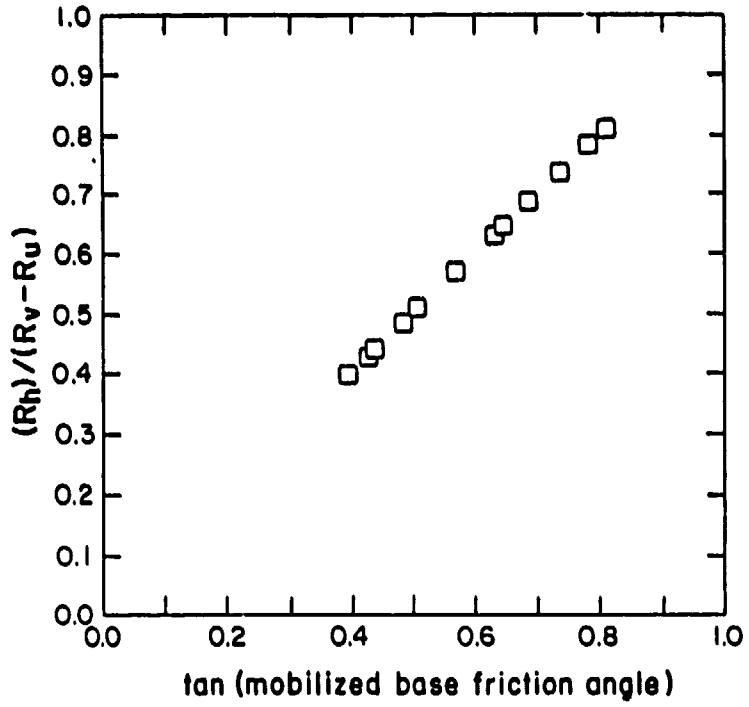

Figure 13. Variation of $\tan(\delta_{bm})$ with $R_h/(R_v - R_u)$

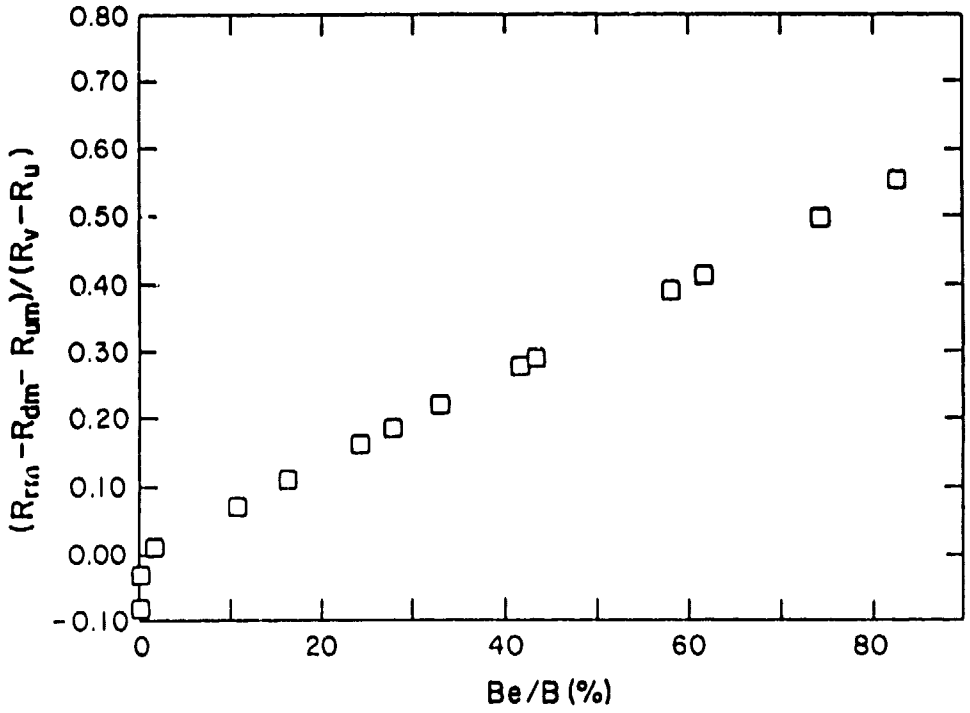

Figure 14. Variation of B_e/B with $(R_{rm} - R_{dm} - R_{um})/(R_v - R_u)$

Hypothetical Structures and Loading Conditions Used in Following Load Analyses

44. A cross section through one of the hypothetical structures used for following load analyses is shown in Figure 15. As shown in Table 3, the heights of the structures evaluated varied from 40 to 70 ft, and the base width-to-height ratio was varied from 0.4 to 0.8. The width of the top of the monolith is maintained at $0.2 \cdot H$ for all structures. The height of the water table behind the monolith, H_w, was maintained at $0.67 \cdot H$.

45. The range of values of the dimensionless parameters for the walls at Emsworth, Montgomery, and Troy locks and the hypothetical cases used in the following load analyses are shown in Table 4. The hypothetical structures cover a range of conditions very nearly the same as covered by the real walls. It seems reasonable to expect, therefore, that study of these hypothetical structures will provide information pertinent to analyses of the behavior of real walls.

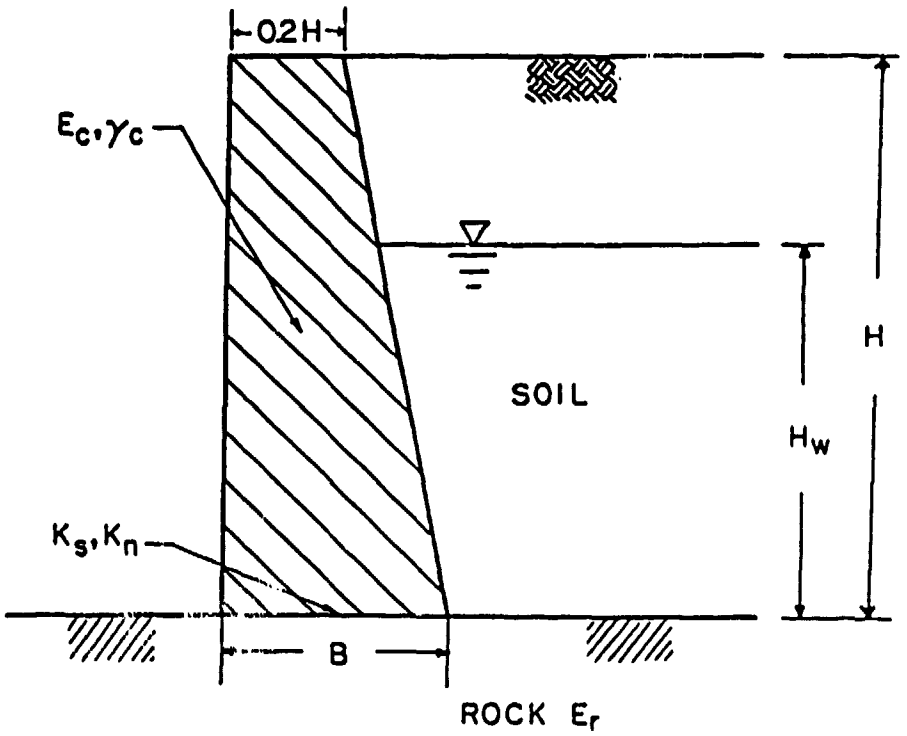

Figure 15. Base case hypothetical structure used in the following load analyses

Table 3

Values of Parameters Used in Following Load Analyses

Constant Parameters	Variable Parameters
T = width at top of wall = 0.2H	H = height of wall
H_w = height of water behind wall	E_r = modulus of rock foundation
γ_d = dry unit weight of backfill = 125 pcf	K_n = normal stiffness of interface
γ_{sat} = saturated unit weight of backfill = 145 pcf	K_s = shear stiffness of interface
γ_c = unit weight of concrete = 150 pcf	B = width of base of wall
E_c = modulus of elasticity of concrete = 3×10^6 psi	

Poisson's ratio of concrete = 0.2
Poisson's ratio of rock = 0.15

Run	H ft	B ft	B/H	H_w ft	E_r psi	K_n psi	K_s psi	Mesh	Loading Increment	Comments
1*	40	16	0.4	26.7	3×10^6	3×10^6	1×10^4	Coarse	Coarse	Base Case
2*	40	16	0.4	26.7	3×10^6	3×10^6	1×10^4	Coarse	[Fine]	Base Case
3*	40	16	0.4	26.7	3×10^6	3×10^6	1×10^4	Fine	Coarse	[UBFM]
4*	40	16	0.4	26.7	3×10^6	3×10^6	1×10^4	Fine	Coarse	[AM]
5*	40	16	0.4	26.7	[1×10^4]	3×10^6	1×10^4	Fine	Coarse	AM
6*	40	16	0.4	26.7	[1×10^7]	3×10^6	1×10^4	Fine	Coarse	AM
7*	40	16	0.4	26.7	3×10^6	[3×10^4]	1×10^4	Fine	Coarse	AM
8*	40	16	0.4	26.7	3×10^6	3×10^6	[1×10^1]	Fine	Coarse	AM
9*	40	16	0.4	26.7	3×10^6	3×10^6	1×10^4	Fine	Coarse	[Construct wall], AM
10*,**	40	[24]	[0.6]	26.7	3×10^6	3×10^6	1×10^4	Fine	Coarse	AM
11*,**	40	[32]	[0.8]	26.7	3×10^6	3×10^6	1×10^4	Fine	Coarse	AM
12*	[70]	28	0.4	46.7	3×10^6	3×10^6	1×10^4	Fine	Coarse	AM

Note: Parameters in brackets are those changed from the values for the base case; UBFM = unbalanced force method; AM = alpha method; Construct Wall = simulate monolith construction using three lifts.

* No hydrostatic uplift pressure.

** Full hydrostatic uplift pressure.

Table 4

Ranges of Values of Dimensionless Parameters for Walls Studied by Corps of Engineers and for Hypothetical Cases Discussed in this Report

Dimensionless Parameter	Range* for Emsworth, Montgomery, and Troy Earth Retaining Monoliths	Range Used in Following Load Analyses	Range Used in Backfill Placement Analyses
R_v	0.705 to 0.961	0.974	0.95 to 0.975
R_h	0.228 to 0.524	0 to 0.534	0 to 0.821
R_u	0.102 to 0.294	0 to 0.278	0
R_{rm}	0.702 to 0.954	0.957	0.917 to 0.958
R_{dm}	0.010 to 1.066	0 to 0.883	0 to 1.365
R_{um}	0.152 to 0.284	0 to 0.278	0
B/H	0.323 to 0.763	0.4 to 0.8	0.4
$\tan(\delta_{bm})$	0.354 to 0.842	0 to 0.646	0 to 0.842
B_e/B, %	0 to 84	0 to 100	0 to 100

* Range from two standard deviations below average to two standard deviations above average.

46. As shown in Table 3, the unit weights of the dry backfill, submerged backfill, and the concrete were kept constant in the analyses, as were the modulus and Poisson's ratio of the concrete and the Poisson's ratio of the rock.

47. The modulus of the rock was varied from 10,000 to 10,000,000 psi. The normal stiffness of the interface between the bottom of the monolith and the rock foundation was varied from 30,000 to 3,000,000 pci, and the shear stiffness was varied from 10 to 10,000 pci. The ranges in rock properties used in the analyses were selected to cover the range of values found to be appropriate for foundation rocks, based on the results of the study described in the report by Benson et al. (1987).

48. Two conditions of uplift pressure were modeled in the analyses. The first was no uplift. The second was full uplift, equal to the height of water behind the structure multiplied by the unit weight of water, acting across the entire base. These conditions were used to bracket actual conditions. Full uplift pressure would correspond to a condition where a crack had propagated from the heel along the base of the monolith to a point just short of the toe; therefore, the entire base of the structure would be subjected to hydrostatic pressure. A condition of no uplift would correspond to an uncracked monolith-foundation interface. Actual conditions of a crack propagation terminating somewhere in the middle of the structure should be bracketed by the results obtained from the full uplift and no uplift analyses.

49. The base case hypothetical structure used in the following load analyses shown in Figure 15 is 40 ft high, 16 ft wide at the base, with a base-to-height ratio of 0.4. The modulus of rock was 3,000,000 psi, and the normal and shear stiffness of the interface between the base of the structure and the rock foundation are 3,000,000 and 10,000 pci, respectively. No uplift pressure was applied to the base of the monolith in the base case.

Hypothetical Structures and Loading Conditions Used in Backfill Placement Analyses

50. Cross sections representing each of the two categories of hypothetical structures used for the backfill placement analyses are presented in Figure 16. In one group of analyses the structure was buttressed by soil at the toe, whereas in the other group there was no toe fill. The geometry of the structure was the same for all analyses and was the same as the monolith

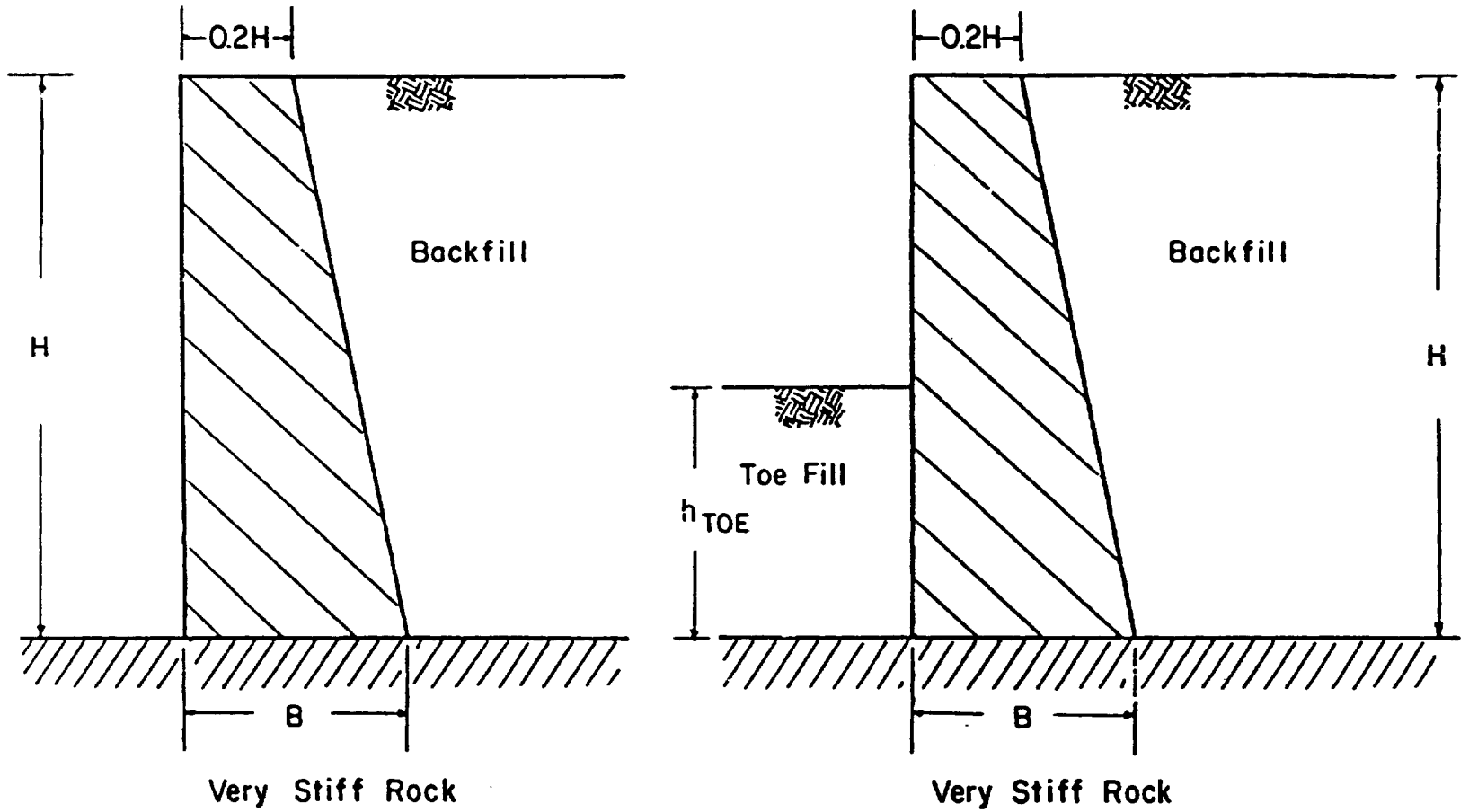

Figure 16. Base case hypothetical structures used in the backfill placement analyses

used in the base case of the following load analyses. It was 40 ft high and had a base width of 16 ft. The width of the top of structure was 0.2·H. For the structure with toe fill, the fill at the toe was 17.8 ft deep, which is equal to the height of structure multiplied by 0.45. In the analyses with toe fill there was no water behind or in front of the wall.

51. As shown in Table 5, the unit weight of the concrete was kept constant in the analyses, as were the modulus and Poisson's ratio of the concrete and the normal stiffness of the interface between the base of the monolith and the rock foundation. The coefficients for the nonlinear stress-strain model for the soil backfill, the normal and shear stiffness for the interfaces between the soil and the concrete and the soil and rock were also maintained as constant during the analyses. The foundation was represented as very stiff rock.

52. The Poisson's ratio of the soil backfill was varied from 0.15 to 0.38, and the shear stiffness of the interface between the base of the monolith and the rock foundation was varied from 10 to 10,000 pci.

53. The base case hypothetical structure used in the backfill placement analysis of monoliths without backfill at the toe was also 40 ft high and 16 ft wide. The normal stiffness of the interface between the base of the structure and the rock foundation was 3,000,000 pci, and the shear stiffness of the interface was 10,000 pci. The dry unit weight of the soil backfill was 135 pcf and the Poisson's ratio was 0.15.

54. The base case hypothetical structure and material properties used in the backfill placement analysis of a monolith with soil backfill present beyond the toe is the same as that described for no backfill at the toe.

Table 5

Values of Parameters Used in Backfill Placement Analyses

Constant Parameters

H - height of wall = 40 ft

B - width of base of wall = 16 ft

B/H = 0.4

H_w - height of water behind wall = 0 ft

T - width at top of wall = 0.2H = 8 ft

γ_c - unit weight of concrete = 150 pcf

E_C - modulus of elasticity of concrete = 3×10^6 psi

K_n - normal stiffness of interface = 3,000,000 pci

K_s - shear stiffness of interface (soil to concrete)

= 20 to 300 pci

Poisson's ratio of concrete = 0.2

Constant Soil Backfill Parameters

ϕ - friction angle of backfill = 39 deg

K - backfill stiffness parameter constant = 450

n - backfill stiffness parameter exponent = 0.4

R_f - backfill failure ratio parameter = 0.7

δ - wall to soil interface friction

Variable Parameters

h_{toe} - height of soil backfill beyond toe

K_s - shear stiffness of interface (rock to concrete)

Variable Soil Backfill Parameters

$\gamma_{backfill}$ - unit weight of backfill

$\upsilon_{backfill}$ - Poisson's ratio of backfill

Run	h_{toe} ft	h_{toe}/h	$\gamma_{backfill}$ pcf	$\upsilon_{backfill}$	K_s* pci	δ/ϕ**	Comments
13a	0	0	135	0.15	1×10^4	0.8	AM
14a	0	0	135	[0.3]	1×10^4	0.8	AM
15a	0	0	135	[0.38]	1×10^4	0.8	AM
16a	0	0	[120]	0.15	1×10^4	0.8	AM
17a	[17.8]	0.45	135	0.15	1×10^4	0.8	AM
18a	17.8	0.45	135	0.15	1×10^4	0.8	[Wall restrained against deformation]
19a	17.8	0.45	135	0.15	[1×10^1]	[1.0]	AM

Note: AM - alpha method. Parameters in brackets are those changed from the values for the base case.

* Concrete-to-rock

** Concrete-to-soil

Equations for soil stress-strain model

$$E_t = \text{tangent modulus} = [1 - R_f \cdot SL]^2 \cdot K \cdot P_a (\sigma_3/P_a)^n$$

$$SL = \text{stress level} = (\sigma_1 - \sigma_3)/(\sigma_1 - \sigma_3)_f$$

$$(\sigma_1 - \sigma_3)_f = (2 \cdot c \cdot \cos\phi + 2 \cdot \sigma_3 \cdot \sin\phi)/(1 - \sin\phi)$$

$$P_a = \text{atmospheric pressure}$$

PART IV: DEVELOPMENT OF FINITE ELEMENT PROCEDURES FOR RETAINING STRUCTURES IN A CONDITION OF INCIPIENT INSTABILITY

55. Finite element procedures for analysis of conventional, stable gravity earth retaining structures are well established (Clough and Duncan 1971; Kulhawy 1974). However, this approach has not been adapted for walls in a condition of incipient instability (the development of a crack at the base due to an applied load). The study of gravity retaining structures in a condition of incipient instability is divided into two phases. The objective of the first phase involves identifying the analytical requirements, and extending the capabilities of the FEA procedure in the program SOILSTRUCT. The improved procedure described in Part IV was used in a series of parametric evaluations of typical retaining structures. The results of these parametric studies are discussed in subsequent parts of this report.

56. Two fundamentally different approaches are used in the finite element studies to treat the loading on the gravity wall. In the first approach, the wall is assumed to be loaded by a predefined lateral pressure of given magnitude and distribution. The soil backfill, per se, is not represented in the analysis. The lateral pressures are established using conventional concepts for earth and water loadings of retaining wall systems. The pressures are applied to the wall in a series of steps so that the response of the structure to gradually increasing loading can be determined. Because of the nature of this approach, the magnitudes and distributions of the loadings are uncoupled from the action of the wall-foundation system. For example, no matter how much the wall moves or regardless of the form of the structure movement, the loading is not changed. Given the nature of this process, this form of loading is termed "following load analysis" in this report. This method is used in all first phase analyses discussed in Parts IV and V. The second method of loading, used in these analyses, is presented in Part VI, and extends the work to include a coupled soil-backfill system.

57. An additional feature of the following load analysis is that with the lateral forces known in both magnitude and distribution, the resultant forces acting along the interface between the base of the monolith and the rock foundation may be determined using conventional equilibrium methods. The total number of unknowns is limited to three, since they must not exceed the number of equilibrium equations. Thus, the magnitude of the shear force resisting sliding, the normal force, and the point of action of this force

along the base are known independent of the FEA. These parameters can be used to evaluate the accuracy of the finite element analyses.

58. The first series of analyses were conducted using the off-the-shelf technology as existed in the program SOILSTRUCT when the project was initiated during the summer of 1986. Their purpose was to define the general nature of the problem and identify the requirements of the analytical procedure. These analyses were exploratory in the sense that this represents the first application of the program to walls that verged on instability. Subsequently, analytical techniques were developed to more closely model the actual conditions of this category of problem.

Comments on Finite Element Analysis and Interface Modeling Techniques

59. The program SOILSTRUCT used in this evaluation of navigation structures is a general-purpose finite element program with the capability of analyzing involved soil-structure interaction problems. Some of the unique features include an ability to model nonlinear material behavior and geometric details such as interfaces along which relative movements occur. In the first phase of analyses, linear material behavior was specified for all materials with the exception of the interface elements used to model the joint between the wall and the foundation.

Interface elements

60. One of the key components in the first phase work is the interface element between the wall and the foundation. The interface element dictates the amount of contact between the wall and foundation and controls the interaction between them to a large degree. The element deformation process is characterized in terms of two parameters: (a) the normal stiffness; and (b) the shear stiffness. Details on these parameters are given in the report by Benson et al. (1987). In the FEA, it is possible to make these parameters single- or multiple-valued functions. In the latter case, different values might be employed depending upon the stress conditions acting upon the interface. For example, one value of normal stiffness might apply for situations where there is compression in the element, and a zero stiffness might be expected to apply if there is any significant amount of tension on the interface.

Interface stiffness

61. In the first phase analyses, the following approach was taken:

a. Normal stiffness. In accordance with the foregoing discussion, this parameter is taken as having two values; a finite value for a state where the interface has normal compressive stresses and a near zero value if the normal stress at the center of the element is shown to be in tension.

b. Shear stiffness. This parameter is assumed to be single-valued when the interface normal stress is compressive. In this instance, it is desired to allow the element to take all of the shear stress it desires to use the accumulated shear stress to check the base friction angle that is mobilized to accommodate the shear loading. The mobilized interface friction angle characterizes the amount of base shear, and as will be seen, this angle is typically within those known to exist for concrete-to-rock interfaces for all the analyses. If the interface normal stress is found to be tensile, the shear stiffness is reduced to a near zero value.

62. The values used for the normal and shear stiffnesses with the element in compression were determined through the literature review given in the report by Benson et al. (1987).

Loading Scheme

63. The loading scheme used in the following load analyses has three basic components. The first involves the vertical loads induced by the weight of the monolith, and the wedge of the soil backfill which is contained in the triangular area that is bounded by the two vertical lines originating at the heel of the monolith; one extending vertically through the backfill and the other along the monolith-backfill interface. The second component of loading is the lateral stress assumed to be generated by the soil backfill and the water in the backfill. Finally, the third loading, used only in special cases, is the upward pressure acting on the base of the monolith generated by hydrostatic uplift. Inclusion of this force is discussed in the parametric studies in Part V.

64. The vertical gravity loads generated by the retaining structure in the following load analyses are accounted for in the analyses in two different approaches. The first of these approaches is described in the following paragraph while the second is discussed in Part V, paragraphs 131 through 138. In the simplest version, the effect of the weight of the concrete monolith and the soil wedge is considered by applying a vertical downward pressure on the

base interface that is equivalent to the overlying material weight. During the application of the downward pressures, the wall stiffness is zero and, thus, does not influence the loading process.

65. The lateral load is applied in a series of steps in which the pressures are assumed to act across the entire face of the monolith. As shown in Figure 17, a total of 10 steps are generally used to bring the lateral loading to full value. As a point of comparison, in one instance the loads are reduced in size so that more than 10 increments are needed to arrive at the full value. This analysis is referred to as a "fine load" analysis, whereas the analysis using 10 load increments is a "coarse load" analysis.

66. When using the coarse load analysis, the first five steps are designed to bring the soil influence to full effect. Total pressures are used for the soil above the water table, and effective pressures act where the soil is below the water table. The magnitudes of the pressures are dictated by the assumed values for the soil parameters given in Table 3. The second of the five steps applies pressures to the portion of the monolith face that is below the water table and model the effects of the hydrostatic loading. By the tenth load step, the full soil and hydrostatic pressures are applied.

67. The upward pressures accounting for the presence of uplift at the base of the monolith are treated in an all or nothing manner. That is, they are assumed to be commensurate with the full uplift or zero. The implementation of the uplift pressure increments is tied to the lateral loading sequence. Basically, as lateral loads are applied that involve water effects, the pressures representing the uplift effects are simultaneously implemented. In the first phase analyses discussed in Part IV, no uplift pressures were applied.

68. A final note relative to the number of load increments applied in an analysis is: In some cases, the system may not be able to absorb the full 10 loading increments. This is due to the fact that before the tenth load increment the system reaches a point where only one interface element along the base of the monolith is left in compression. Loading beyond this serves no purpose, since the system is inherently unstable numerically, and from a statics point of view, the base contact area is zero or even less than zero.

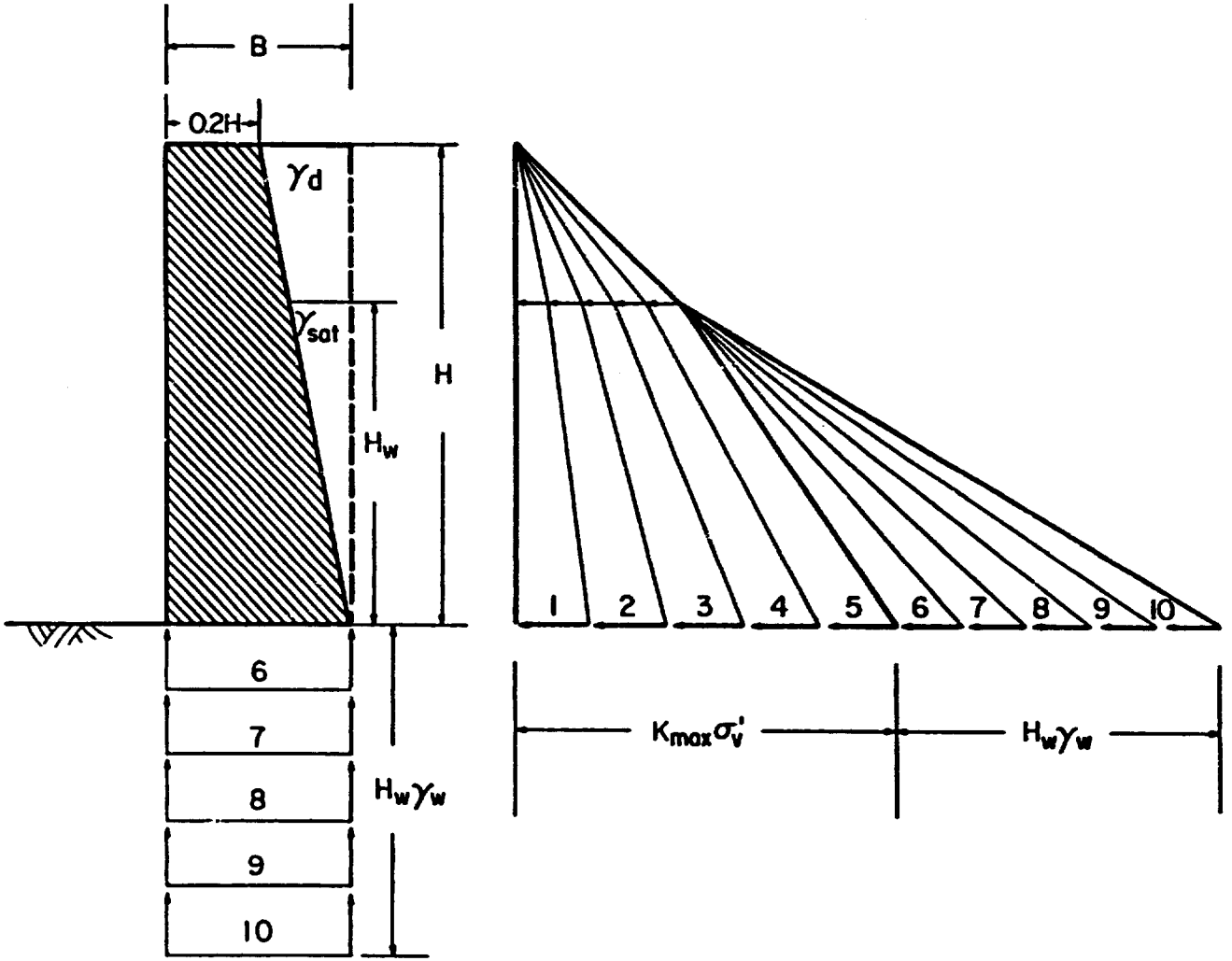

Figure 17. Incremental pressure applications used in following load analysis

Coarse Mesh for Base Case

69. The finite element mesh designed for the initial phases of the investigation is shown in Figure 18. The cross section shows the base case hypothetical structure (Figure 15), a 40-ft-high monolith with a 16-ft base or a base-to-height ratio of 0.4. The depth of rock foundation included in the mesh is two and one-half times the width of the monolith's base and extends a distance equal to three times the monolith's height beyond the toe and heel. The mesh contains a total of 167 two-dimensional and interface elements; 24 of which represent the concrete monolith, 138 the rock foundation, with 5 interface elements between the monolith and its foundation. The early analyses showed this mesh to be too coarse, and refinements were added in subsequent analyses. The mesh of Figure 18 is referred to as the "coarse mesh" in this report.

Material Properties

70. Linear material behavior was assumed for the concrete monolith and the rock foundation for all phases of analyses. For the base case, the modulus of the concrete and rock is 3,000,000 psi, and the Poisson's ratio is 0.15 and 0.2 for the respective materials. The normal and shear stiffnesses of the interface between the wall and foundation are 3,000,000 and 10,000 pci, respectively.

Results from the Following Load Analyses

71. The results for the following load analyses are characterized in terms of these parameters:

a. The distribution of normal and shear stresses along the interface between the wall and foundation.

b. The percent contact area for the base of the wall with the foundation, B_e/B .

c. The ratio of residual tensile load, produced in the interface elements to the overlying total gravity load of the structure and the backfill. In theory, a perfect analysis would produce a zero residual tensile load.

d. The ratio of residual shear load, produced in the interface where tensile stresses are developed, to the total shear force developed along the entire interface, F_h .

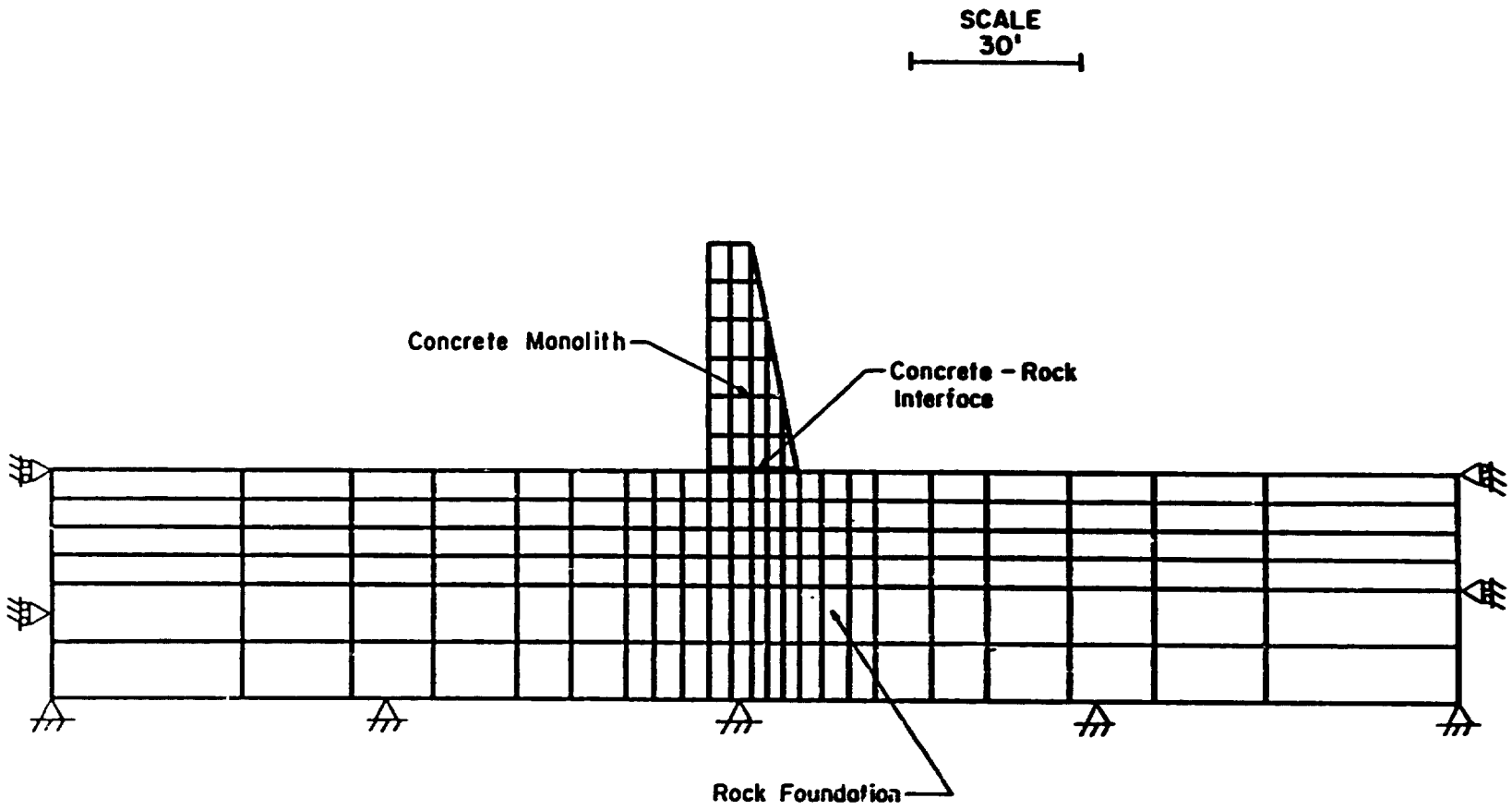

Figure 18. Coarse finite element mesh used to model the base case hypothetical structure

e. The location of the resultant normal force for the portion of the base that is in compression as computed in the finite element analysis compared to the location of the resultant force computed from the conventional equilibrium analysis.

f. The ratio of the lateral deformation at the crest of the wall, u_x , to its height, H .

Results from the Coarse Load Step Analysis Coarse Finite Element Mesh

72. In Figure 19, the interface normal and shear stress distributions on the base of the structure for the initial condition and with various stages of lateral loading are shown. In this analysis, no uplift pressures along the base are assumed. The first distribution presented in the initial stress prior to any lateral loading. Since only gravity induced forces are acting and no lateral loads are applied at this stage, the initial shear stress is zero. The second distribution shown is for the case of $0.3 \cdot \sigma_v$ lateral loading, the first indication that the wall is attempting to separate from the foundation. The analysis results show that tensile stresses have developed in the first interface element at the heel of the wall. For subsequent load stages, the normal and shear stiffnesses are assigned a near zero value so that no additional stresses are accumulated within the element. At this point in the analysis, 13.3 ft of the base remains in compression and this is referred to as the effective base contact area, B_e . The first interface element, representing 2.7 ft of the wall length, is removed from stiffness computations for subsequent stages.

73. By the application of the full lateral soil load, equivalent to $0.5 \cdot \sigma_v$, three of the five interface elements on the base have developed tension stresses (Figure 19). Figure 19 also shows the normal stress distribution from the CEA for full lateral soil loading. It indicates a smaller length of effective base, and a higher compressive stress within the toe region, as compared to the results from the FEA. In spite of the differences in base pressure distributions between the finite element and conventional analyses, the resultant forces computed using the normal and shear stresses predicted by the FEA for the interface elements are in equilibrium with the applied forces. This is because the finite element solution minimizes the total potential energy for the problem, the basis for the series of equations used in the finite element procedure.

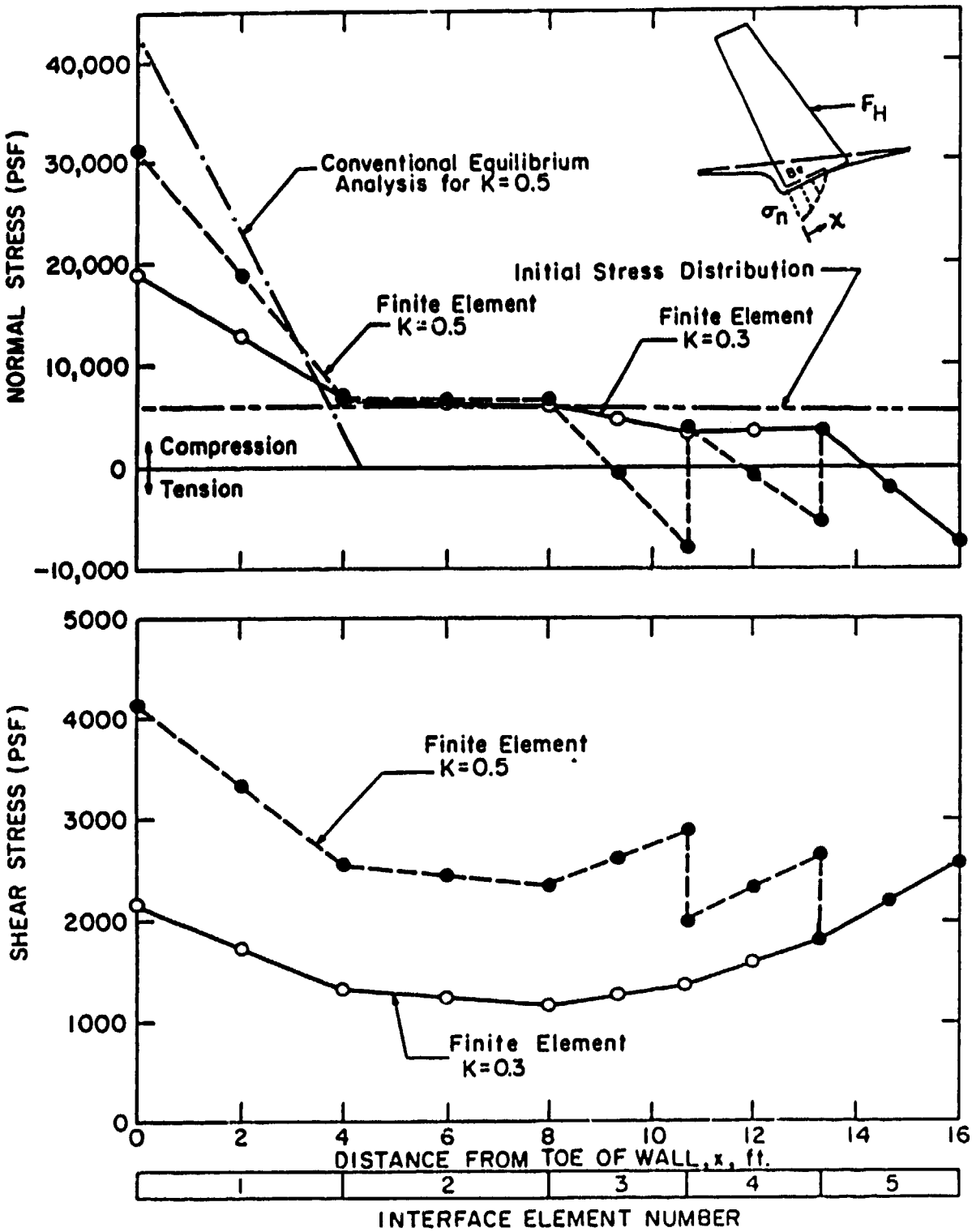

Figure 19. Stress distributions along the base for various stages of loading, coarse mesh/coarse load step

74. Figure 20 presents information on the development of the effective base contact area, B_e, as a function of the loading for the FEA, and the conventional rigid body static analysis. The value of B_e is defined as the area of the base over which the pressure distribution is in compression. The normalized base contact area, B_e/B, decreases as the lateral load is increased. Notably, the reduction in the computed B_e is less for the FEA as compared to B_e from the CEA. Taking the results at face value, they would suggest that the conventional analysis is conservative. This would be true if all factors were equal in the analyses, but as Figure 19 indicates, the FEA have, in essence, built in a structure-to-foundation tension that does not exist in the conventional case.

75. The magnitude of tension and shear stress in the cracked zone may be considered as an index to the error in the FEA. In this document, the stresses are converted to resultant forces and normalized by the total applied vertical and horizontal forces, respectively, as convenient simplified parameters to assess the accuracy of the analyses. The normalized normal and shear resultant forces within the tensile region are referred to as the overshoot, since they represent forces which would not exist on a no-tension interface.

76. Figure 21 presents information on the development of normalized overshoot forces as a function of the loading for the coarse mesh/coarse load step analysis. As the lateral loading increases, the overshoot increases. It is observed that the normalized overshoot shear force ($\Delta T/F_h$) decreases in magnitude after the entire earth pressure load is applied, whereas the normalized overshoot tensile force ($\Delta N/F_v$) remains constant. This decrease results from the fact that the normalizing force F_h increases during the loading sequence, whereas F_v, which reflects the gravity load, is constant. At the end of the earth pressure loading, a significant amount of force is retained within the interface elements representing the open joint; 10 percent of the gravity load and 45 percent of the shear force. Later analyses will put this magnitude of error in perspective.

77. In Figure 22 the location of the resultant normal force for the region in compression as computed by the FEA is compared to that of the CEA. If they were in agreement, the results would plot on the diagonal line through the figure. It is observed that as the loading increases and the location of the resultant normal force moves toward the toe, the error in the computed point of action in the finite element results increases.

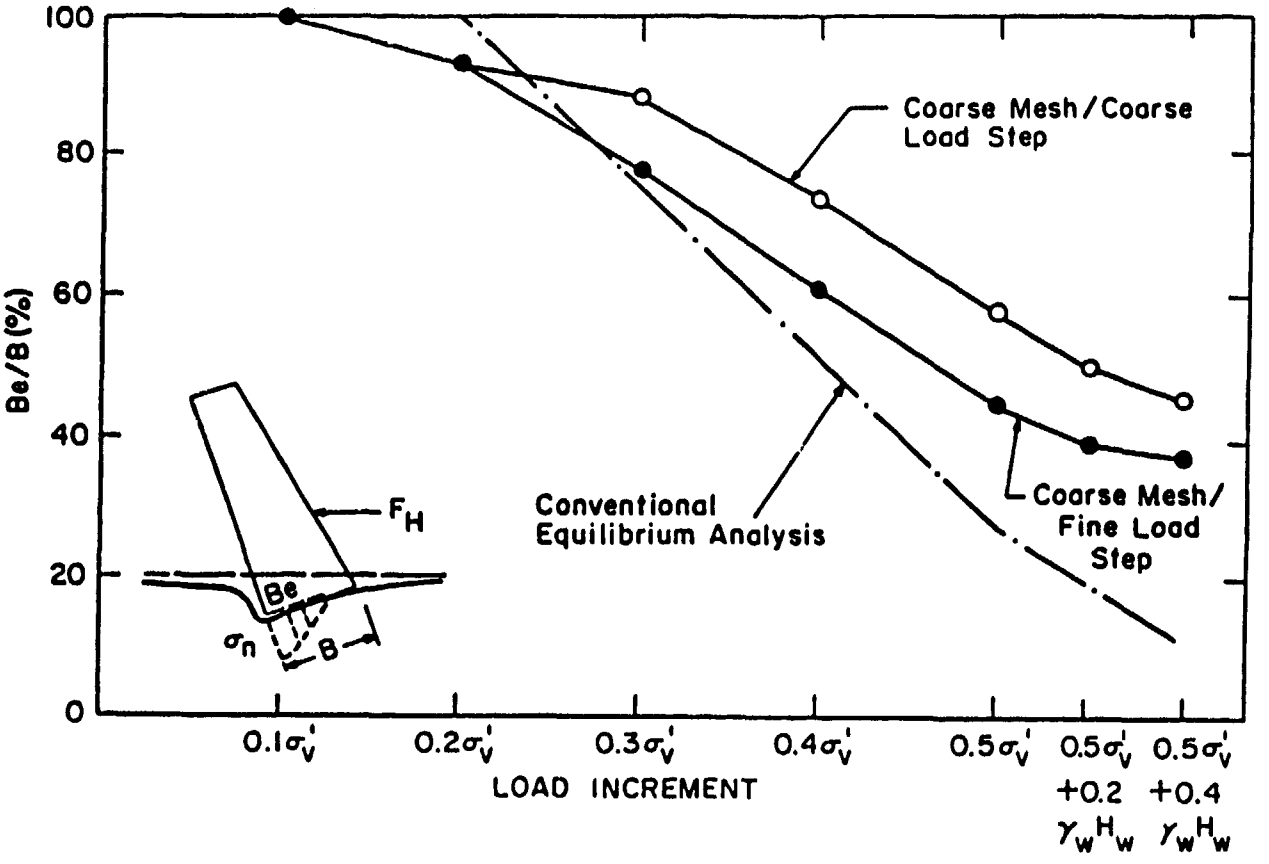

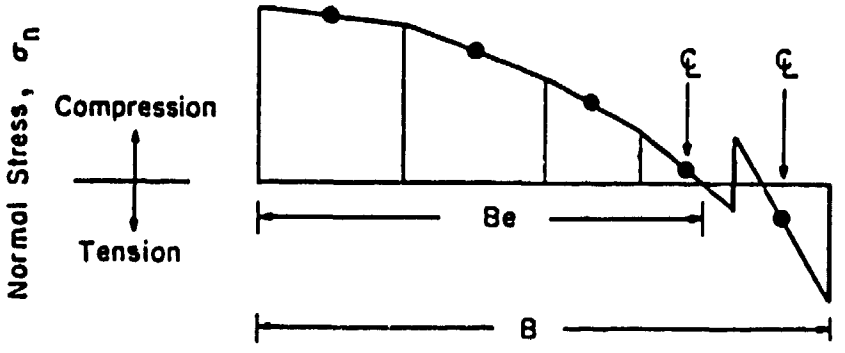

Figure 20. Variation of B_e/B with lateral load, coarse mesh

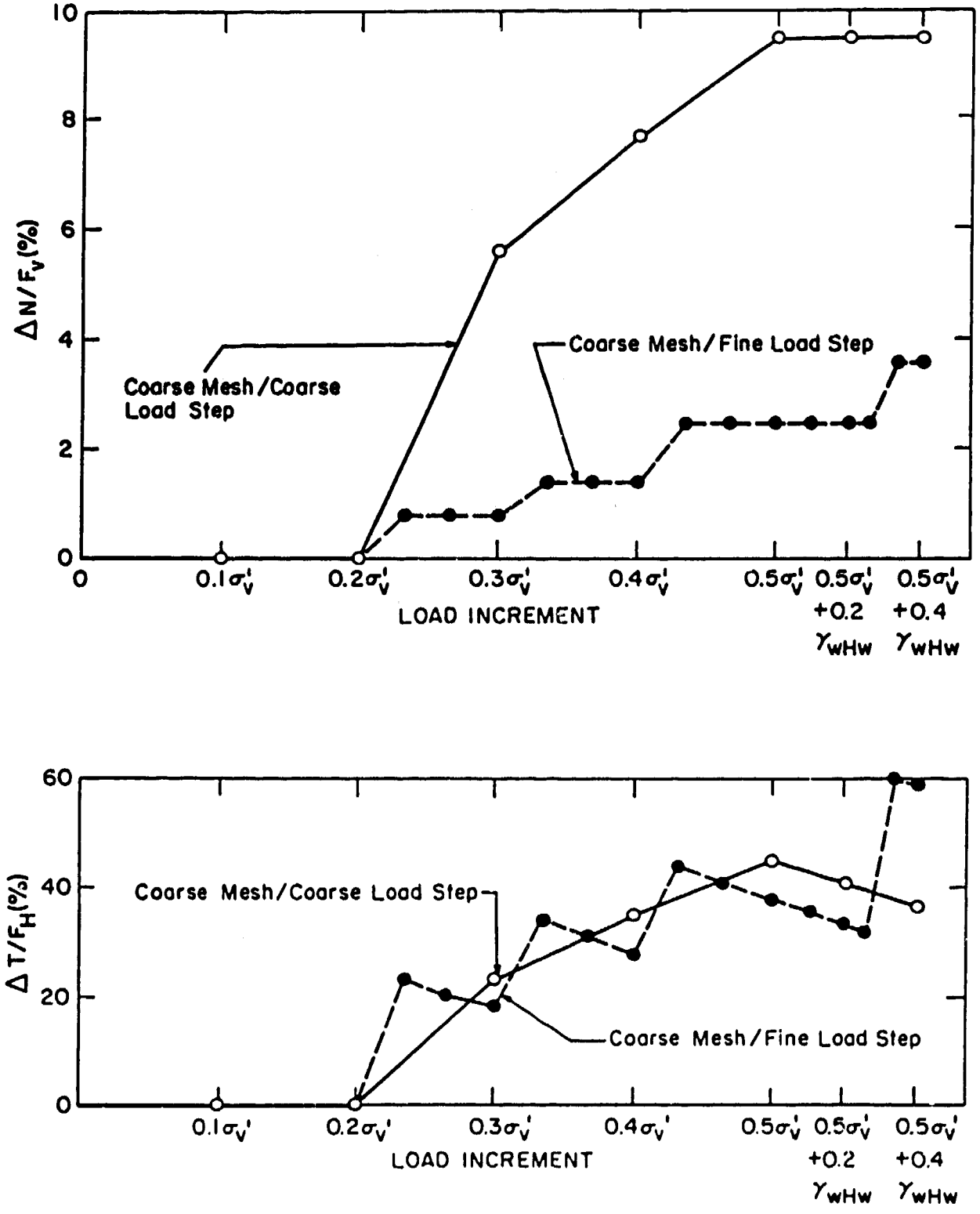

Figure 21. Development of overshoot forces with lateral load, coarse mesh

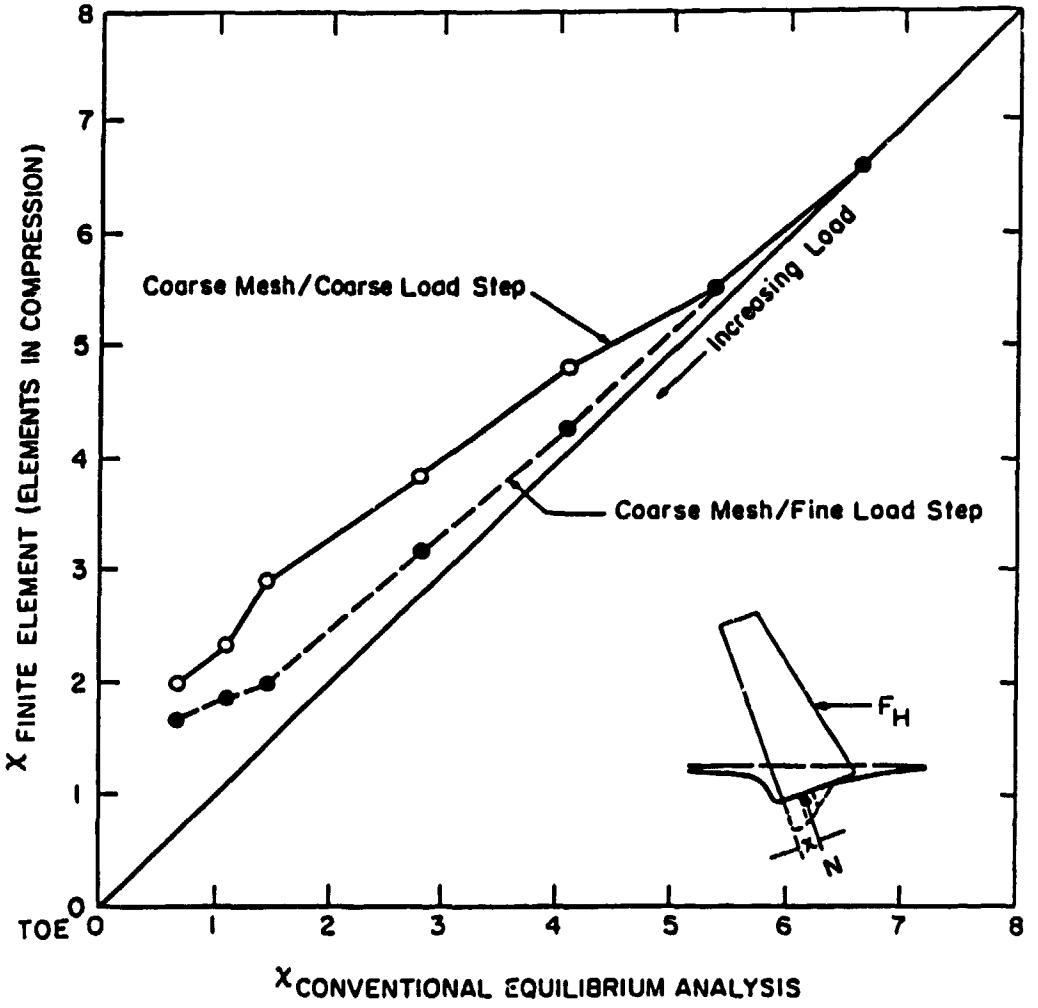

Figure 22. Location of resultant normal force as computed using finite element and conventional equilibrium methods

Conclusions for the Coarse Load Step Analysis

78. It has been shown that the results of the following load analysis, using the coarse mesh/coarse load step, results in errors when compared to a solution based on a no-tension interface. These errors result from the stress retained within elements representing the opened crack between the wall and the foundation.

Results from the Fine Load Step Analysis Coarse Finite Element Mesh

79. In an attempt to reduce the errors found in the first analyses, finer load steps were used. In this approach the same total load is applied as before, but the load increments are about one-third as large, and, hence approximately triple the load steps are needed to reach the full load. For example, to reach the earth loading of $0.3 \cdot \sigma_v$, 9 load increments are applied and for $0.5 \cdot \sigma_v$, 15 load increments are needed.

80. Figure 23 presents the interface normal and shear stress distributions for $0.5 \cdot \sigma_v$, lateral load. It may be remembered that in the coarse load step analysis, the entire interface element closest to the heel developed tensile stress when the load increment was applied and increased the total load from $0.2 \cdot \sigma_v$, to $0.3 \cdot \sigma_v$. However, the fine load step analysis uses three load increments to achieve this same increase in load. This difference leads to the program logic sensing the fact that tension is beginning to develop on the base for the fine load analysis before it develops for the coarse load analysis; hence, the stiffness is reduced in time to hold tension and shear stresses to a minimum. By the point at which the entire lateral effective stress is applied, the fine load analysis predicts lower tension on the base than does the coarse load analysis and agrees more closely with the base pressure distribution of the conventional approach.

81. In Figure 20, it is observed that the analysis using the finer load steps results in a smaller effective base width, B_e , as compared to the coarse load analysis. However, it is still larger than that calculated by the CEA.

82. The development of overshoot forces for the fine load step analysis is presented in Figure 21. As expected, the use of the finer load steps results in a lower tension overshoot force, as compared to the coarse load step. However, the magnitude of the overshoot error continues to be significant. At the stage of loading equal to the full lateral effective stress, the tensile overshoot force is 2.5 percent, and the shear overshoot force is 38 percent.

83. The resultant normal force location for elements exhibiting compressive stress in the fine load analysis is closer to that from the conventional equilibrium method, as seen in Figure 22. For example, at the stage of full lateral effective stress loading, the resultant normal force acts at a

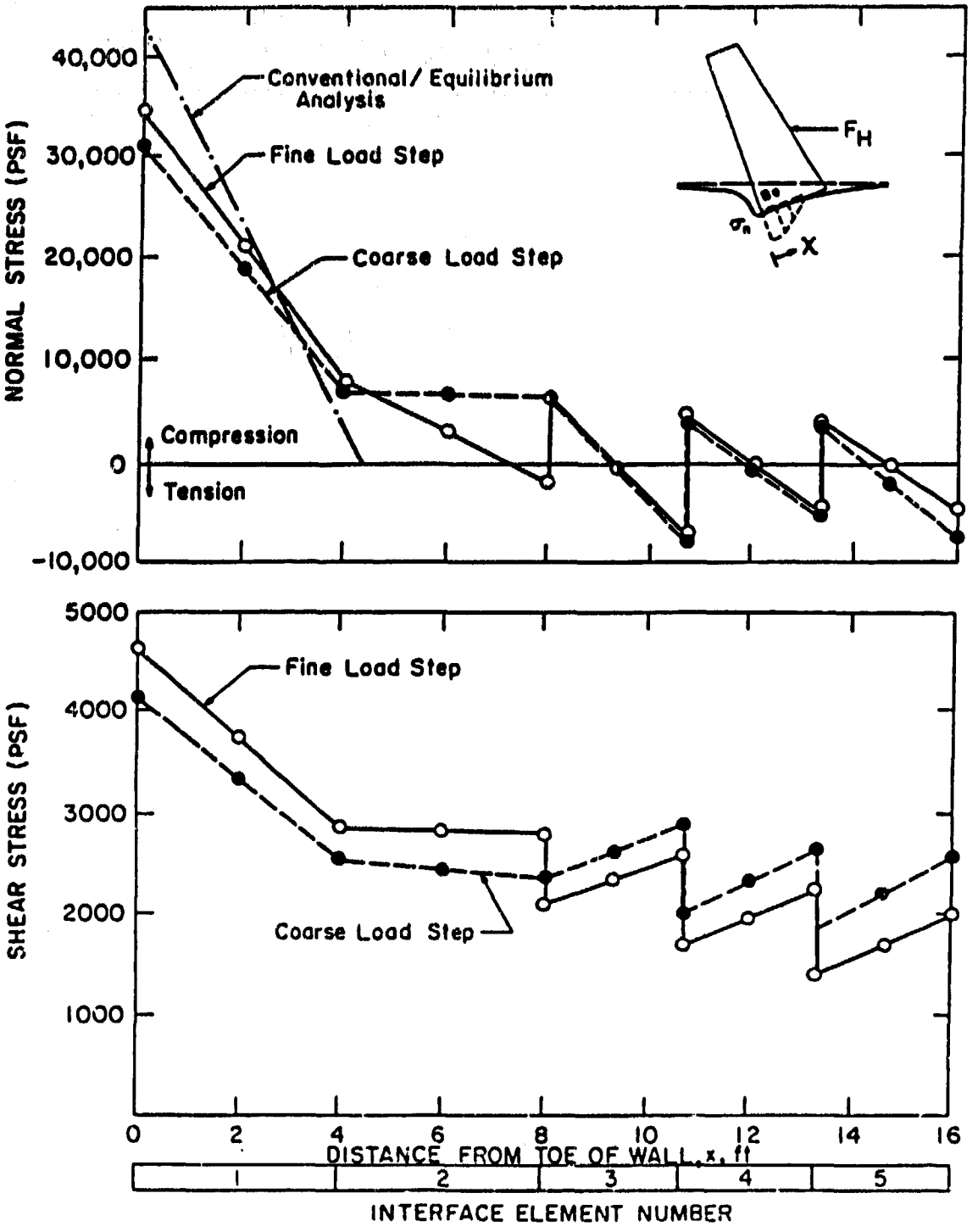

Figure 23. Stress distributions along the base for $0.5 \cdot \sigma_v$ load, coarse and fine load steps

point 1.45 ft from the toe, as computed using the conventional equilibrium method. The resultant compressive force for the coarse and fine load step analyses are located at a distance of 2.94 and 2.02 ft, respectively. Thus, the error in the point of action of the resultant decreased from 103 to 39 percent.

Conclusions for the Fine Load Step Analysis

84. It is observed that by tripling the number of load steps used in the following load analysis, the error in the overshoot forces and the point of action of the resultant normal force is reduced. It is tempting to believe that the base tension could be completely eliminated if more increments were used successively to apply the load. Taken to the extreme, this logic is correct, but it does not necessarily follow that the tension will be reduced in a monotonic fashion with the application of larger numbers of increments. This problem is caused by the fact that the tension that develops in each interface element is a function of the level of compressive stress in the element prior to its going into tension, as well as the size of the load increments. This means that since we are unable to use an infinite number of load increments, there will always be some tension generated within an element during the course of the FEA, and thus, a nonzero error. Two alternative approaches, to be discussed in the following paragraphs, are needed to solve this problem.

Following Load Analysis Using the Unbalanced Force Method

85. The residual normal and shear stress in the interface elements that develop tension should be zero, ideally, since we are making the assumption that the base interface is incapable of transmitting tension. As one alternative approach to reduce the amount of overshoot stress, the unbalanced force method logic was built into the program to (a) check for the development of tension, and if found, (b) then reduce this overshoot stress retained within the element(s). This process is conducted after each load step is completed.

86. The technique used is known by several names: Zienziewicz (1977) described it as the initial stress method, and later it became known as the residual force method, stress transfer method, or the unbalanced force method.

All these phrases describe specific aspects of the same general method implemented in the program SOILSTRUCT. Briefly, the principle of the procedure is to: (a) convert a stress regime into an equivalent set of nodal point forces; (b) transfer this equivalent force into the adjacent elements by applying it as an external force at the nodes; and (c) maintain equilibrium by subtracting the equivalent internal stress from within the element(s) used to formulate this force.

87. After each load step is completed and prior to any modulus adjustment, all interface elements are checked for the development of tensile stress at their centers. If none is found, the analysis proceeds with the next increment of load as usual. When tensile stresses are observed in the interface element(s), the following series of computations (idealized in Figure 24) are made prior to analysis of the next load increment:

a. For each interface element that develops tensile stresses at its center, artificial restraining forces are applied to reduce this tensile stress to zero. Two sets of artificial restraining forces, Q_n and Q_s, are computed for each element; one for the normal stress and the other for the shear stress. These artificial restraining forces are given as:

$$Q_n = \iiint_V [B]^T \{\sigma_n\} dv \tag{7}$$

$$Q_s = \iiint_V [B]^T \{\sigma_s\} dv \tag{8}$$

where $\{\sigma_n\}$ and $\{\sigma_s\}$ are the element normal and shear stresses to be restrained by the nodal forces. $[B]^T$ is the transformation matrix that relates element strains to the nodal point displacements. In the program code, this is accomplished by subtracting this equivalent normal and shear stress from the stress regime existing across the entire element, as shown in Figure 24.

b. Since the forces Q_n and Q_s do not actually exist, an analysis is made of the entire mesh with these nodal point forces applied in the opposite direction at the nodes. Essentially, the tensile and shear stresses are redistributed. The largest effect of this redistribution occurs in the elements adjacent to the interface elements undergoing corrective action.

c. Steps a and b are repeated until the resulting stresses or, conversely, the restraining forces are small. Then the moduli are updated, and the conventional analysis is resumed with the application of the next load increment.

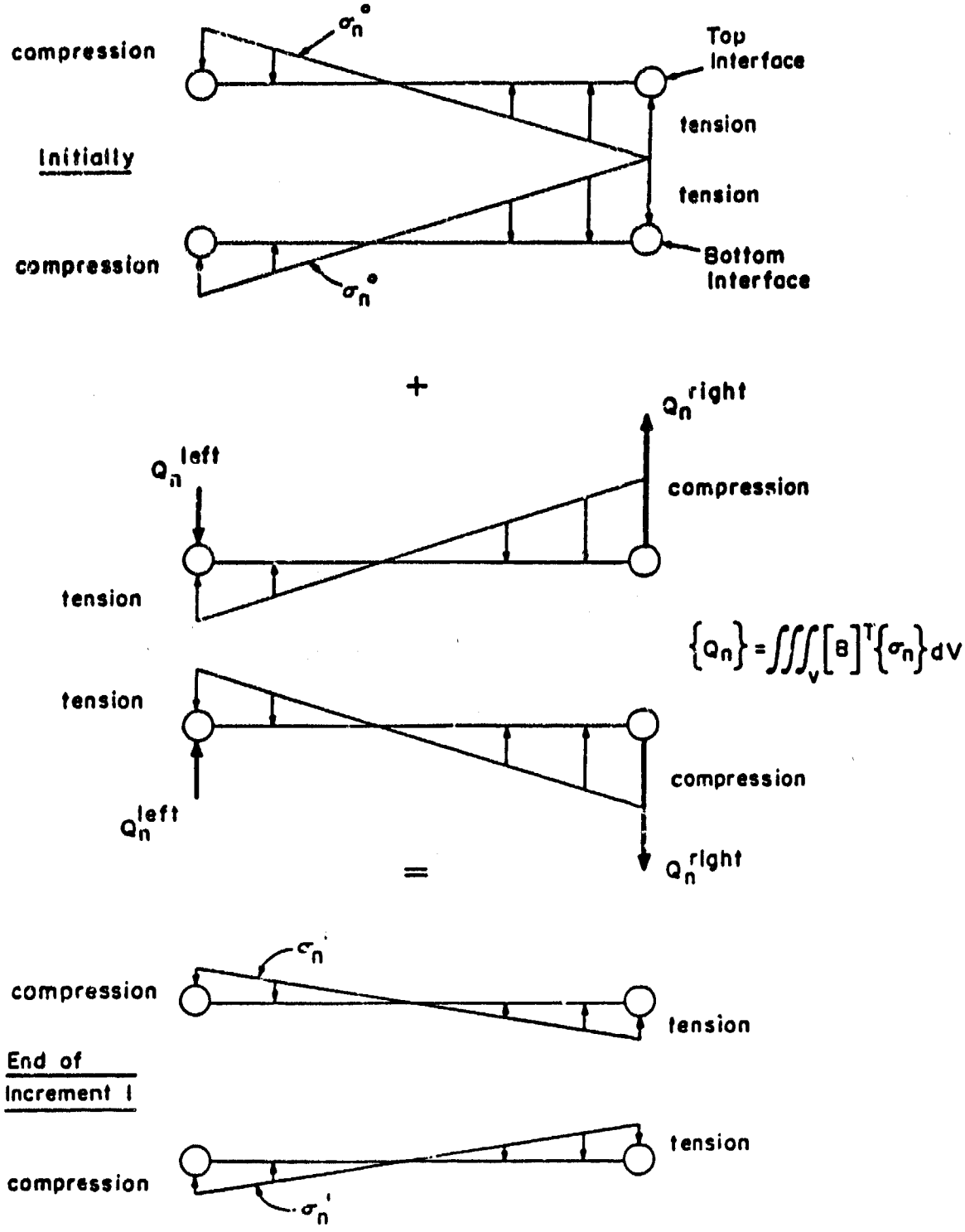

Figure 24. Idealization of the unbalanced force method

88. This unbalanced force procedure is iterative because, as a result of the application of forces Q_n and Q_s in step b, additional displacements

are generated within the entire mesh and especially at the nodes defining the interface element(s). This results in the development of additional tensile and shear stress within the interface element. However, the magnitude of the accrued stresses are less than those applied in step a so that the net result is the reduction in total stress at the end of each pair of operations for the interface element(s).

89. The unbalanced force procedure is terminated when the overshoot force is less than a specified value. In this case, the iterations were concluded when the overshoot force was less than 100 lb which corresponds to less than one-tenth of 1 percent of the weight of the monolith and soil wedge.

90. For comparison, the base case following load analysis of the hypothetical structure in Figure 15 was repeated using the updated program with the unbalanced force method logic. The same 10-step coarse load analysis was used as before. However, due to the amount of base separation that occurred in the previous analyses, a finer mesh was developed to allow for refinement of the stress distributions.

Fine mesh for base case

91. The refined finite element mesh is shown in Figure 25. As before, it represents a 40-ft-high monolith with a 16-ft-wide base. The depth of rock foundation included in the mesh is two and one-half times the base width of the monolith and extends a distance equal to three times the height of the monolith beyond the toe and heel. The mesh contains a total of 329 two-dimensional and interface elements with 113 representing the concrete monolith, 200 representing the rock foundation, and 16 interface elements between the monolith and its foundation.

Results from the following load analysis
using coarse load steps-unbalanced force method

92. Figure 26 presents the interface normal and shear stress distributions for the loading stage of $0.5 \cdot \sigma_v$, along with the distribution for the CEA at this stage. The results labeled "alpha method" in this figure will be discussed in the final section of Part IV. For the first time, the normal stresses from the FEA at the toe of the wall are higher than those from the CEA. The maximum compressive stress (q_{max}) of 59,000 psf, by the FEA with the unbalanced force routine, exceeds the 43,000 psf from the conventional analysis. This reverse in trend compared to the earlier finite element results is

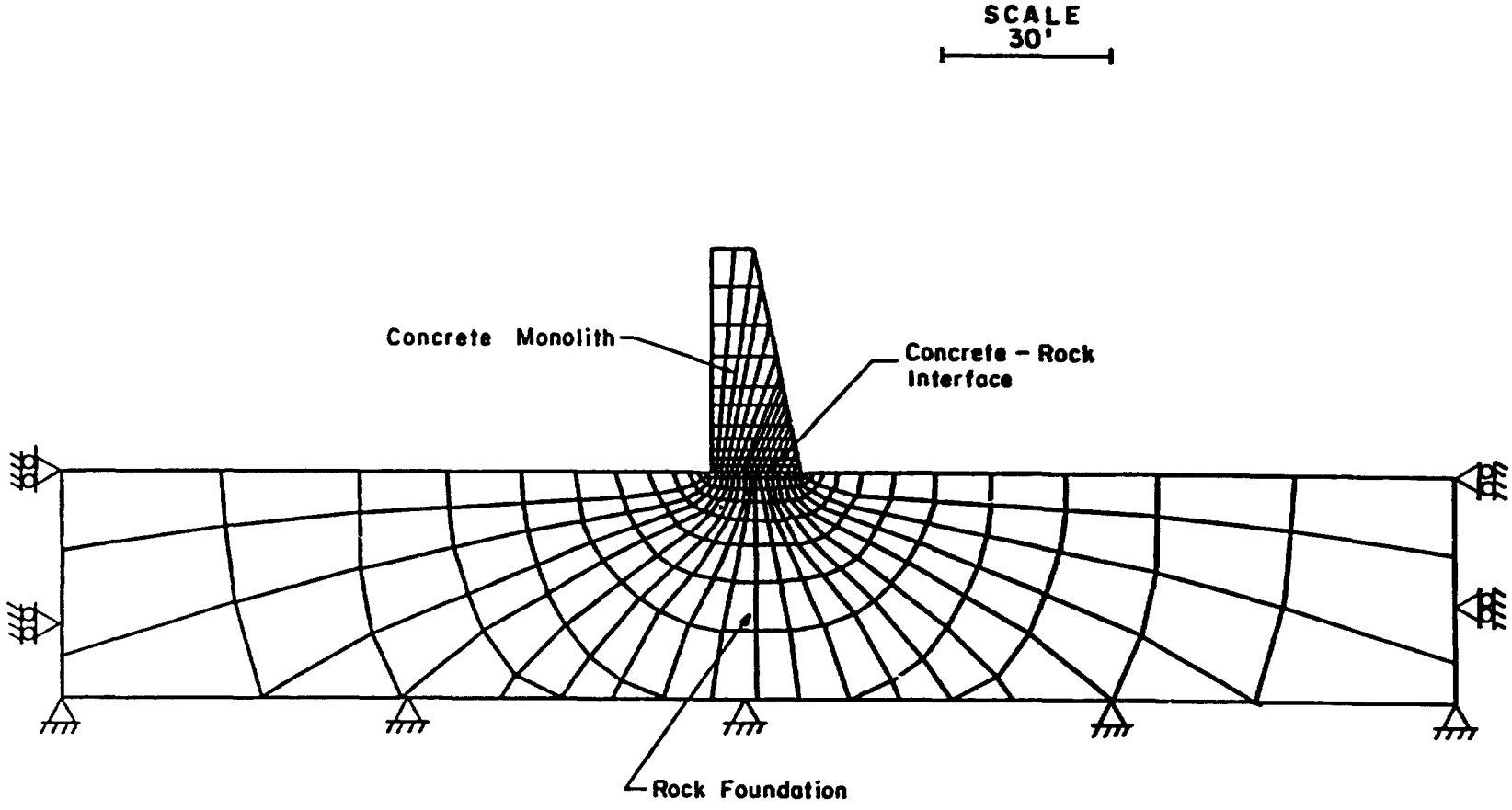

Figure 25. Fine finite element mesh used to model the base case hypothetical structure

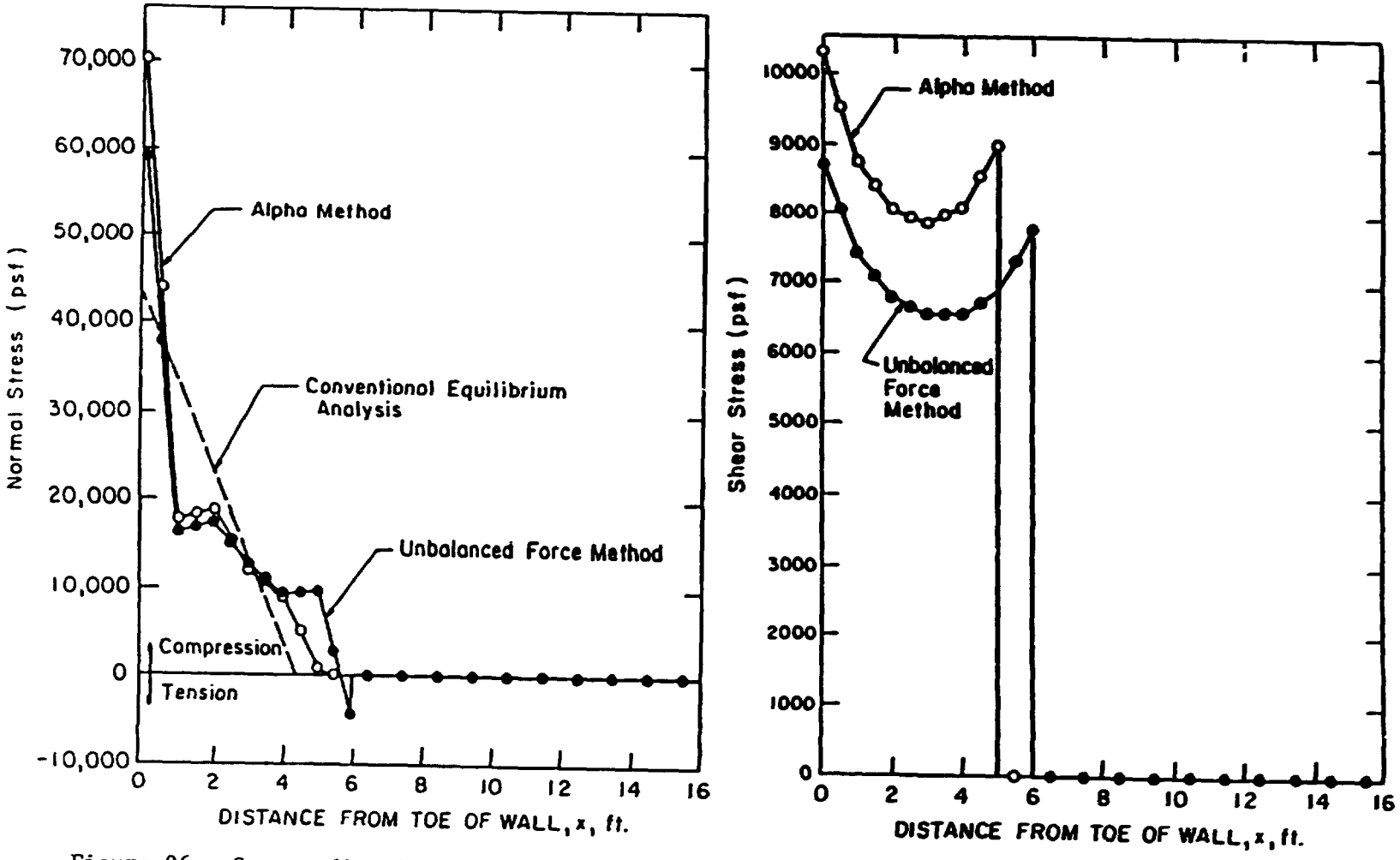

Figure 26. Stress distributions along the base for $0.5 \cdot \sigma_v$ load, fine mesh/coarse load step

attributed to solution of the overshoot problem by the unbalanced force method.

93. The effective base contact area, B_e, normalized by the total base width, B, as a function of loading is presented in Figure 27. It is observed that the general trend is for closer agreement in B_e/B with that from the CEA than achieved in either of the earlier two analyses.

94. Figure 28 presents information on the development of overshoot forces, both normal and shear, as a function of the loading for all the analyses. As noted, the unbalanced force method as specified in the program reduces the overshoot forces to a total maximum specified value of 100 lb. It is observed that this technique reduces the normalized overshoot shear force ($\Delta T/F_h$) to a near zero value at all stages, while the normalized overshoot tensile force ($\Delta N/F_v$) remains constant at less than 1 percent.

95. The location of the resultant normal force for elements exhibiting compressive stress is closer than those for previous FEA's to that from the conventional equilibrium method, as seen in Figure 29. For example, at the stage of full lateral effective stress loading, the resultant normal force acts at a point 1.45 ft from the toe, as computed by the conventional equilibrium method. The location of the resultant compressive force for the three FEA's are computed to be 2.94 ft from the coarse load/fine mesh analysis, 20.02 ft from the fine load/coarse mesh analysis, and 1.87 ft for the coarse load/fine mesh analysis using the unbalanced force method. The error in the point of action of the resultant for the three are; 103 percent, 39 percent, and 29 percent, respectively.

Improved cost efficiency in
the unbalanced force method

96. A point of consideration when evaluating the usefulness of any procedure of analysis is its efficiency. Efficiency is determined not only in terms of execution cost, but also the number of computations conducted to reach an acceptable solution. Due to the iterative nature of the unbalanced force method, a total of 549 complete solutions of the problem were required to attain the final solutions. This increased the central processing time on the IBM 3090 model 200VF mainframe computer to 19 min, as compared to less than 0.5 min in previous analyses. The analysis represents about a tenfold increase in computer run charges for use of the VPI IBM mainframe computer. To aid in reducing this cost, the computer program SOILSTRUCT was modified to

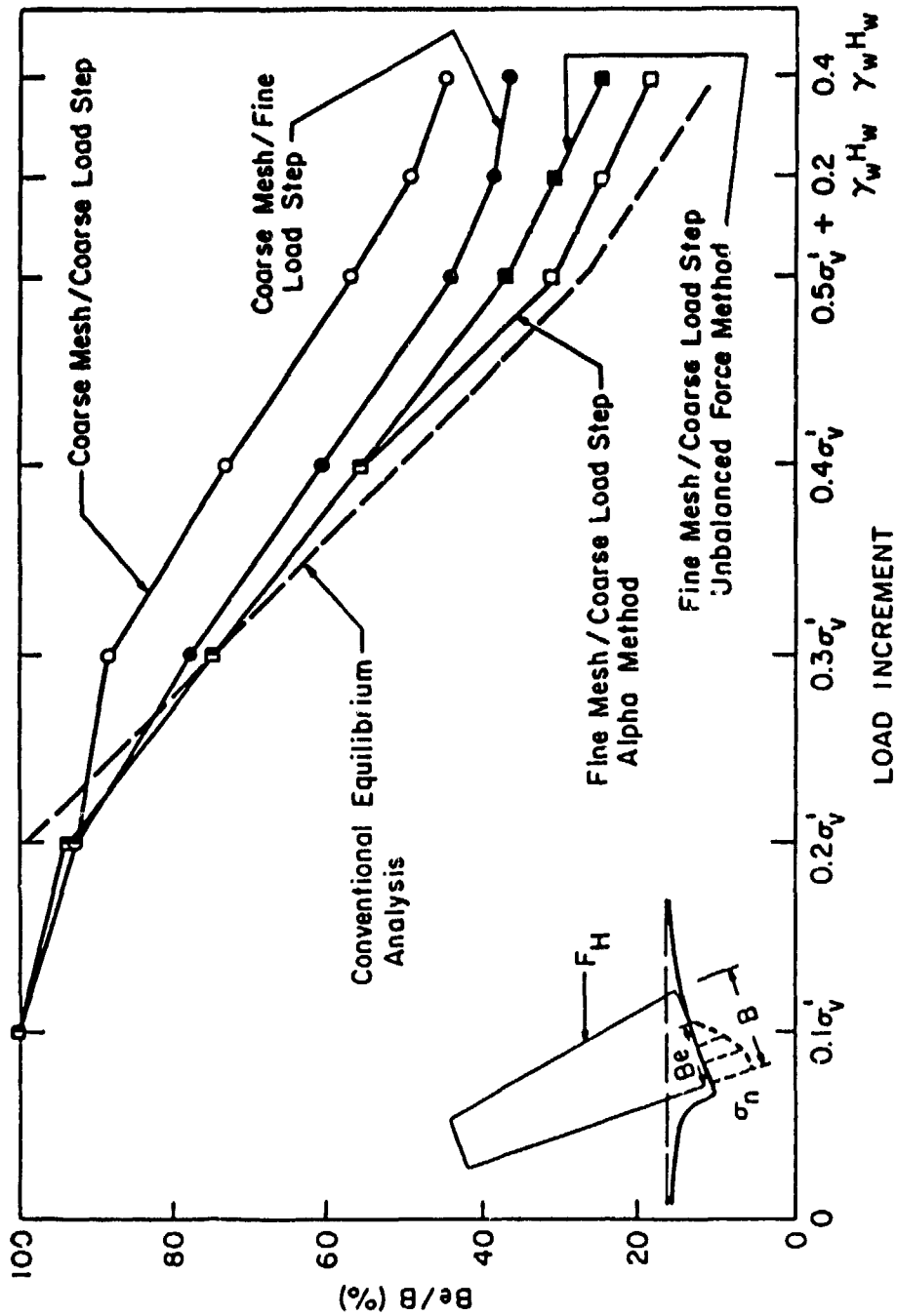

Figure 27. Variation of B_e/B with lateral load

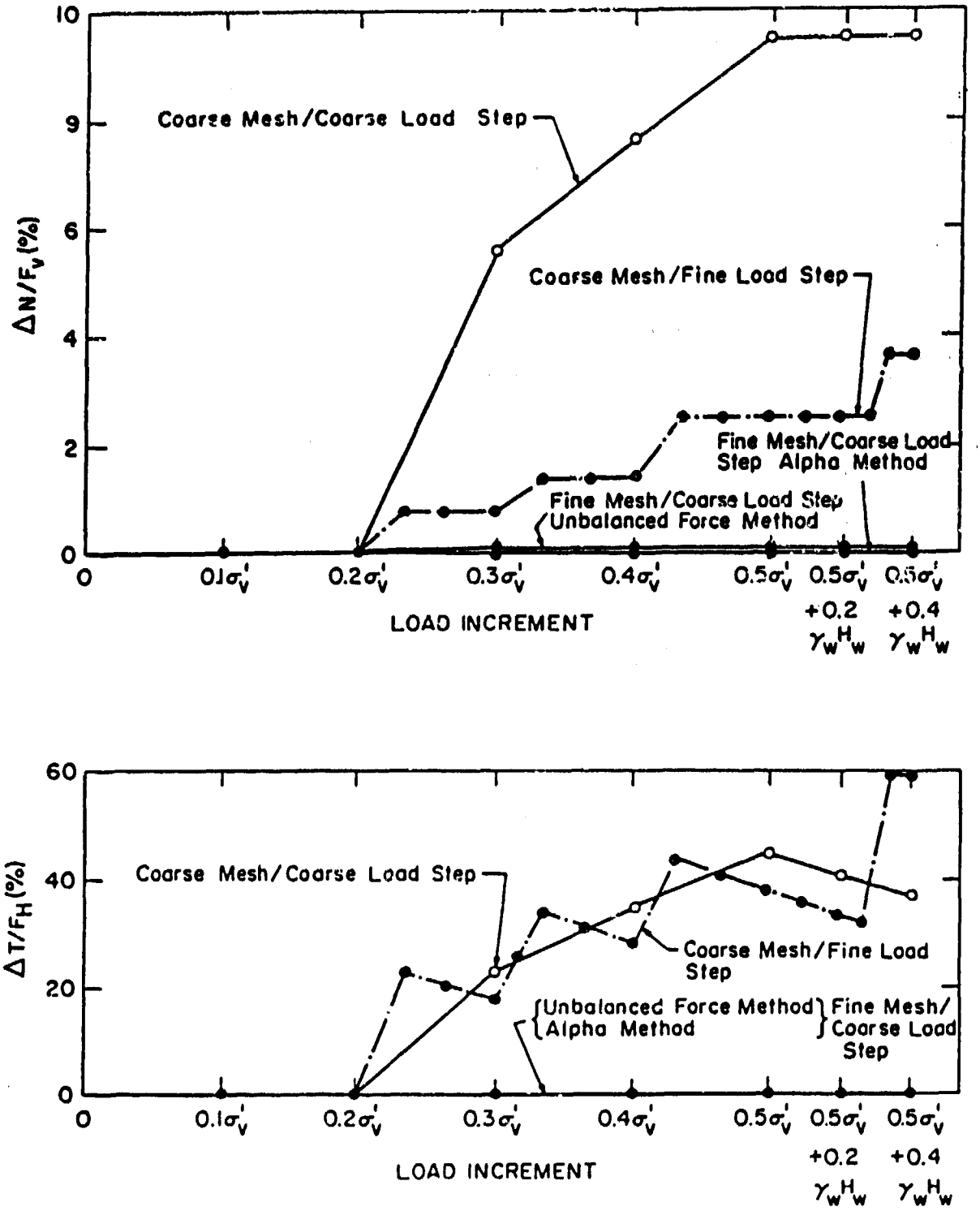

Figure 28. Development of overshoot forces with lateral load

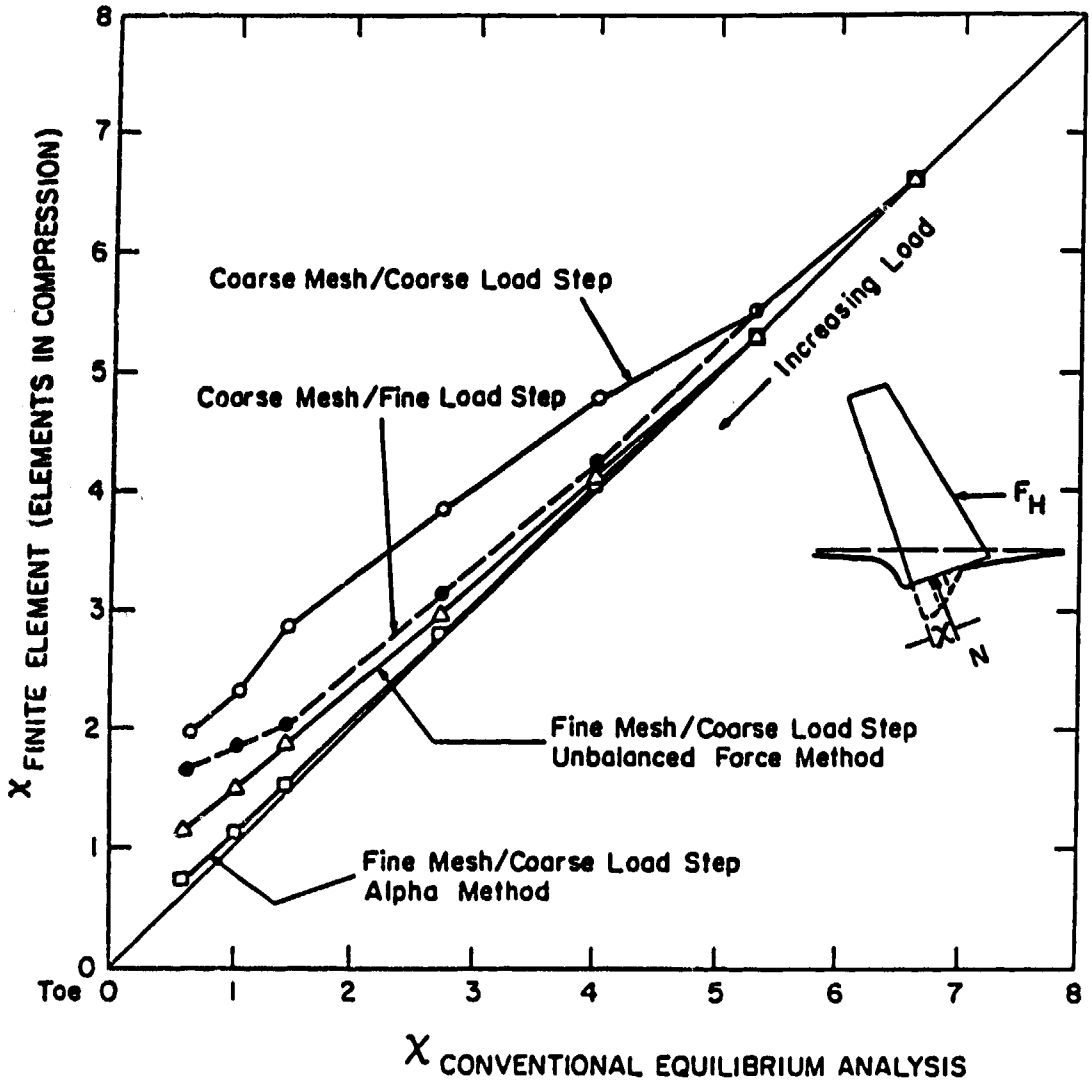

Figure 29. Location of resultant normal force as computed using finite element and conventional equilibrium methods

take better advantage of one of the features of its equation solver algorithm.

97. In SOILSTRUCT, a large proportion of the computer time is used in the solution of linear simultaneous equations of the form;

$$[K](u) = (Q) \tag{9}$$

where

[K] = global stiffness matrix

{u} = unknown nodal point displacements

{Q} = global force vector

For each computation in the unbalanced force method, a load vector, {Q} , is created based upon the stress regime existing within interface elements that develop tensile stress at their centers. At all stages of these particular following load analyses, the moduli of the elements are maintained at their original values. Since the elastic properties are constant, there is no need to reformulate the stiffness matrix, [K] , prior to each iteration. This fact allows us to expedite the computations by taking advantage of a unique feature of the equation solver used in SOILSTRUCT.

98. The equation solver in SOILSTRUCT uses the Crout Reduction procedure to solve the set of linear simultaneous equations. One of the features of this equation solver is that the reduction of the stiffness matrix, [K] , occurs independently of the reduction of the load vector, {Q} . Thus, once the original stiffness matrix, [K] , is reduced to its final values in the fully triangularized matrix at the first computation stage, it is stored in this form and used in all subsequent analyses for this load step. This modification results in a significant savings in computation time and thus cost of analysis.

99. The implementation of the new logic resulted in a significant reduction in computation cost for the unbalanced force method of analysis. For example, to attain the previously discussed results for the fine mesh/coarse load analysis of the base case hypothetical structure, 549 complete solutions are required. To produce the same results, the new logic reduced the central processing time of the IBM mainframe computer from 19 to 0.5 min. This analysis represents only about a twofold increase in computer run charges, as compared with earlier analyses without the unbalanced force routine.

Conclusions for the unbalanced force method

100. It is observed that using the unbalanced force method results in a significant reduction in overshoot force and location of resultant normal compressive force errors, as compared to previous FEA's. Also, the modification of the sequence of computations used in conjunction with the equation solver algorithm resulted in a significant savings in central processing time

and thus cost per analysis. However, a second procedure, referred to as the alpha method, will be shown to further reduce the errors, number of computations, and costs.

Following Load Analysis Using the Alpha Method

101. The alpha method addresses the same fundamental issues as the unbalanced force method, namely; the reduction of the stresses retained within interface elements developing tensile stress. However, the objective of this procedure is: (a) a further reduction in the magnitude of the overshoot forces and error in location of resultant compressive force, and (b) reductions in computations as compared to the unbalanced force method.

102. This method evolved from the unbalanced force method analyses, and retains some of its key steps. Briefly, the principle of the procedure is to: (a) factor the applied load vector so that zero normal stress results in the center of the element which previously developed tensile stress at its center; (b) convert a shear stress regime for this element into an equivalent set of modal point forces; (c) transfer this equivalent force into the adjacent elements by applying it as an external force at the nodes; and (d) maintain equilibrium by subtracting the equivalent internal stress from within the element used to formulate this force. The name given to this method is derived from the factor applied to the load vector, alpha.

103. After each load step is completed, all interface elements are checked for the development of tensile stress at their centers. This occurs prior to updating the stress, displacement, and modulus arrays. If none are found, the analysis proceeds with the array updates and the next increment of load as usual. When tensile stresses are observed in the interface element(s), the following series of computations (idealized in Figure 30 for a single interface element developing tension after application of the full load increment, $\{Q_0\}$) would be made prior to any array updates or the analysis for the next load increment:

a. For each interface element that develops tensile stress at its center, the fraction of the applied force that would result in zero normal center stress is computed. This fraction is referred to as alpha and is computed for all elements that develop tensile stress at their centers. Each of these alpha values may be described as the fraction of the total force which results in zero overshoot normal force for that interface element. The linear relationship is due to the incremental

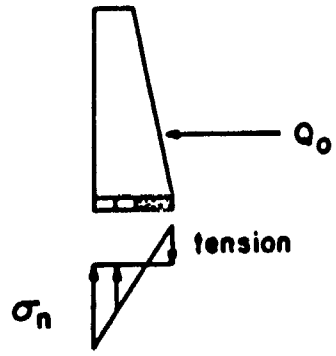

Alpha Method

a. Apply full load increments (Q_0) , develop tension in single interface element

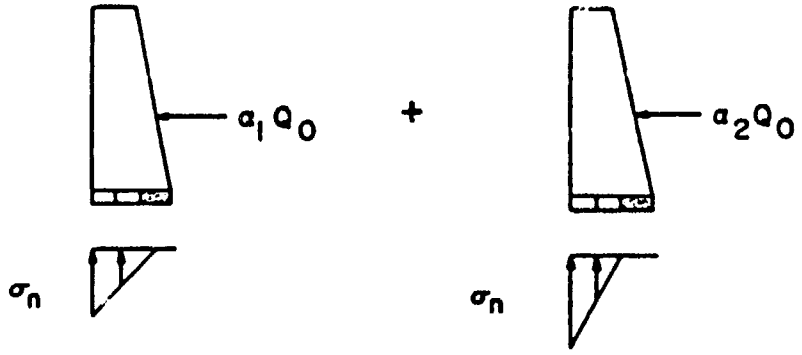

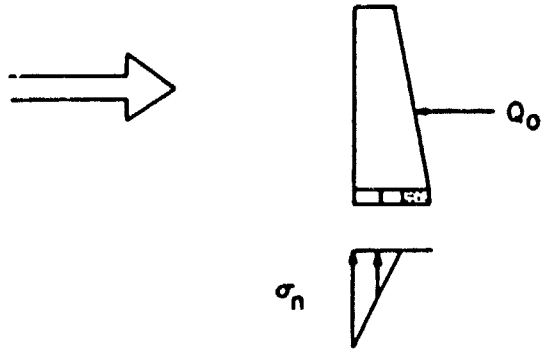

b. Apply factored loads; $\alpha_1 Q_0 + \alpha_2 Q_0$

Figure 30. Idealization of the alpha method

linear elastic analysis procedure used in the program. Due to the mechanics of the crack development, it is observed that the interface element closest to the heel, which has not developed tensile stress at its center in a previous load increment, possesses the smallest value of alpha.

b. The load vector, $\{Q\}$, is then redefined as the product of the smallest value of alpha, α_1, and the original load vector for this load step, $\{Q_0\}$.

$$\{Q\} = \alpha_1 \cdot \{Q_0\} \tag{10}$$

A new analysis is conducted using the reduced load vector, and all displacements and stresses are updated.

c. Zero normal and shear stiffness is then assigned to the interface element. This prevents the accrual of stress in step d.

d. For the critical interface element the tension stress at its center is now zero, but artificial restraining forces are needed to reduce the built-in shear stress to zero. The artificial restraining force, Q_s, is computed for the element. Using the unbalanced load procedure, Q_s is:

$$Q_s = \iiint_V [B]^T \{\sigma_s\} dv \tag{11}$$

where $\{\sigma_s\}$ is the element shear stress to be restrained by the nodal forces. It is equal to the actual linear shear stress distribution across the element. $[B]^T$ is the transformation matrix that relates element strains to the nodal point displacements. In the program code, this is accomplished by subtracting this equivalent shear stress from the stress regime existing across the entire element.

e. Since the force Q_s does not actually exist, an analysis is made of the entire mesh to these nodal point forces applied in the opposite direction at the nodes. All displacements and stresses are updated. Essentially the shear stresses are redistributed. This step, applied in conjunction with the fourth, maintains equilibrium within the system.

f. The next fraction of the initial load to be applied is computed. The load vector, $\{Q\}$, is defined as;

$$\{Q\} = \alpha_1 \cdot (1 - \Sigma\alpha) \cdot \{Q_0\} \tag{12}$$

where

α_i = the smallest of the remaining values of alpha

$\Sigma\alpha$ = the sum of previously applied alpha values

(Q_0) = the original load vector

The analysis is then conducted using (Q), and all resulting displacements and stresses are updated.

g. Steps c through f are repeated until the total original load vector for this load step, (Q_0), is applied. Then the conventional analysis is resumed with the application of the next load increment.

104. For the purposes of comparison to the other methods, the base case problem was analyzed with the alpha method. In this analysis, the fine mesh (Figure 25), with the coarse load steps, were used.

Results from the following load
analysis using coarse load steps, alpha method

105. Figure 26 presents the predicted interface normal and shear stress distributions for the full lateral soil loading stage from the alpha method, along with the distributions for the CEA and the unbalanced force method. The shape of the normal and shear stress distributions are similar for the two improved finite element methods, and both yield a q_{max} at the toe higher than that computed by the conventional equilibrium method. Notably, the q_{max} for the alpha method is 70,000 psf, larger than that computed using the unbalanced force method by 11,000 psf.

106. The effective base contact area, B_e, normalized by the total base width, B, as a function of loading, is presented in Figure 27. Note that B_e/B using the alpha method is in close agreement with that from the CEA.

107. Figure 28 presents information on the development of overshoot forces as a function of the loading for the four FEA's. In all cases, as the lateral loading increases, the crack propagates from the heel toward the toe, generating tensile stresses and thus overshoot forces within the interface elements. However, the alpha method reduces this overshoot force to zero at all stages of loading.

108. With the alpha method, the location of the resultant normal force for elements remaining in compression is closer than previous analyses to that from the conventional equilibrium method (Figure 29). At the stage of full lateral effective stress loading, the resultant normal force acts at a point

1.45 ft from the toe, as computed using the conventional equilibrium method. Using the unbalanced force method and the alpha method, the locations of the normal force are computed to be 1.87 and 1.52 ft, respectively. The error in the point of action of the resultant decreased from 29 to 5 percent in using the alpha versus the unbalanced force method.

109. The implementation of the alpha method logic also results in a reduction in computational cost as compared to the unbalanced force method of analysis. To attain the solution for the fine mesh/coarse load analysis of the base case hypothetical structure, only 47 complete solutions are required for the alpha method, as compared to 549 using the unbalanced force method. The central processing time of the IBM mainframe computer for the alpha method was less than 0.5 min.

110. Figure 31 shows the normalized lateral deformation at the crest of the wall (u_x) by its height (H) as a function of the load. In general, the lateral deformation increases as the load increases. The lateral deformation also increases as the magnitude of the tensile stress retained within interface elements is reduced. Further, due to the difference in the approach used to reduce these overshoot forces, deformations resulting from the alpha method are larger than those using the unbalanced force method.

Conclusions for the alpha method

111. It has been shown that the response of a structure in a condition of incipient instability may be predicted by the computer program SOILSTRUCT using a new computational technique called the alpha method. Further, the results are accurate when compared to those using the conventional equilibrium method. When compared to other methods of FEA, the alpha method results in much smaller errors. It eliminates the overshoot forces, and results in a reduced error associated with the location of resultant normal compressive force. It also resulted in a significant reduction in the number of solutions required when compared to the unbalanced force method.

The Alpha Method and the Backfill Placement Analysis

112. The previous discussion on the implementation of the alpha method was associated with the analysis of structures subjected to following loads. A second category of loading used in the second phase study of analyses is termed the "backfill placement analysis." It differs from the following load

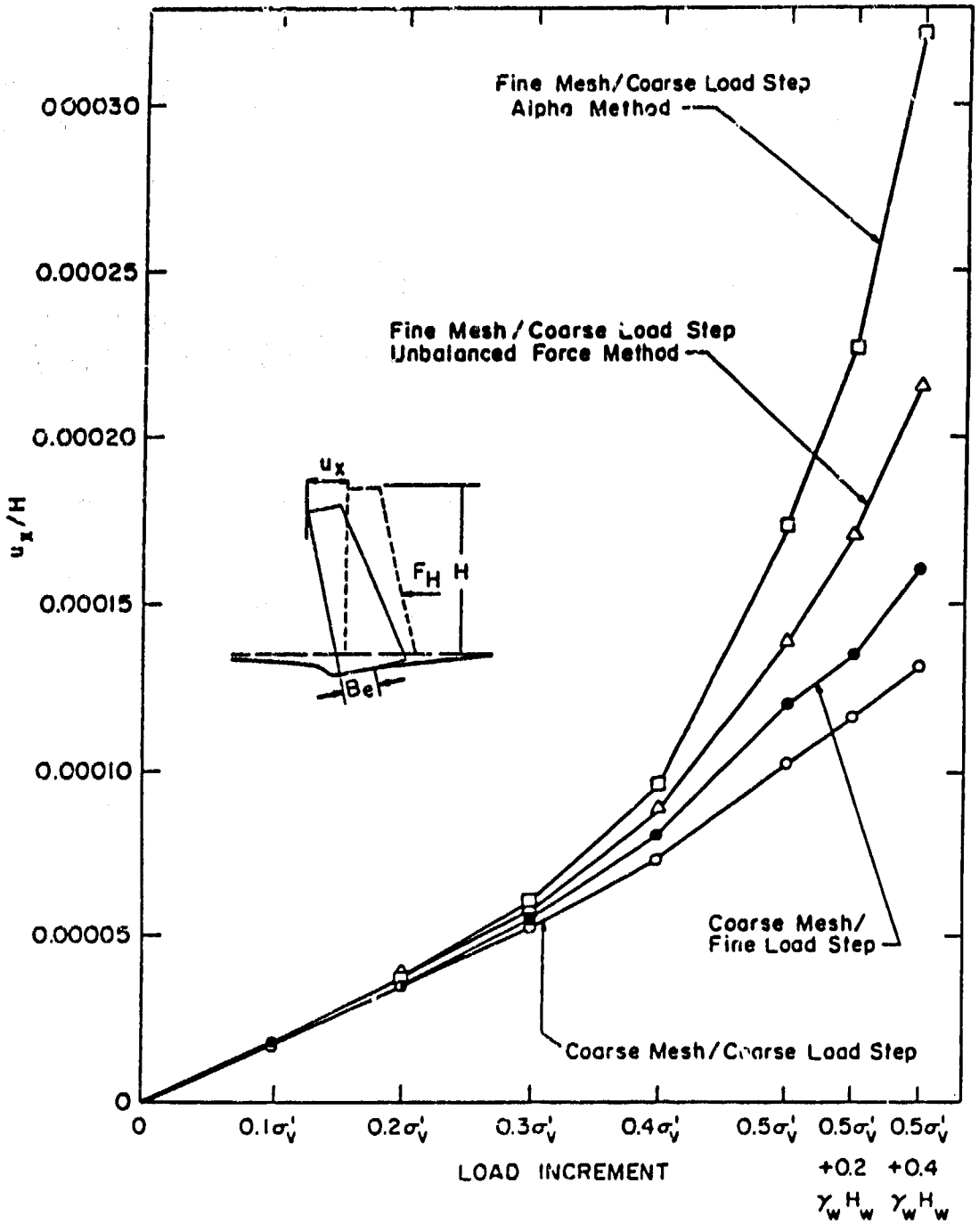

Figure 31. Variation of normalized lateral crest displacements (u_x/H) with lateral load

analysis by the method in which the forces acting on the structure are developed. The soil backfill is incorporated in the mesh and the forces acting on the wall are developed through a backfill operation simulation. The details of this procedure and the results are discussed in Part VI.

113. In the backfill placement analysis, the backfill operation is simulated by the placement of the soil in a series of lifts. For each lift, the soil placed generates a set of forces that are applied to the wall and previously placed backfill system. With an equivalent linear stress-strain soil model used, the moduli within the existing soil backfill are adjusted to be consistent with the current level of loading. In the analyses presented in Part VI, two iterations are used for each lift, and the alpha method is not implemented until the second computation is completed for each lift. In the unbalanced force analyses, the alpha method is applied after the first computation for each load step is completed.

114. In the backfill placement analysis, the soil backfill is incorporated within the mesh. Interface elements are placed between several different material regions in the mesh; concrete wall-to-rock foundation, concrete wall-to-soil backfill, and soil backfill-to-rock foundation. Due to the involved nature of the response of the system to the analytical simulation of the backfill operation, the alpha correction is applied only to the interface elements between the base of the wall and the foundation.

PART V: RESULTS OF FOLLOWING LOAD PARAMETRIC ANALYSES OF RETAINING STRUCTURES USING THE ALPHA METHOD

115. This part describes an investigation into the influence of geometry, material, and loading parameters on retaining structures founded on rock and subjected to a following load. The finite element program SOILSTRUCT with the alpha method incorporated is used in the analyses. Since the loads are predefined in the following load approach, the response that is predicted focuses on the movement of the wall and foundation system and their interaction along the base of the wall.

116. The influence of seven parameters are evaluated, with the range in values presented in Table 3. These parameters include;

a. Height of the wall.

b. Initial normal and shear stress distributions developed along the interface between the wall and its foundation, prior to lateral loading.

c. Width of the wall.

d. Magnitude of the uplift pressure applied to the interface.

e. Modulus of the rock foundation.

f. Interface normal stiffness.

g. Interface shear stiffness.

117. The results for the following load analyses are characterized in terms of:

a. Distribution of normal and shear stresses along the interface between the wall and its foundation.

b. Percent contact area for the base of the wall with the foundation, (B_e/B).

c. Magnitude of the mobilized angle of friction at the base of the wall.

d. Ratio of the lateral deformation at the crest of the wall, u_x , to its height, H .

e. Magnitude of the maximum compressive stress developed within the toe region of the structure.

118. In the analyses, the two dimension ratios are kept constant. Namely, the width of the top of the monolith always equals $0.2 \cdot H$, and the height of the water table within the backfill (H_w) is always $0.67 \cdot H$. Several of the material properties are also constant: the unit weight of the concrete and the modulus and Poisson's ratio of the concrete and the rock.

Effect of Height of the Wall

119. Study of the effects of wall height are accomplished by comparing results for two FEA's: one for the base structure that is 40 ft high, and a second for a structure that is identical to the first in terms of proportions, but is 70 ft high. The scale factor between the two cases is 70/40 or 1.75.

120. The base case structure is modeled using the fine mesh in Figure 25. A second mesh was developed for the larger structure by multiplying x and y coordinates of the nodal points defining the fine mesh by 1.75. This results in a 70-ft-high monolith with a 28-ft-wide base, while maintaining the same base-to-height, B/H , ratio of 0.4.

Loading scheme

121. As discussed in Part IV for the basic following load problem, there are three components of loading: (a) the vertical loads induced by the weight of the monolith; (b) lateral effective earth pressures due to the soil backfill (usually applied in five increments); and (c) lateral pressure due to water within the soil backfill (usually applied in five increments).

122. If the pressure distributions applied to the two different size structures are normalized by the maximum pressure and plotted versus the distance normalized by the length over which the pressure acts, then the two distributions are identical. This holds true for the gravity stress distribution along the base as well as the earth and water pressures on the back of the wall. When the applied pressure is converted into equivalent nodal point forces, the forces acting upon each of the structures will differ in magnitude by the square of the scale factor, at the same normalized distance. This results from the equivalent force being equal to the integral of pressure over the region upon which it acts, and each of these terms differ in proportion to the scale factor between the meshes. The difference in magnitude between the equivalent resultant force applied to each of the structures also varies with the square of the scale factor. This resultant force has the same normalized point of action since the distribution of normalized pressure versus normalized distance is the same for both meshes.

Material properties

123. The standard material properties as used in Part IV are assigned to both the small and large monolith problems. The modulus of the concrete

and rock is 3,000,000 psi, and the Poisson's ratio is 0.15 and 0.2 for the respective materials. The normal and shear stiffness of the interface between the monolith and foundation are 3,000,000 and 10,000 pci, respectively.

Theoretical considerations of scale effects on the results

124. Due to the characteristics of both the analysis procedure and the structural system, the effects of scale can be predicted theoretically. This follows from four factors;

a. Although the analysis allows nonlinear response from one step to another, the computational procedure used in the FEA is based on a linear elastic response within each step.

b. The geometry of the two structures and their equivalent meshes is the same when compared using normalized dimensions.

c. The same material properties are used.

d. The applied load increments are the same based on normalized pressures and normalized distances.

125. With these considerations and theory given in Appendix B, several conclusions may be drawn with regard to the effect of the scale of a structure upon the computed variables for each load increment.

a. The incremental stresses induced by the loading will vary in proportion to the scale factor.

b. The incremental strains induced by the loading also will vary in proportion to the scale factor.

c. The work done by the applied forces and the strain energy stored within the system varies with the scale factor to the fourth power.

d. The incremental displacements vary with the square of the scale factor.

Results--scale effects

126. Figure 26 presents the interface normal and shear stress distributions for the loading stage where the full lateral soil load is applied. In terms of normalized distance along the base (x/B), the stress distributions for the 70-ft-high monolith are the same as those for the 40-ft-high monolith. The actual magnitudes of these stresses differ from those obtained for the 40-ft-tall base case monolith. For example, the maximum compressive stresses developed within the toe region of the 40- and 70-ft-high monoliths are 70,000 and 125,000 psf, respectively. The compressive stresses differ by a factor of 1.78, a value approximately equal to the difference in scale between the

structures, or 1.75. The small variance from 1.78 to 1.75 results from larger approximation errors developed for the mesh representing the monolith 70 ft in height.

127. The effective base contact area, B_e, normalized by the total base width, B, as a function of loading is presented in Figure 32. It is observed that B_e/B agrees for all stages of loading in both analyses, and is, therefore, independent of the scale of the structure, as expected.

128. The mobilized base friction angle, δ_{bm}, on the interface between the base of the wall and its foundation is given as:

$$\tan(\delta_{bm}) = T/N' \tag{13}$$

where:

T = net horizontal interface shear force

N' = net effective normal interface force

For either size monolith, the mobilized base friction angle is the same. This follows since the interface forces must equal the applied vertical and horizontal forces. Both of these forces vary with the square of the scale factor, so when substituted into Equation 13, the same factor appears in the numerator and denominator, and the scale factors cancel out.

129. Figure 32 also shows the normalized lateral deformation at the crest of the two monoliths (u_x/H) as a function of the load. There are two general trends common to both structures: (a) the lateral deformation increases as the load increases; and (b) the rate of deformation increases as the effective base area decreases. Another trend observed in the figure is that the normalized displacement is larger for the taller of the two structures. For example, upon application of the $0.5 \cdot \sigma_v$ soil loading, the normalized lateral displacements are 0.00029 and 0.00017 for the 70- and 40-ft-high walls, respectively. The ratio of the displacements occurring at the crest of the two structures for the same level of loading is 2.91. Theoretical considerations indicate that this ratio should actually be the square of the scale factor, or 3.06.

130. With all factors considered equal, it is observed that for the same level of load, the scale of the structure influences the magnitude of the

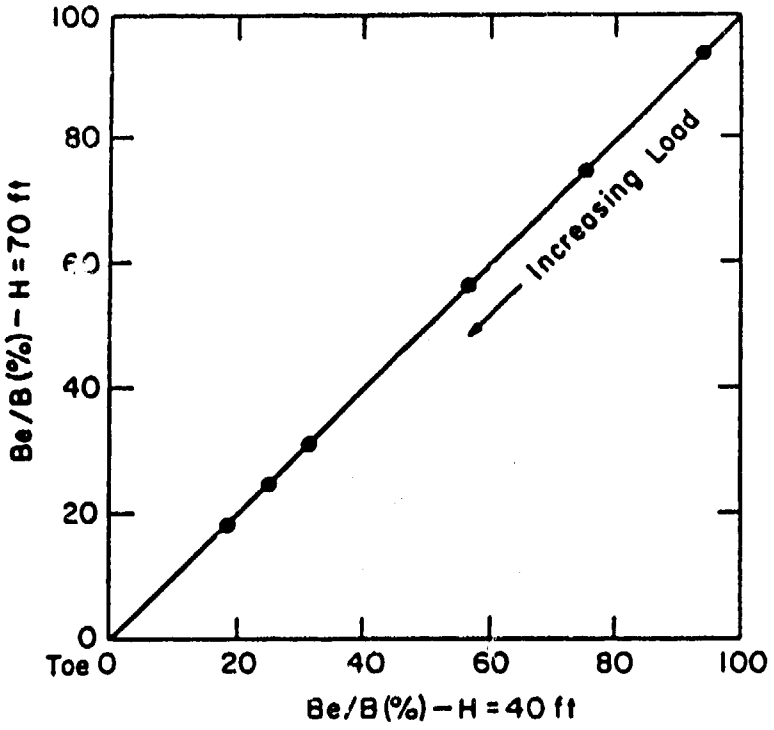

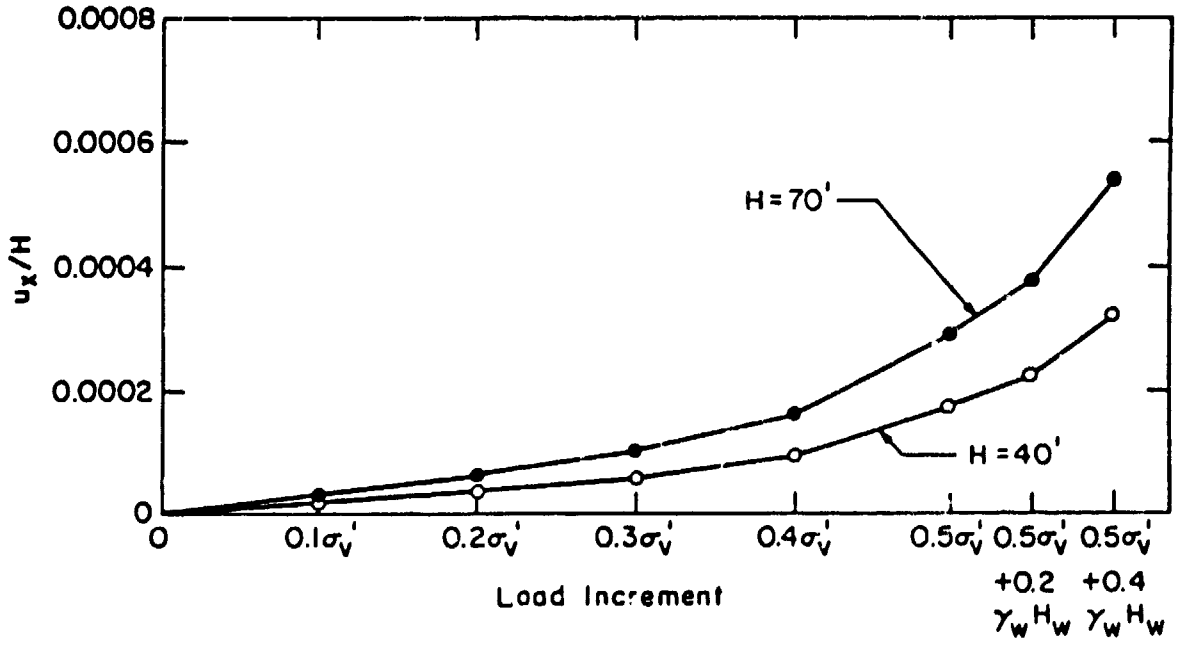

Figure 32. Variation of B_e/B and u_x/H with lateral load, scaled structure

stresses developed within the structure and the displacements. Importantly, the distribution of the resulting stresses in terms of normalized distance, normalized effective base contact area, and mobilized base friction angle are not influenced by scale. Wherever small differences exist between expected and calculated scale factors, they are likely a result of inherent approximations in the finite element method and the relative fineness of finite element meshes.

Effect of Initial Stress Distribution

131. The influence of the initial stress distribution on the results for the base case structure is examined in the following paragraphs. Two types of gravity stress simulations are used to develop the initial interface normal and shear stress distributions. In one case, the loads are applied through vertical pressures acting downward on the interface, where the vertical pressures are simply a reflection of the weight of the material above the elements. The other approach uses the scheme of loading that involves a construction simulation where the wall stiffness gradually comes into effect, using three increments, allowing for hardening of the concrete after each layer is placed.

132. The fine mesh of the base case structure is used with the 40-ft-high wall with a 16-ft-wide base (Figure 25). The loading used on the structure for all analyses is the 10-step coarse load application shown in Figure 17, with no uplift pressures. Material properties were unchanged from previous analyses.

Results--initial stress distribution

133. The initial pressure distribution in the interface for the simple approach is, as expected, a mirror image of the applied pressures (Figure 33), with the normal pressure increasing from the heel of the monolith because the amount of concrete overlying the base increases and the amount of soil decreases. Since the overlying material is all concrete, the pressure is constant. No shear stresses are generated in this instance.

134. The initial normal pressure distribution in the interface with the construction sequence simulation is different from that for the applied pressure approach in that it is concave in shape, with the pressures at the edges

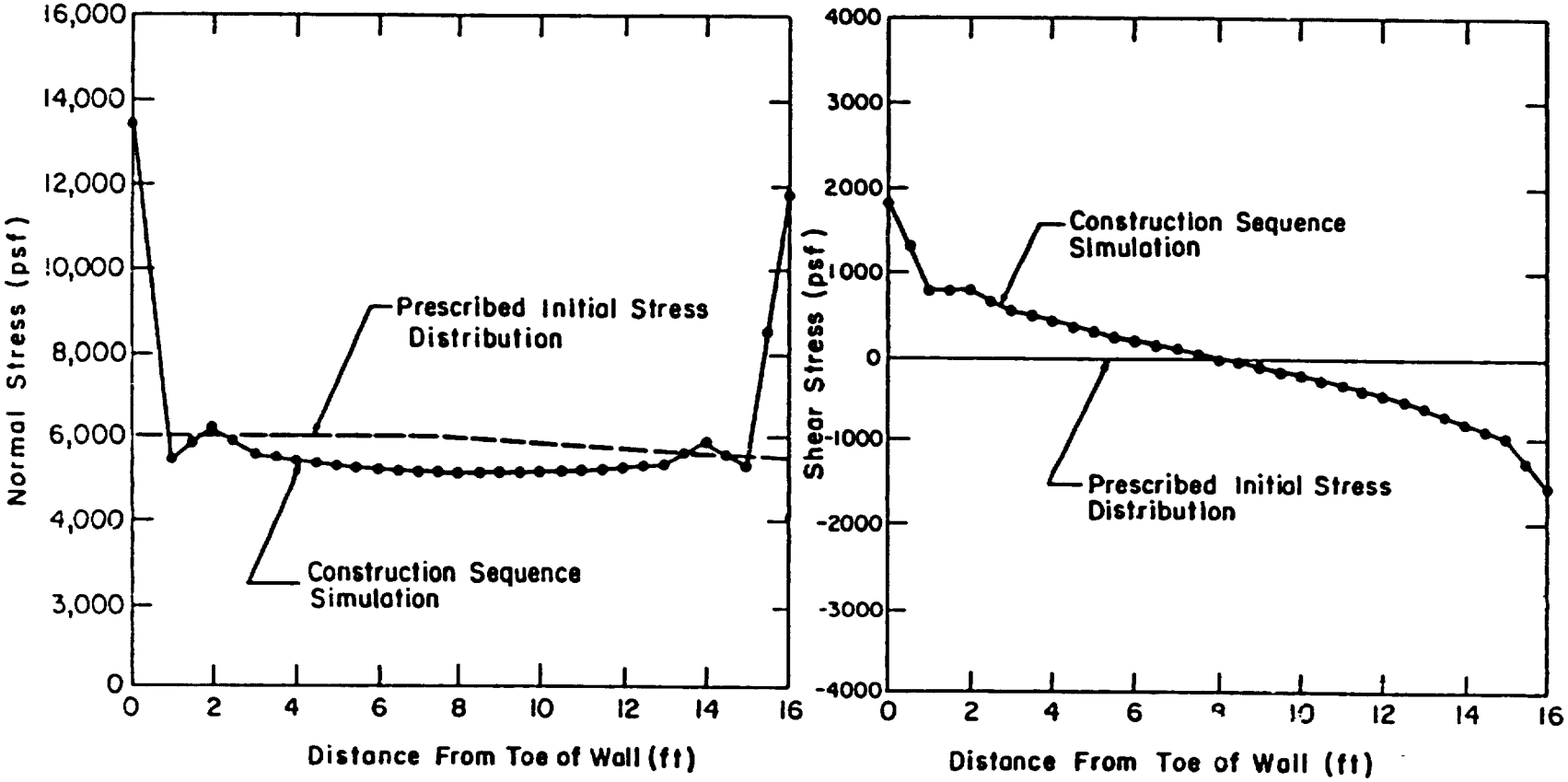

Figure 33. Initial stress distributions along the base

of the wall larger than those at the center. This effect is caused by the interplay of the wall stiffness and the foundation. As is known from elastic theory, the normal pressure distribution beneath a rigid foundation shows theoretically that the edge pressures are infinite. The finite element results are not so extreme since the wall is not rigid, and its stiffness is only gradually engaged in the incremental construction simulation. Due to the interaction effect, shear stresses are also developed along the interface.

135. As the lateral loads are applied, the trend is toward similar distributions for the normal and shear stress along the interface regardless of the initial pressure model. Figure 34 shows the stress distributions for the loading stage of $0.4 \cdot \sigma_v$, along with the distribution for the conventional equilibrium method. At this stage of loading, the effective base areas are approximately the same for both analyses, and slightly larger than that obtained by the conventional equilibrium method. The nonlinear distributions of normal and shear stresses have the same general features, and both results exceed q_{max} get the toe compared to the conventional equilibrium method. The difference between the magnitudes of the maximum stresses developed within the toe region of the monolith predicted by the analyses with the different initial stress distributions decrease with continued loading. For example, after the gravity loads are applied, the maximum compressive and shear stresses for the simple pressure-induced initial stresses are 6,000 and 0 psf, respectively. This compares with values of 13,500 and 1,800 psf, for the construction simulation analyses. At the loading stage of $0.4 \cdot \sigma_v$, the maximum normal and shear stresses for the two approaches are very close.

136. The effective base contact area, B_e/B, is presented in Figure 35 for the two analyses. For the first three stages of the lateral loading, the B_e/B values are larger by 5 percent for the structure with the initial interface stress determined by a construction sequence simulation. The values of B_e/B resulting from both analyses are in agreement for all subsequent load stages. The mobilized base friction angle agrees for the two analyses at all stages of loading, due to equilibrium considerations.

Normalized lateral deflection

137. Figure 35 also shows the normalized lateral deflection at the crest of the wall, u_x/H, as a function of load. The lateral deflection increases as the load increases, and the rate of deformation increases as the

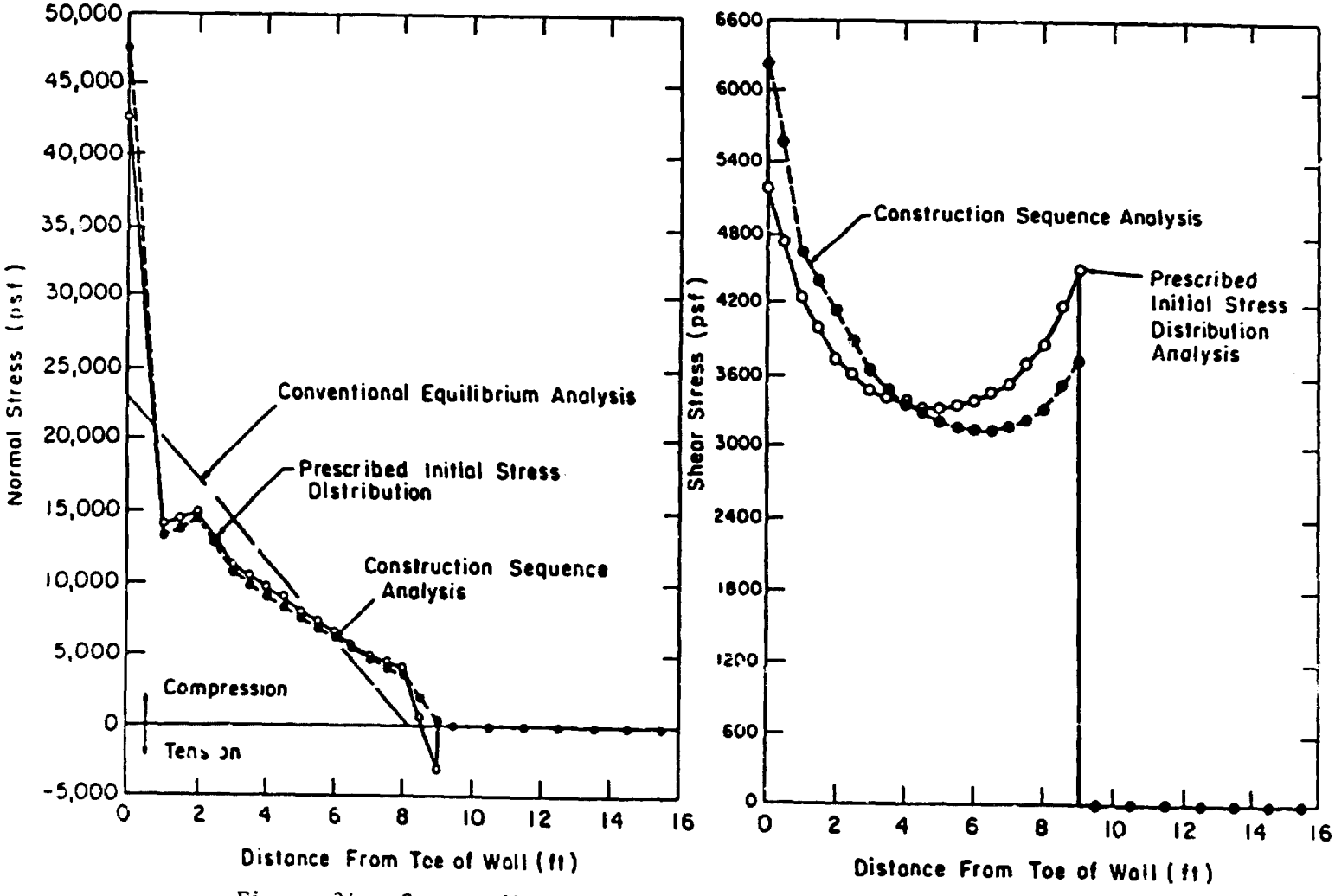

Figure 34. Stress distributions along the base for $0.4 \cdot \sigma_v$ load, effect of initial stress distributions

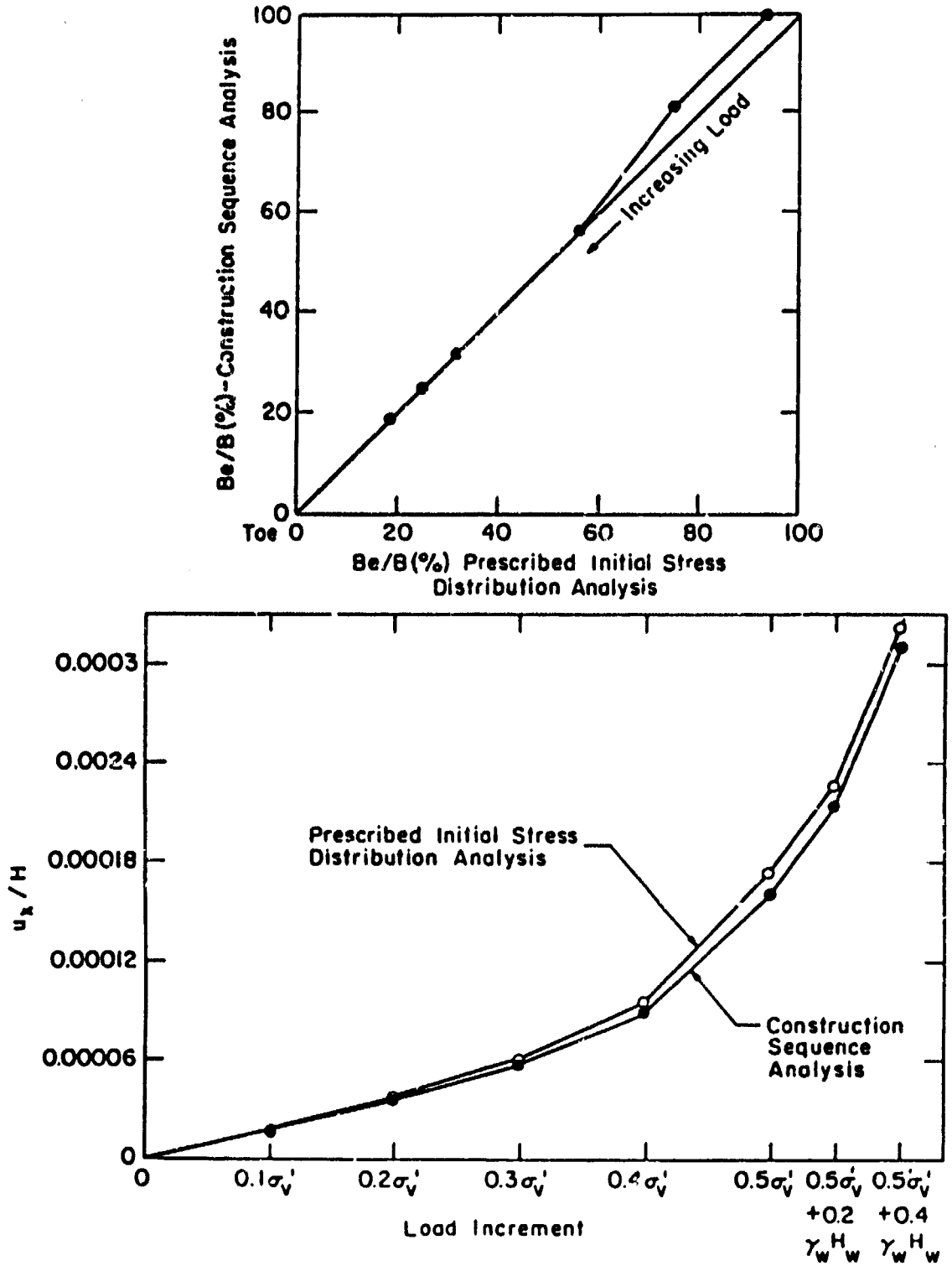

Figure 35. Variation of B_e/B and u_x/H with lateral load, effect of initial stress distributions

effective base decreases. In general, the lateral deflections at the crest of the monolith for both initial stress approaches are in agreement for all stages of loading.

138. The initial stress distribution has an influence on some of the computed variables, but the difference in the results for the two analyses decreases as the loading proceeds. This suggests that this variable is unimportant in the overall behavior of the retaining wall system, except at small loadings.

Effect of Width of Wall

139. To determine the influence of the width of the structure, the results for three structures with B/H ratios of 0.4, 0.6, and 0.8 are compared. The prescribed loads are the same for all structures so that only the factors influenced by the lateral geometry affect the results.

140. The base structure with a B/H ratio of 0.4 is shown in the fine mesh in Figure 25. The two additional meshes for the other structures are developed by multiplying x coordinates of the nodal points defining the fine mesh by 1.5 and 2.0. This results in respective base widths of 24 and 32 ft and a height of 40 ft for all structures, with B/H values of 0.6 and 0.8. The finite element meshes are shown in Figure 36.

141. The loading used on the three structures is the 10-step coarse load analyses shown in Figure 17. No uplift pressures are assigned. The same standard material properties are assumed for all three meshes as were used in previous analyses.

Results--width of wall

142. In general, as the width of the base of the wall increases, there is a decrease in the magnitude of the normal and shear stresses developed along the base. When the loading stage $0.5 \cdot \sigma_v$ is applied to the three monoliths, the maximum compressive stress within the toe region decreases from 70,000 psf to 24,000 psf and 16,000 psf, as the B/H ratio increases from 0.4 to 0.6 and 0.8. After completion of the full 10-step lateral load sequence, the resulting maximum compressive stress is 32,000 and 20,000 psf, respectively, for the two wider monoliths.

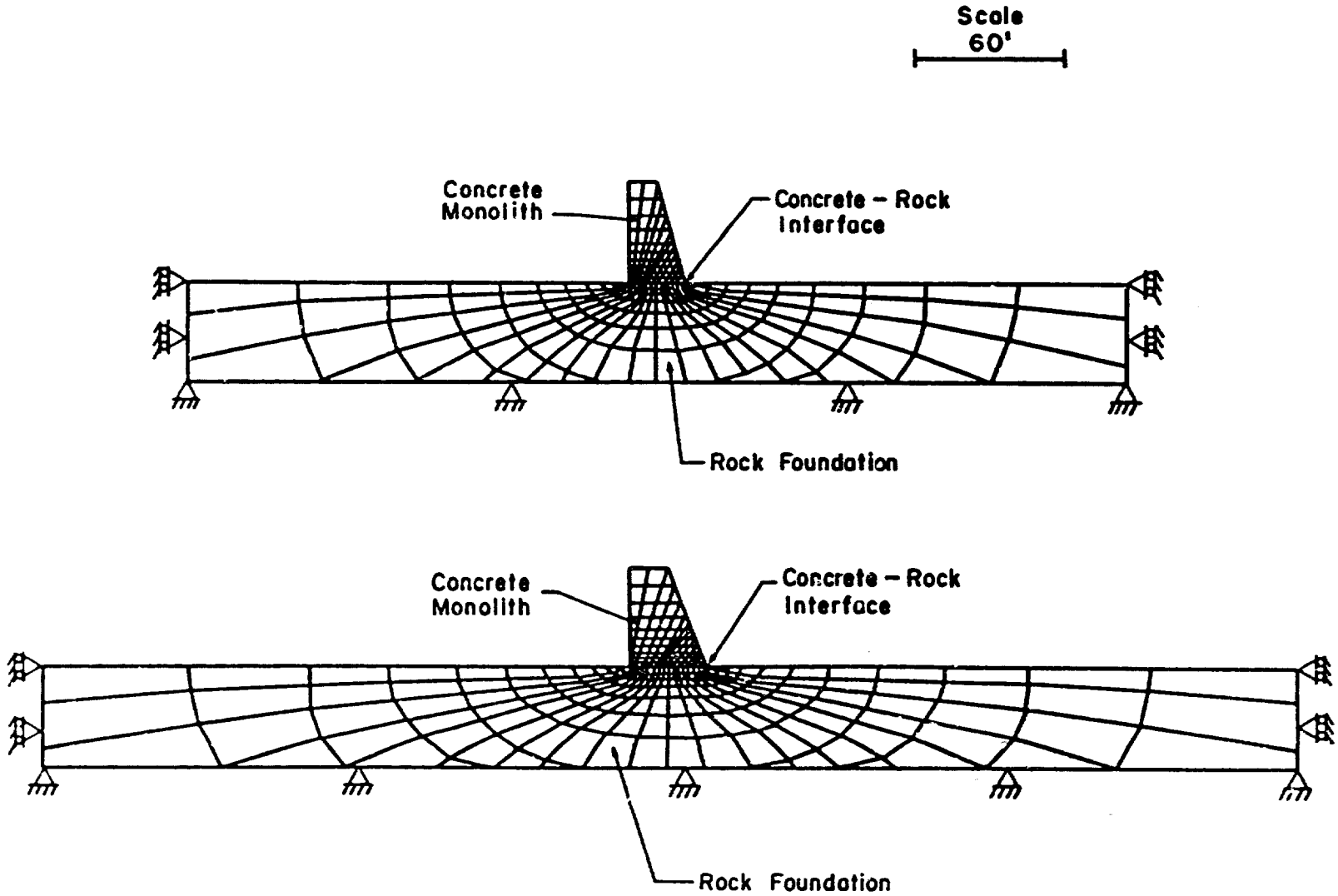

Figure 36. Finite element meshes, B/H ratios equal to 0.6 and 0.8

143. The normalized effective base contact area, B_e/B, as a function of loading is presented in Figure 37. For the same set of applied forces, the resulting B_e/B ratio is larger when the B/H ratio of the structure is increased from 0.4 to 0.6. In fact, structures possessing a B/H ratio equal to or exceeding 0.6 meet the Corps of Engineers criterion with respect to having an effective base contact area of 75 percent for full lateral loading.

144. The mobilized base friction angle, δ_{bm}, increases with load for all the analyses (Figure 37). This is attributed to the same magnitude and distribution of lateral force being applied to all structures at each stage of loading. As the width of the structure increases, δ_{bm} decreases, since wider structures are heavier.

Trends common to all structures

145 Figure 38 presents the normalized lateral deformation at the crest of the three monoliths, u_x/H, as a function of the load. There are two trends common to all structures: (a) the lateral deformation increases as the load increases; and (b) the rate of deformation increases as the effective base decreases. Another trend observed in the figure is that the normalized displacement becomes larger as the structure itself narrows for the same level of load.

146. With all factors equal, it is observed that for the same applied load, the width of the structure influences all the computed variables; the stresses, effective base contact area, mobilized base friction angle, and displacements. In general, the wider the structure the more its stability is enhanced and the smaller the lateral deformations.

Effect of Uplift Pressure Applied to the Interface

147. In these analyses the influence of the magnitude of uplift pressure applied to the interface between the monolith and its foundation is considered. For this evaluation, two structures with B/H ratios of 0.6 and 0.8, but possessing the same height of 40 ft, are used. The procedure for determining the vertical and lateral applied loads is the same for both structures, so that only the factors influenced by the uplift pressures affect the results. The finite element meshes are shown in Figure 36. The same standard

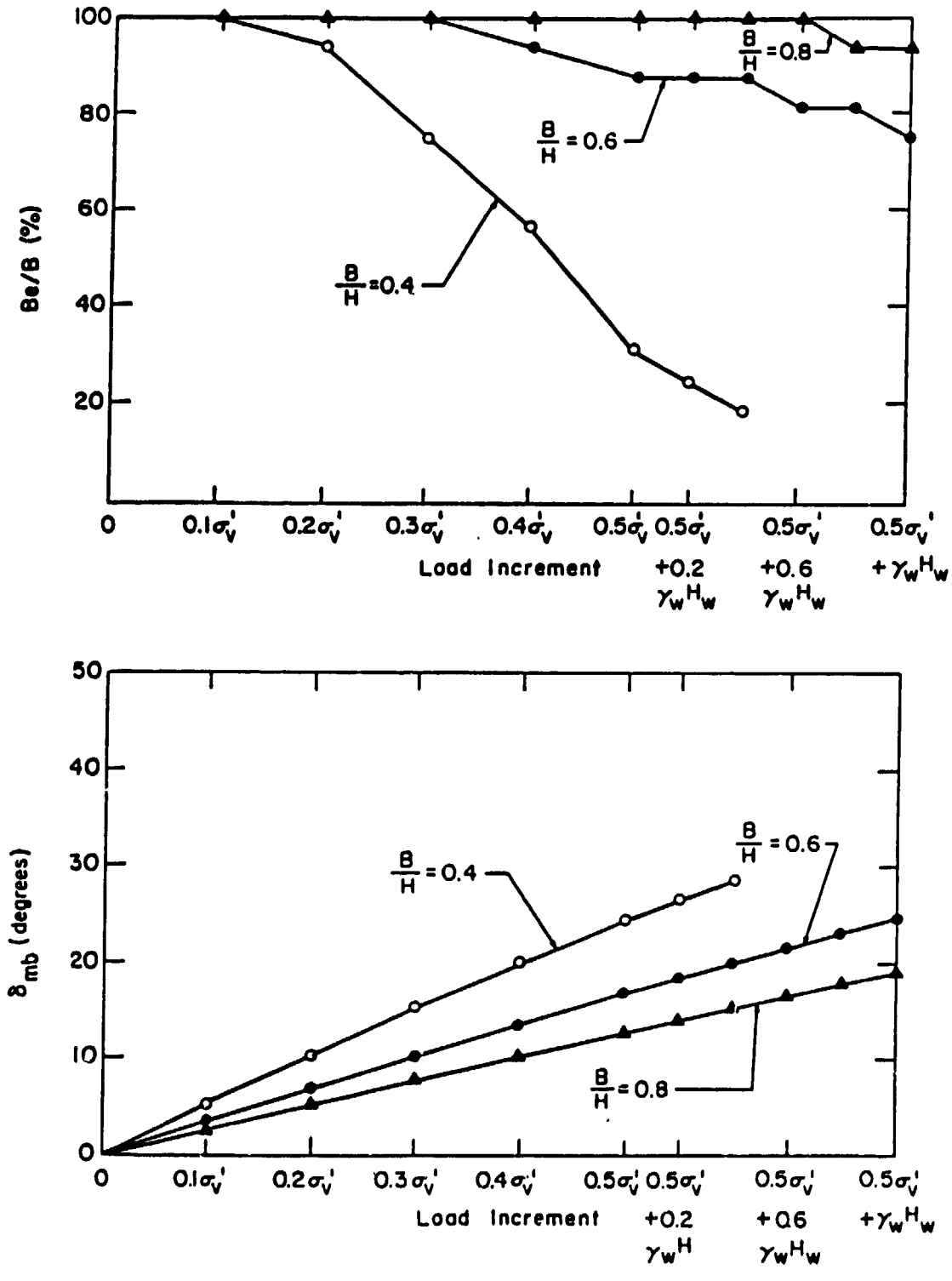

Figure 37. Variation of B_e/B and δ_{bm} with lateral load, walls with B/H ratios equal to 0.4, 0.6, and 0.8

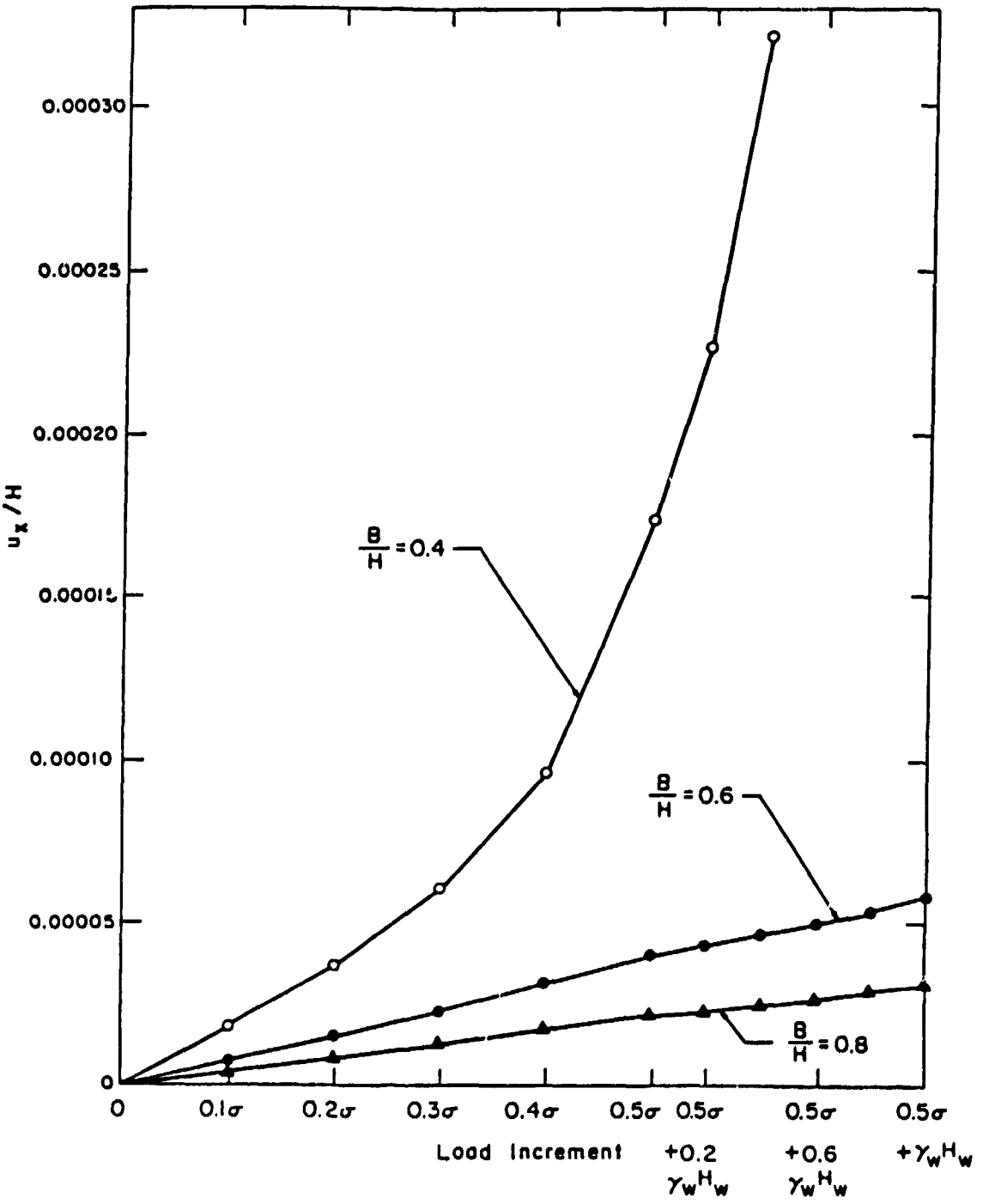

Figure 38. Variation of u_x/H with lateral load, walls with B/H ratios equal to 0.4, 0.6, and 0.8

material properties are assigned to the two meshes as were used in previous analyses.

Loading scheme

148. The loading used on the two structures is the 10-step coarse load shown in Figure 17. For this problem, two pairs of analyses are conducted for each structure; one for no uplift, and the second using full uplift pressures. As explained previously in Part IV, the uplift pressures are assigned during the second 5 increments of the 10-step load sequence and model the effects of full hydrostatic loading. At the end of loading, the magnitude of this pressure, acting upon the entire length of interface, equals the unit weight of water multiplied by the height of water in the backfill, $0.67 \cdot H$. This is the most severe boundary condition possible and thus represents the upper bound in the magnitude of uplift pressure.

Results--uplift pressures

149. The influence of the magnitude of the uplift pressures on the computed stresses on the base depends on the width of the structure. For example, at the completion of the 10-step load sequence, $0.5 \cdot \sigma_v + \gamma_w \cdot H_w$, the monolith possessing a B/H ratio equal to 0.6 develops a maximum compressive stress of 32,000 psf within the toe region for the case when no uplift pressures are applied. This value increases to 37,000 psf when the full uplift pressures are applied. However, in the corresponding pair of analyses for the monolith with a B/H ratio of 0.8, there is very little difference in the computed maximum compressive stress; 20,000 psf for no uplift and 19,000 psf for the case when full uplift pressures are assigned. A similar trend is also observed for the maximum shear stress. The difference in the trends for the two structures is attributed to the overall size of the structure and its interaction with the applied uplift pressures.

150. The normalized effective base contact area, B_e/B , as a function of loading is presented in Figure 39. Given the same height structure, lateral load, and uplift pressure, the resulting B_e/B ratio increases as the width of structure increases. There is a trend toward smaller differences in B_e/B as the width of the monolith increases, when comparing the results for the analyses with no uplift pressures and those with full uplift pressures. Another observation is that structures possessing a B/H ratio equal to 0.6 would meet the Corps of Engineers criterion only, with respect to having an

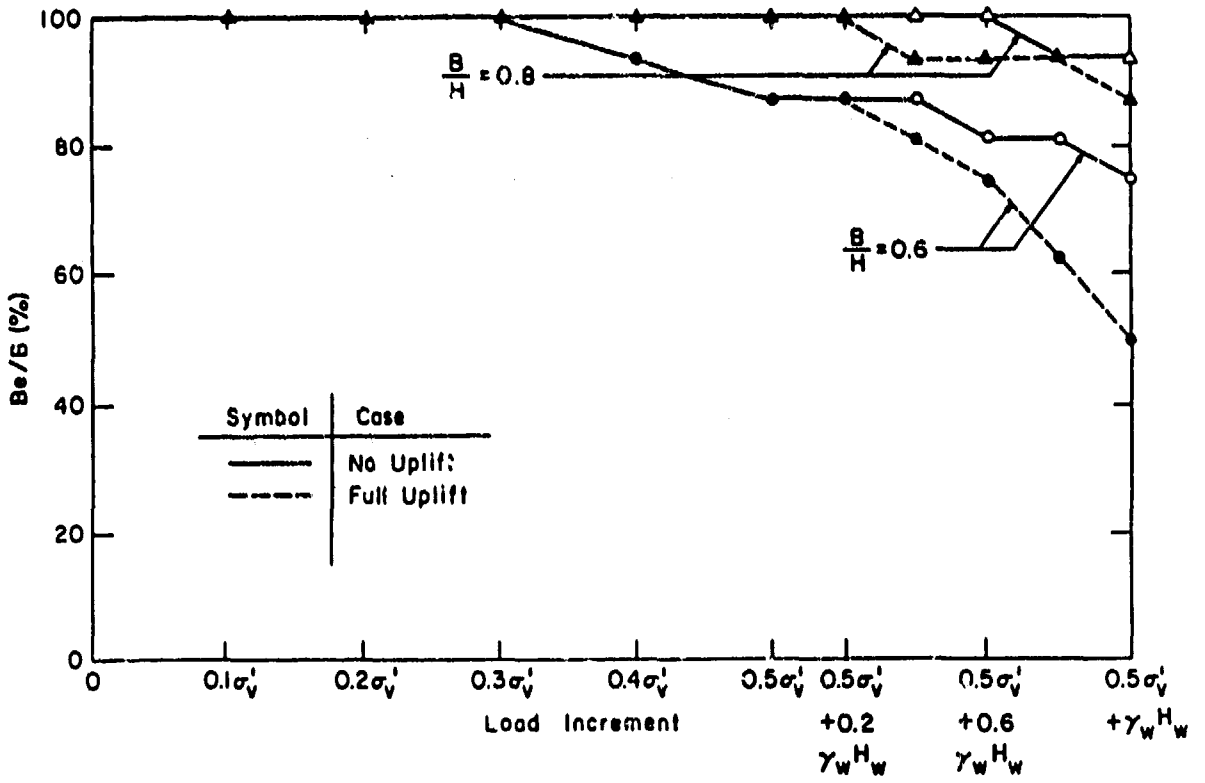

Figure 39. Variation of B_e/B with lateral load, walls with no uplift and full uplift pressures

effective base contact area of 75 percent, if no uplift pressure were applied. However, a structure possessing a B/H value of 0.8 meets this criterion for both load conditions.

151. With application of uplift pressures, the rate of change of δ_{bm} increases because the net effective interface pressure decreases (Figure 40). For example, at the end of the 10-step load sequence, the presence of uplift pressures results in an increase in δ_{bm} by 7 to 8 deg, depending upon the B/H ratio of the structure. As expected, as the width of the structure increases, δ_{bm} decreases.

152. Figure 41 presents the lateral deformation at the top of the two walls (u_x) normalized by the height (H). There are several trends: (a) the lateral deformation increases as the load increases; (b) the rate of deformation increases as the effective base decreases; and (c) the deformations increase as the uplift pressures are added.

153. It is observed that for the same height of structure and applied lateral load, the magnitude of the uplift pressures applied to the base of the

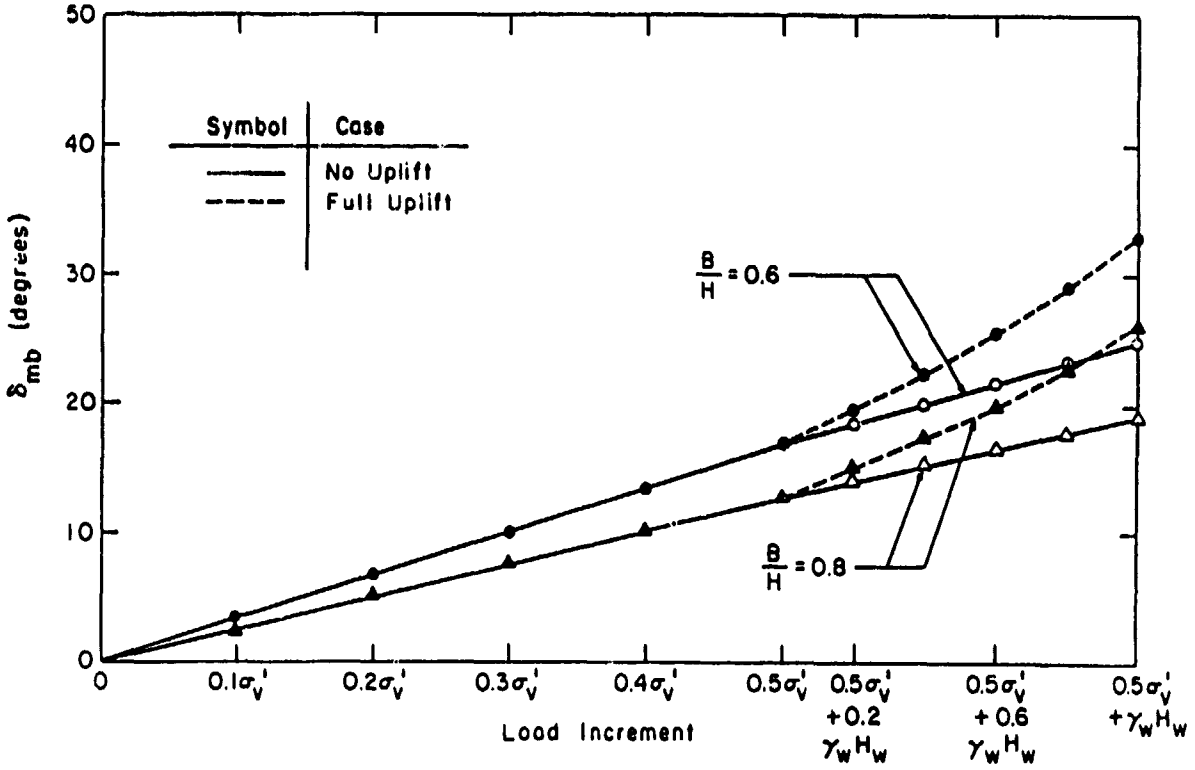

Figure 40. Variation of δ_{bm} with lateral load, walls with no uplift and full uplift pressures

structure influences all the computed variables; the stresses, effective base contact area, mobilized base friction angle, and displacements. The degree to which these variables are influenced depends upon the width of the structure.

Effect of Modulus of the Rock Foundation

154. In this first of a series of analyses of the effects of material parameters, the influence of rock modulus is determined. The base case structure is used, and the loads are the same for all analyses. The fine mesh of the base case structure as shown in Figure 25 is used.

Loading scheme

155. The loading for all analyses is the 10-step coarse load scheme (Figure 17). For this problem, no uplift pressures were assigned.

Material properties

156. The same material properties are used for the monolith and the interface between its base and the foundation as in previous standard analyses.

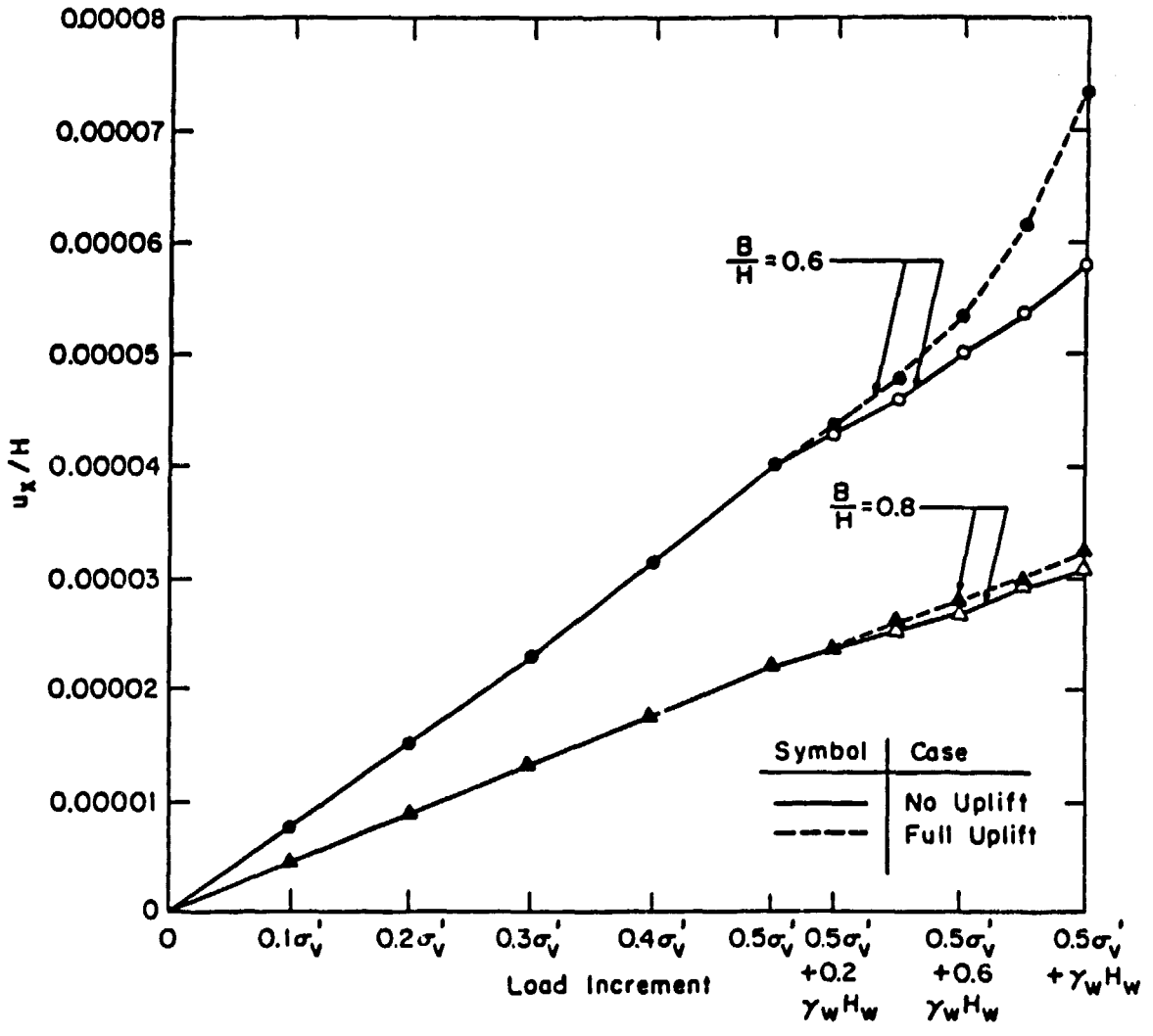

Figure 41. Variation of u_x/H with lateral load, walls with no uplift and full uplift pressures

The modulus values for the rock are 10,000, 3,000,000, and 10,000,000 psi. The Poisson's ratio is maintained at 0.2.

Results--rock foundation modulus

157. The normal and shear stress distributions on the interface between the monolith and the rock foundation as predicted by the FEA are shown in Figure 42 along with the values determined by the conventional equilibrium method. The following trends are apparent:

a. The effective base contact area is not significantly impacted by the rock modulus.

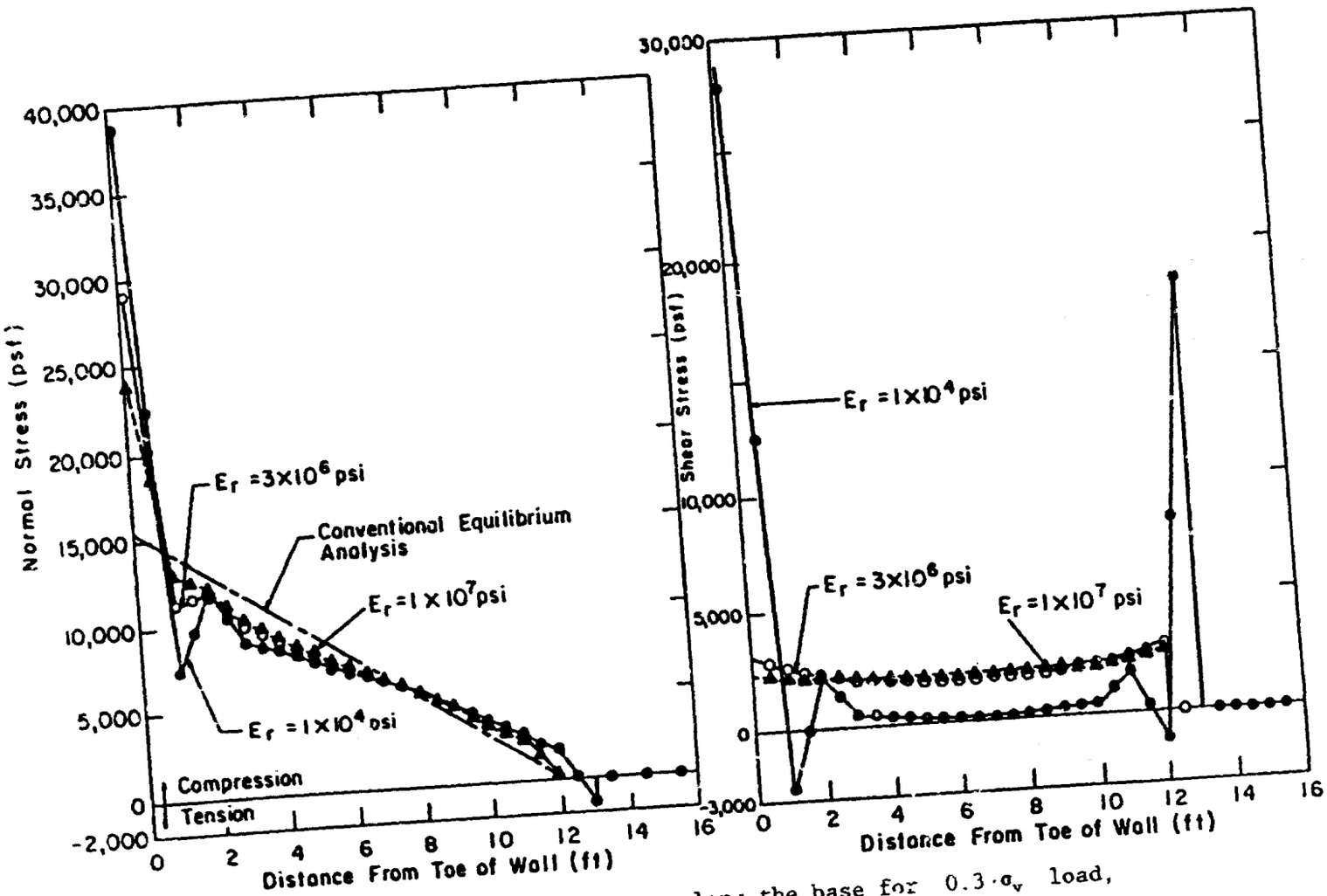

Figure 42. Stress distributions along the base for $0.3 \cdot \sigma_v$ load, three rock moduli

b. The FEA results for all rock modulus values show higher normal stresses at the toe of the wall than is indicated by the CEA.

c. The maximum normal stress at the toe of the wall is affected by the rock modulus, with higher values occurring as the rock modulus decreases.

d. The distribution of the shear stresses on the interface for the two higher rock modulus values are very similar, but there is a wide shift relative to the values for the lowest rock modulus. At the lowest rock modulus, there is a large concentration of shear stresses at the toe and the heel of the wall that does not exist for the stiffer rock foundations.

The behavior of the wall on the soft rock foundation can be better understood by examining Figure 43, showing the lateral displacements of the wall as a function of the lateral loading. It is observed that the deformations are considerably larger for the soft rock case than for the other two cases. This behavior is logical in that the soft rock modulus is less than the other two by two to three orders of magnitude. It is useful to note that the displacements do not scale in direct order with the differences in modulus since the lateral displacement shown in Figure 43 includes movement generated on the interface, a constant movement for all cases.

158. The larger deviation of the soft rock foundation stress distributions from the conventional analysis is consistent with the fact that the conventional analysis assumes the rock foundation to be perfectly rigid. Notably, the finite element results show that as the rock foundation becomes stiffer, the predicted behavior fits closer to the conventional model.

159. The normalized effective base contact area, B_e/B , as a function of loading is presented in Figure 44. There is a tendency for closer agreement between the conventional equilibrium method and the FEA as the magnitude of the rock modulus increases. The reasons for this are as described previously. The mobilized base friction angle agrees for the three analyses at all stages of loading, due to equilibrium considerations. For the three analyses, the same set of gravity and lateral forces are applied to the structures at each load stage, and thus the same magnitude of interface shear forces are developed.

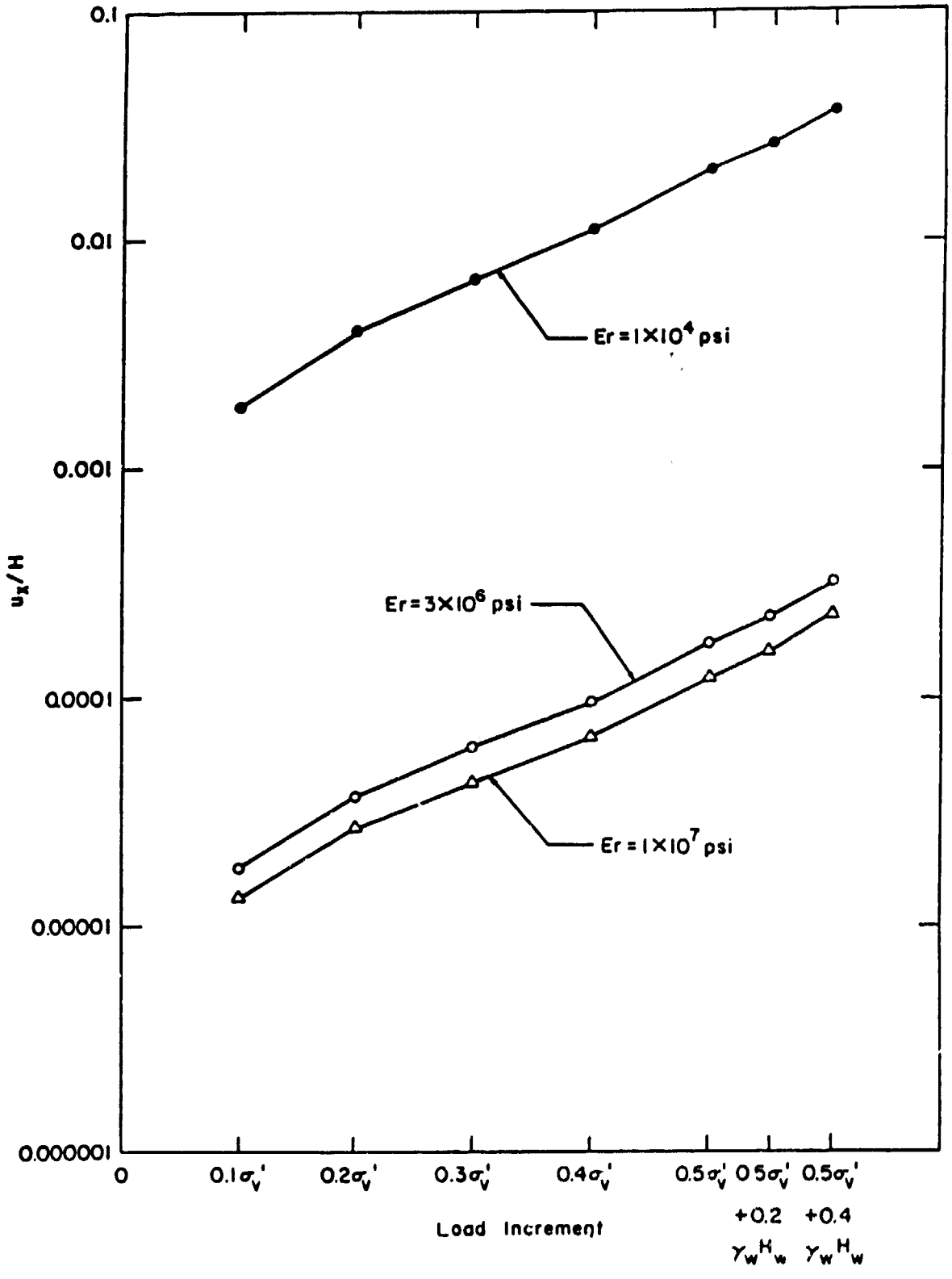

Figure 43. Variation of u_x/H with lateral load, three rock moduli

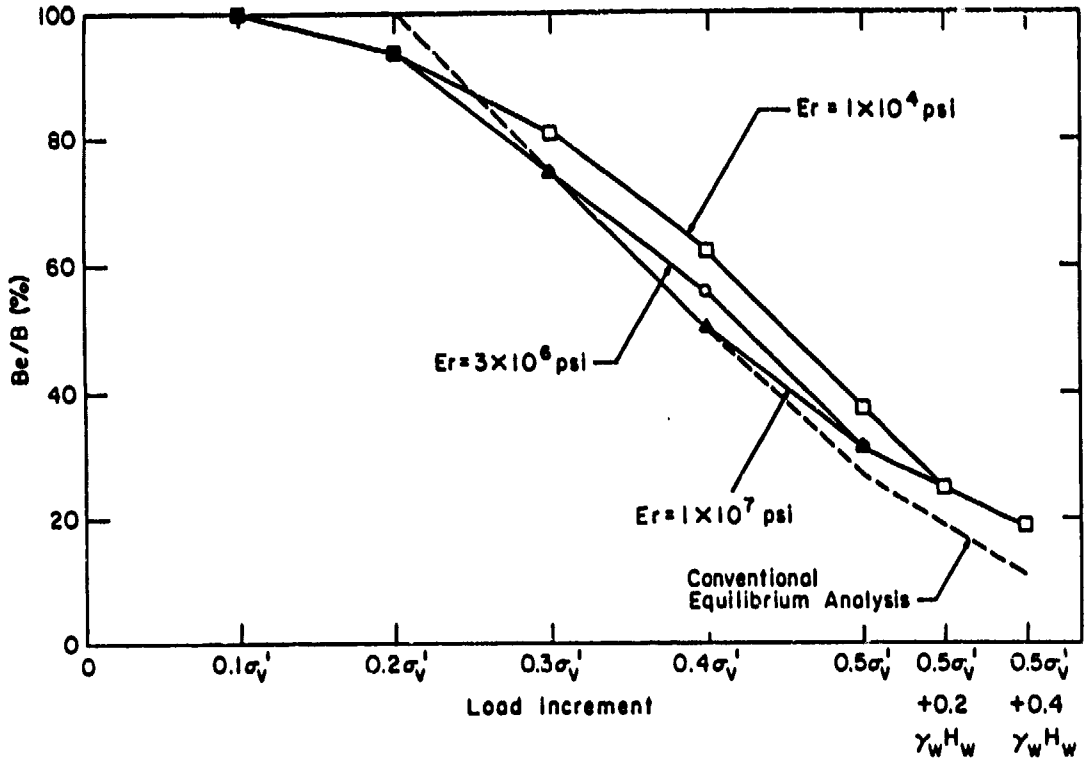

Figure 44. Variation B_e/B with lateral load, three rock moduli

Effects of Normal and Shear Stiffnesses of Interface Between the Wall and the Rock Foundation

160. To this point, the normal stiffness of the interface has been assumed to be a value of 3,000,000 pci. Thus, the interface is assumed to represent sound contact between the rock and wall. However, if the interface should have deteriorated over time due to erosive action by water flow or chemical effects, then the normal stiffness could be lower, and in this parameter study, a value of 30,000 pci is used. Assuming a similar deterioration for the shear capacity of the interface, the use of a shear stiffness of only 10 pci rather than the standard value of 10,000 pci would be recommended.

161. All other parameters in these analyses are the same as for the standard case. The fine mesh for the 40-ft wall is used as shown in Figure 25, and the loading is the 10-step coarse scheme of the previcus analyses.

162. In Figures 45 and 46, the results are given showing the effects of varying the normal stiffness of the interface (the shear stiffness in these

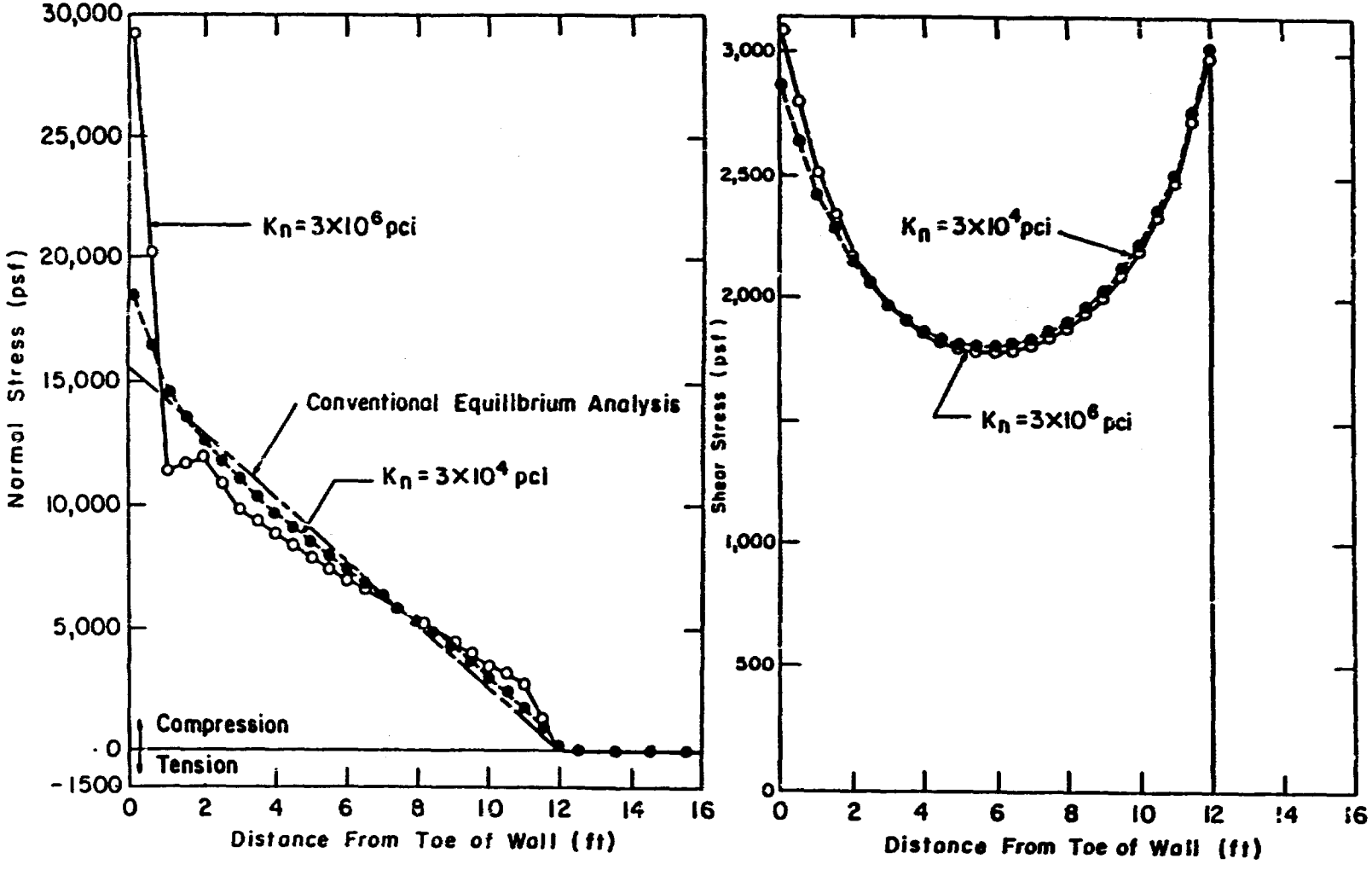

Figure 45. Stress distributions along the base for $0.3 \cdot \sigma_v$ load, two interface normal stiffnesses

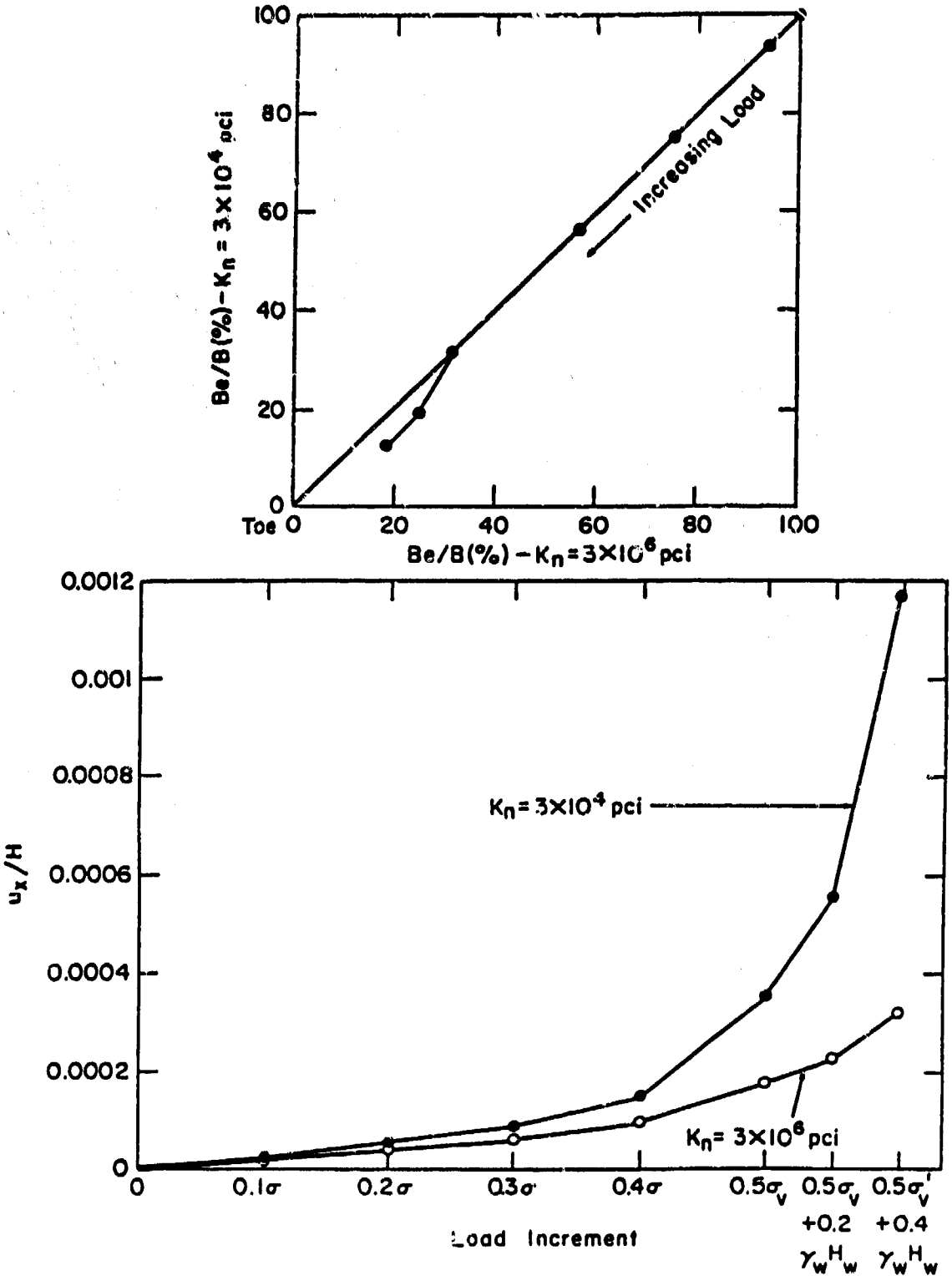

Figure 46. Variation of B_e/B and u_x/H with lateral load, two interface normal stiffnesses

stress distribution for the change in normal stiffness, there is a reduction in the normal stress generated at the toe of the wall with the use of the lower stiffness value. This reduction occurs since the soft interface prevents the mobilization of the high normal stresses that develop for the stiff interface.

163. Figure 46 shows that while little difference exists in predicted effective base contact area with either value of normal stiffness, there is a large increase in wall deformation with the softer interface versus the stiffer interface. The larger displacements are to be expected since there are two orders of magnitude difference in the two values of interface normal stiffness.

164. Figures 47, 48, and 49 give the results of the softer interface shear stiffness (the standard value of the interface normal stiffness is used in these cases). As shown in Figure 47, the softer shear stiffness has no effect on normal stress distribution on the interface, but it dramatically evens out the shear stress distribution on the interface. This is reasonable in that the softer interface provides less opportunity to develop stress concentrations. Figures 48 and 49 show the expected results that the shear stiffness value has little impact on base contact area, but that larger lateral displacements develop with the softer shear stiffness.

165. The general impact of using either a softer normal or shear stiffness for the interface is to increase lateral displacements and to modify the distribution of the interface stresses. In these following load analyses, the effect on lateral displacements is not important, since there is no soil-structure interaction involved. However, the impact of this behavior in the analyses that include soil-structure interaction can be considerable. In the presence of more lateral displacement of the wall, as induced by the softer interface, soil pressures on the active side of the wall would be reduced and those on the passive side of the wall would be increased. The wall movements will also cause changes in the vertical shear stresses acting on the wall faces. Thus, while there is little impact of interface stiffness on the following load analyses, this conclusion cannot be extrapolated to more sophisticated soil-structure interaction analyses.

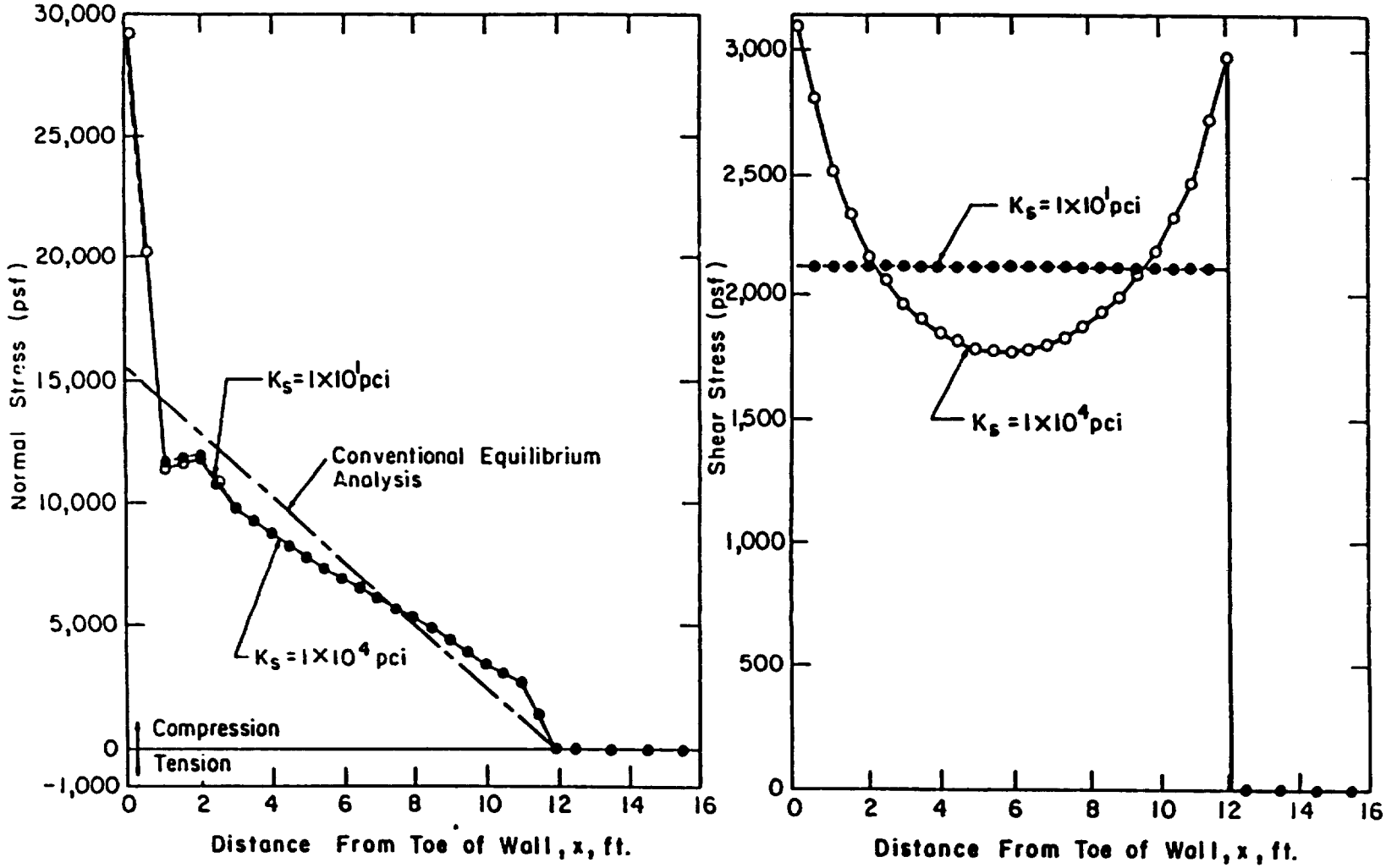

Figure 47. Stress distributions along the base for $0.3 \cdot \sigma_v$ load, two interface shear stiffnesses

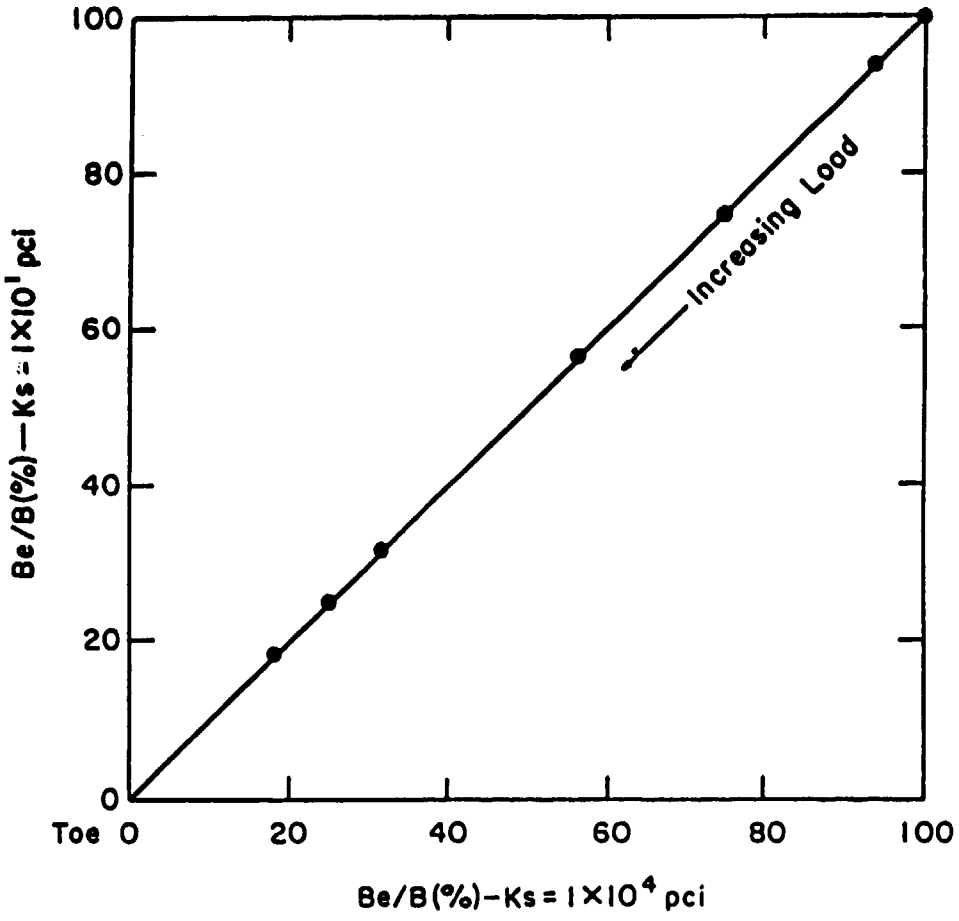

Figure 48. Variation of B_e/B with lateral load, two interface shear stiffnesses

Summary

166. The influences of seven geometric, material, and loading parameters on the response of retaining structures to following loads have been investigated. The finite element analyses used the alpha method, allowing for the separation of a monolith from its foundation (i.e. a condition of incipient instability). The results of the parametric evaluations indicate:

a. The height of the structure influences the magnitude of the stresses and the displacements resulting from the applied loads. However, normalized stress distributions formulated by dividing the actual stress by the maximum value and distance by the geometry scale factor are the same for structures of different sizes.

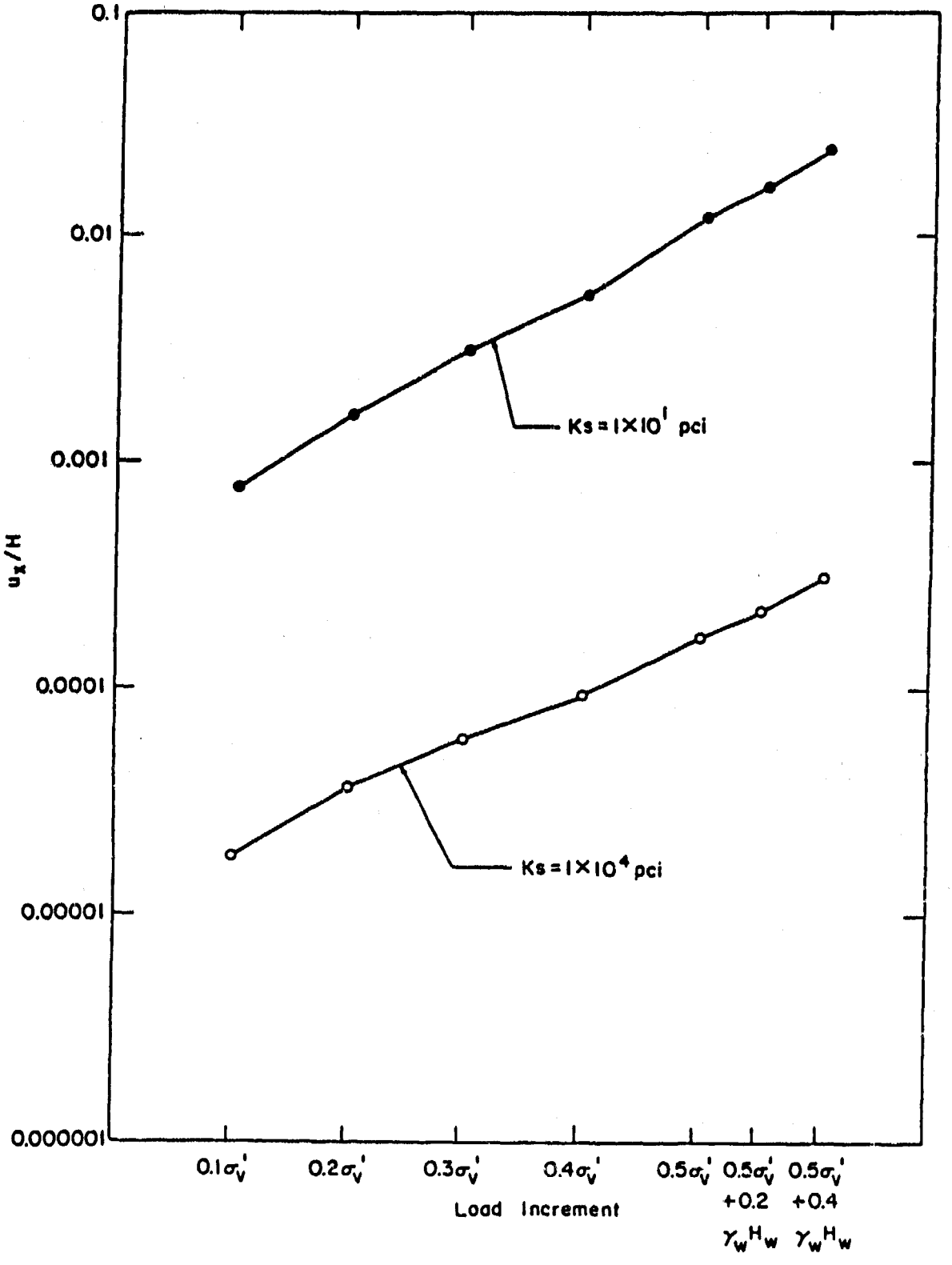

Figure 49. Variation of u_x/H with lateral load, two interface shear stiffnesses

b. At very early loading stages, the distribution of initial stress along the base of the wall influences the resulting stresses on the base and effective base contact area. Otherwise, this variable is unimportant in the computed behavior of the wall.

c. The width of the wall influences all of the computed variables. The value of B_e/B increases with increasing values of width, while the magnitudes of the stresses on the base, the mobilized angle of base friction, and displacements all decrease with increasing width. Additionally, the stability of the structure increases with increasing width.

d. The magnitude of the uplift pressures applied to the base of the wall influences all the computed variables. The level to which they are influenced depends upon the width of the structure. In general, the narrower the wall, the greater the influence of the uplift pressures.

e. The rock foundation modulus influences all the computed variables, but the level of influence is not the same for all parameters. The value of the rock modulus has a greater effect on the movements of the wall, the maximum value of compressive stress, and distribution of shear stresses on the base than on the distribution of normal stresses on the base and the effective base contact area.

f. The magnitude of the normal stiffness of the interface between the wall and its foundation influences the computed normal stresses on the base of the wall, but has little effect on the shear stresses on the base. The reverse trend is observed for the interface shear stiffness; the shear stresses are influenced by changes in the value of the interface shear stiffness, but this change does not affect the normal stresses on the base. Changes in the magnitude of either the interface normal or the shear stiffnesses affect the computed displacements but have little influence on the effective base contact area.

167. In addition to the influence of particular parameters, other conclusions can also be drawn:

a. Values of mobilized base friction angle calculated by FEA are in precise agreement with values calculated using CEA procedures.

b. Values of percentage effective base contact area calculated by FEA are somewhat larger than those calculated using CEA.

c. The maximum values of contact pressure between the base of the structure and the foundation calculated by the FEA are somewhat higher than those calculated using conventional analyses.

d. While certain of the parameters showed no significant influence on the results of the following load analyses, this does not necessarily extrapolate to backfill placement analyses. In particular, this applies to base-foundation interface properties.

PART VI: BACKFILL PLACEMENT ANALYSES OF RETAINING STRUCTURES USING THE ALPHA METHOD

168. The final series of the second phase analyses are presented in Part VI. This group of analyses differs from those described previously with regard to the method used to simulate loading on the monolith. In the analyses described in the following paragraphs, the soil backfill was represented in the finite element mesh, and the loadings exerted by the backfill on the wall were generated automatically during placement of the backfill behind the wall. This procedure is termed "backfill placement analysis." Use of this soil-structure interaction method of analysis eliminates the necessity of estimating or assuming the loads imposed on the structure by the backfill. It is believed to afford the most realistic representation of the behavior of the walls that can be performed using the finite element method.

169. The influence of several parameters on the computed results were studied in the analyses described in this part. Some of the structures evaluated had soil in front of as well as behind the monoliths. Comparisons were made between the results of the FEA and the results of CEA of the type used by the Corps of Engineers. The FEA were performed using the program SOILSTRUCT. This program is capable of modeling the development of a crack between the monolith and its foundation using the alpha method, as described in Part IV.

Structures Analyzed

170. The structures analyzed are shown in Figure 50. Both of the monoliths have the same geometry, differing only in the fact that one of the structures had soil in front of it as well as behind it. The monoliths are 40 ft high with base widths of 16 ft, resulting in a B/H ratio of 0.4. The width at the crests of the monoliths is 8 ft, corresponding to a normalized crest width of $0.2 \cdot H$. These monoliths have the same geometry as the base case structure used in the following load analyses described in Part III. The backfill extends to the top of the monolith. For the monolith with toe fill, the height of the toe fill was 17.8 ft, resulting in a normalized height of toe fill, h_{toe}/H, equal to 0.45.

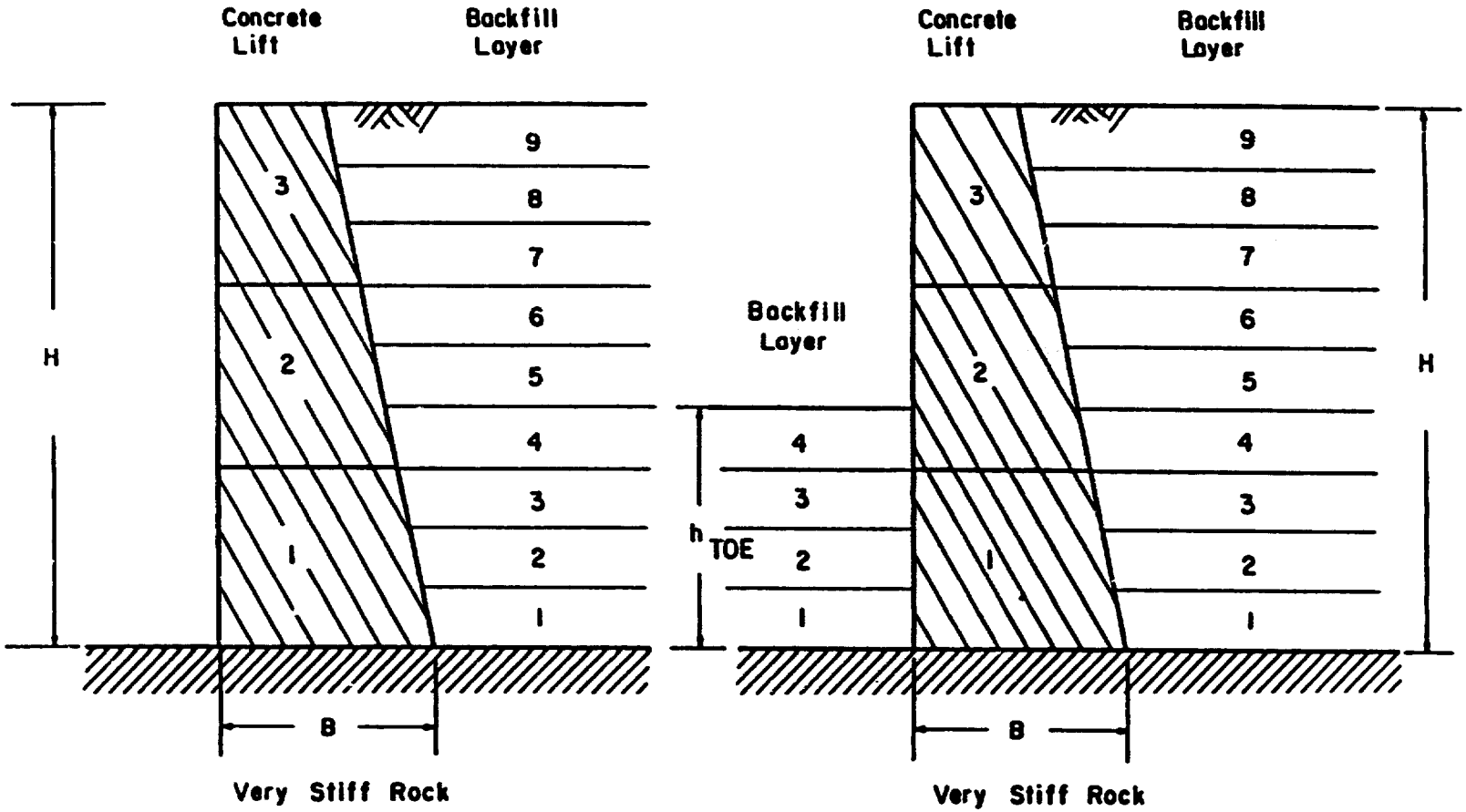

Figure 50. Idealization of base case structures for backfill placement analysis

Loading Scheme

171. There are two important differences between the backfill placement analyses and the following load analyses already described in this report:

a. The loadings exerted on the wall by the backfill and the toe fill are dependent on soil-structure interaction and are not explicitly controlled to take a certain form or magnitude. The loadings are dependent on how much and in what direction the wall moves.

b. The mode of interaction between the wall and the backfill is not predetermined. This allows for the development of interface shear, or downdrag, on the back of the wall, as well as horizontal earth loads.

As shown in Figure 50, placement of the backfill was simulated using nine layers of backfill, each 4.44 ft thick. Prior to placement of backfill, construction of the wall was simulated in three lifts, each 13.33 ft high. In the analyses where fill was placed in front of the wall, the backfill and toe fill were placed simultaneously to a depth of 17.8 ft, the final thickness of the toe fill. No water pressures were represented in the analyses.

Finite Element Meshes

172. The finite element meshes used for the backfill placement analyses discussed in this part are shown in Figures 51 and 52. Both meshes are identical, with the exception that for the mesh shown in Figure 52 additional nodal points and elements were used to model the toe fill. These meshes were designed to model a gravity wall on very stiff rock. The nodes along the base of the meshes were fixed, and thus simulated a rigid boundary at the top of rock. Interface elements were included in four regions; between the wall and the backfill, between the wall and the foundation, between the backfill and the rock, and between the toe fill and the rock.

173. There are 204 two-dimensional and interface elements in the mesh shown in Figure 51, and 258 two-dimensional and interface elements in the mesh shown in Figure 52. Of these, 57 elements model the wall, 117 model the backfill, and 40 model the toe fill. The remaining elements model the interfaces between the foundation and the structure and the fills above.

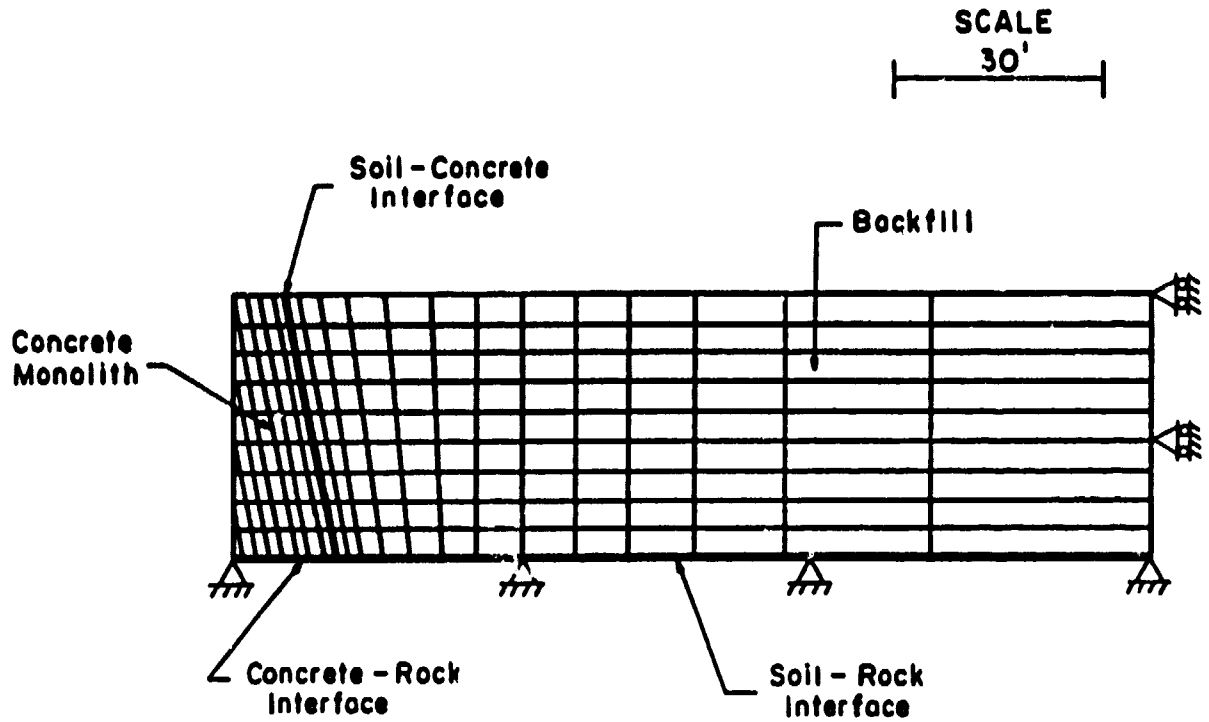

Figure 51. Finite element mesh used to model a base case hypothetical structure

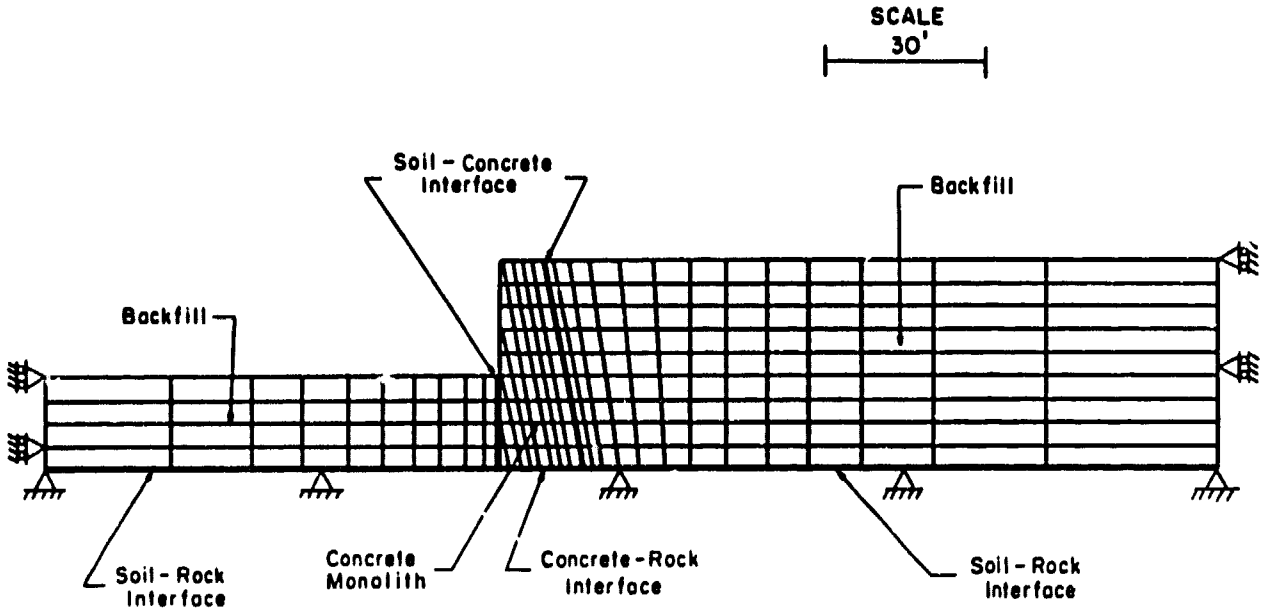

Figure 52. Finite element mesh used to model a base case hypothetical structure with additional backfill beyond the toe

Material Parameters Used in The Finite Element Analyses

174. As in the following load analyses, the wall was modeled as a linear elastic material. The soil was modeled as a hyperbolic nonlinear stress-dependent material. The modulus of each soil element was adjusted during the course of the analysis in accordance with the stresses in the element. A full explanation of the characteristics of the hyperbolic model is given by Duncan and Chang (1970) and by Clough and Duncan (1971). This model has been found to yield reasonable behavior for soils in many types of problems, and particularly those where the stresses are at working levels, and not near failure. This condition is satisfied in the analyses described in this part.

175. The values of the parameters used in these analyses are listed in Tables 3 and 5 (Part III). Table 5 also lists some of the key equations used in the hyperbolic stress-strain relationships.

176. As noted, three interfaces were used in these analyses; the first at the base of the wall, a second between the wall and the backfill, and the third between the backfill and the foundation. The details of the interface models have been discussed in Part IV. The interface between the wall and its foundation provided the capability of modeling the development of a crack by the alpha method of analysis. The original linear interface model, as discussed in the section titled "Comments on Finite Element Analysis and Interface Modeling Techniques," paragraphs 59 through 62 was used for the interfaces between the backfill and the wall and between the backfill and the underlying rock. The same normal stiffness was used for all three types of interfaces, while the shear stiffnesses of the interfaces between soil and wall and between soil and rock varied as shown by the parameter values listed in Table 5. The shear stiffness assigned to the interface between the wall and its foundation was the same as that used in the following load analyses.

177. Soil-to-concrete direct shear tests conducted by Clough and Duncan (1969) and by Peterson et al. (1976) showed that shapes of shear stress versus displacement curves for soil-to-concrete interfaces are dependent on the magnitude of the normal stress on the interface. The shear stiffness values used in these analyses were therefore varied in accordance with the calculated values of normal stress in the interface elements. The interface strength was considered to result entirely from friction, with zero adhesion.

Analyses Performed

178. Analyses were performed to study the influence of five geometrical and material parameters. The ranges of values considered for the variables are shown in Table 5. The purpose of these analyses was to determine the influence of these parameters on the calculated results;

a. The magnitude of the Poisson ratio assigned to the backfill.

b. The unit weight of the backfill.

c. The presence of toe fill in front of the wall.

d. The movement of the wall.

e. The shear stiffness for the interface between the monolith and its foundation.

179. The results of these backfill placement analyses were evaluated with regard to a number of factors that control the stability of the wall. These are:

a. The distribution of stresses along the base of the wall, the front and back of the wall, and along several planes through the backfill.

b. The magnitudes of the resultant forces on these planes, and the positions of their points of action.

c. The magnitudes of the mobilized angles of friction on these planes.

d. The magnitudes of the earth pressure coefficients that characterize the magnitudes of the earth pressures on vertical planes within the backfill.

e. The percent of effective contact between the base of the wall and the foundation B_e/B .

f. The lateral displacement of the monolith.

g. The magnitude of the maximum compressive stress developed in the toe of the wall.

h. Stress paths at various key locations within the backfill.

180. Finally, a comparison was made between the results of the FEA and the conventional equilibrium method used by the Corps of Engineers to evaluate the stability of walls on rock.

Effect of Poisson's Ratio of the Backfill

181. The first analyses were performed to investigate the influence of the magnitude of Poisson's ratio of the backfill. The structure shown in

Figure 50, with no toe fill, was used in the evaluation. Three analyses were performed, in which the value of Poisson's ratio assigned to the backfill was increased from its standard value to a value large enough to reach a state of impending instability for the wall.

Material properties used in the analyses

182. The properties of the concrete and the interface between the monolith and its foundation were the same as those used in the following load analyses discussed in paragraphs 46 and 49. The modulus of the concrete was 3,000,000 psi, and the Poisson's ratio was 0.15. The normal stiffness of the interface between the wall and the foundation was 3,000,000 pci, and the shear stiffness was 10,000 pci.

183. The properties assigned to the backfill and to the backfill/wall and backfill/foundation interfaces were characteristic of a clean granular backfill with a Unified Soil Classification of SW or SP and a relative compaction of 100 percent, as determined using the American Society for Testing and Materials (ASTM) D 698-70 (ASTM 1970). This corresponds to an approximate relative density of 75 percent. The unit weight was 135 pcf, and the angle of internal friction was 39 deg. The magnitudes of the parameters used to model the hyperbolic stress-strain behavior were: the modulus constant, $K = 450$; the modulus exponent, $n = 0.4$; and the failure ratio, $R_f = 0.7$. Three values of Poisson's ratio were used: 0.15, 0.3, and 0.38.

184. The shear stiffness assigned to the interfaces between the soil and the concrete and between the soil and the rock ranged from 20 to 300 pci, depending upon the confining pressure. The normal stiffness assigned to all of the interfaces was 3,000,000 pci. The friction angle of the wall/soil interface was 31 deg, corresponding to 80 percent of the angle of internal friction for the soil.

Results of the backfill placement analyses

185. The results of the analyses (runs 13a, 14a, and 15a) are summarized in Table 6. The stress distributions computed using the program SOILSTRUCT were converted into equivalent resultant forces. Their magnitudes and points of action were determined for several planes shown in Figure 53. The sections labeled A-A and C-C pass through the heel of the monolith, the former extends vertically within the backfill, and the latter along the soil-to-wall interface. A vertical section B-B is located far behind the heel of the wall, so that the stresses developed on this plane are not influenced by

Table 6

Summary of Results for Backfill Placement Analyses

Run	$\gamma_{backfill}$ pcf	$\nu_{backfill}$	Section B-B Vertical Section Beyond Heel				Monolith							
							Base							Crest
			F_h lb	K_o	h_{Fh} ft	h_{Fh}/H	T lb	N lb	X_n ft	X_n^* ft	B_e/B	q_{max} psf	δ_{mb} deg	U_X/H
13a	135	0.15	55,329	0.51	14.2	0.36	48,922	107,408	2.192	2.270	0.45	39,918	24.5	0.000063
14a	135	0.30	67,473	0.63	13.9	0.35	59,108	107,095	0.902	1.116	0.25	71,727	28.9	0.000134
15a	135	0.38	78,517	0.73	14.0	0.35	67,074	107,382	-0.009	0.308	<0.09	>165,096	32.0	0.000325
16a	120	0.15	49,180	0.51	14.2	0.36	43,460	103,493	2.505	2.585	0.5	35,246	22.8	0.000053
17a	135	0.15	55,329	0.51	14.2	0.36	37,299	110,671	2.808	2.886	0.5	33,474	18.6	0.000050
18a	135	0.15	55,329	0.51	14.2	0.36	--	72,000	6.222	6.222	1.0	--	--	--
19a	135	0.15	55,202	0.51	14.2	0.36	5,475	108,276	4.137	4.175	0.75	22,098	2.9	0.000607

Note: -- indicates not aplicable in each case

(Continued)

Table 6 (Continued)

Run	Section C-C Soil-to-Concrete Interface-Heel					Backfill Wedge			Section A-A, Vertical Section Through Heel						
	F_S lb	F_n lb	ℓ ft	ℓ/L	δ_m deg	W_S lb	W_S/area pcf	X_{W_S} ft	F_v lb	F_h lb	K_v	K_h	h_{Fh} ft	h_{Fh}/H	δ_m deg
13a	25,126	54,916	14.2	0.35	24.6	20,520	128	2.88	14,888	48,922	0.14	0.45	14.7	0.37	16.9
14a	22,822	64,843	14.1	0.35	19.4	20,818	130	3.11	14,278	59,108	0.13	0.55	14.3	0.36	13.6
15a	21,541	72,711	14.0	0.34	16.5	21,329	133	2.5	14,053	67,074	0.13	0.62	14.3	0.36	11.8
16a	22,358	48,792	14.2	0.35	24.6	18,251	114	3.07	13,242	43,460	0.14	0.45	14.6	0.37	16.9
17a	25,031	54,986	14.2	0.37	24.5	20,480	128	2.84	14,795	49,008	0.14	0.45	14.7	0.37	16.8
18a	24,838	55,500	14.1	0.35	24.1	20,570	129	2.15	14,570	49,542	0.14	0.46	14.9	0.37	16.5
19a	26,981	42,522	17.0	0.42	32.4	19,934	125	5.63	14,863	36,405	0.14	0.34	16.8	0.42	22.2

(Continued)

Table 6 (Concluded)

Run	Section A-A		Section H-H Vertical Section Beyond Toe				Section E-E Soil-to-Concrete Interface, Toe							
	$\frac{K_h A\text{-}A}{K_o B\text{-}B}$	EPI	F_h lb	K_o	h_{Fh} ft	h_{Fh}/h_{toe}	F_v lb	F_h lb	K_v	K_h	h_{Fh} ft	h_{Fh}/h_{toe}	δ_m deg	$\frac{K_h E\text{-}E}{K_o H\text{-}H}$
13a	0.88	0.21	--	--	--	---	--	--	--	--	--	---	---	---
14a	0.87	0.20	--	--	--	---	--	--	--	--	--	---	---	---
15a	0.85	0.22	--	--	--	---	--	--	--	--	--	---	---	---
16a	0.88	0.21	--	--	--	---	--	--	--	--	--	---	---	---
17a	0.88	0.21	12,714	0.6	6.6	0.37	3,342	11,711	0.16	0.55	6.62	0.37	15.9	0.92
18a	0.90	0.18	12,714	0.6	6.6	0.37	3,490	11,311	0.16	0.53	6.59	0.37	17.1	0.89
19a	0.67	0.61	12,829	0.6	6.6	0.37	1,479	30,930	0.07	1.45	5.43	0.31	2.7	2.41

(Sheet 3 of 3)

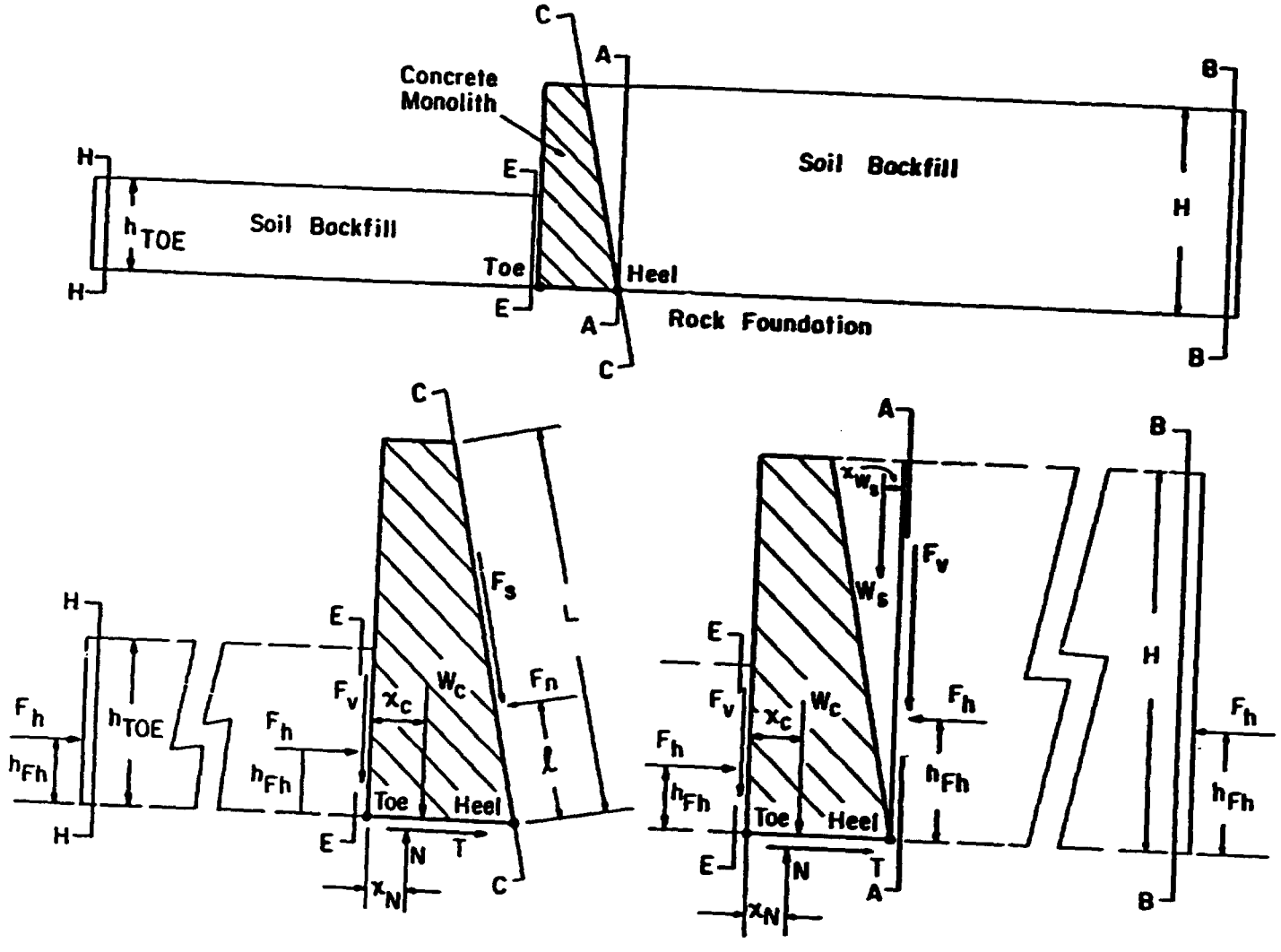

Figure 53. Planes along surfaces of the monolith and within the backfill on which resultant forces are computed

the soil-structure interaction. The resultant forces acting on this plane were used to determine the at-rest earth pressure coefficient that characterizes the maximum potential lateral load that could be developed on an unyielding wall.

Forces on section B-B

186. Due to its distance from the monolith, the stresses developed on the vertical section B-B are not influenced by soil-structure interaction. The stresses on this plane therefore reflect only the influence of the material parameters assigned to the soil.

187. The magnitude of the resultant lateral force, F_h, acting on section B-B was found to increase with increasing value of Poisson's ratio. This is consistent with the fact that it has been shown previously (Dunlop, Duncan, and Seed 1968) that the equivalent value of K_o for an elastic material increases with increasing value of Poisson's ratio. For a simple linear elastic material, Dunlop, Duncan, and Seed (1968) showed that K_o and ν were related as follows:

$$K_o = \frac{\nu}{1 - \nu} \tag{14}$$

For the model used in these analyses, the relationship is more complex. The value of the bulk modulus used in the program is calculated using Poisson's ratio and the initial tangent modulus value (E_i), whereas the stiffness of the soil in shear is governed by the tangent modulus value (E_t). Because E_i is larger than E_t, the relationship between K_o and ν is changed, and

$$K_o > \frac{\nu}{1 - \nu} \tag{15}$$

in this case. In this case it is necessary to perform FEA to determine the value of K_o that corresponds to a given value of Poisson's ratio.

188. The lateral earth pressure coefficient (K_h) on section B-B corresponds to the at-rest earth pressure coefficient (K_o). Values of $K_h = K_o$ were calculated from the finite element results using the expression

$$K_h = \frac{F_h}{0.5 \cdot \gamma_{backfill} \cdot H^2} \qquad (16)$$

As the value of Poisson's ratio of the backfill increases from the standard value of 0.15 to 0.3 and 0.38, the value of K_o increases from 0.51 to 0.63 and 0.73. The value of K_o serves as a convenient index to the magnitude of the loading this wall would be subjected to if it did not move.

189. The resultant lateral force acts at $0.35 \cdot H$ above the base in all three analyses. This is slightly larger than the value of $0.33 \cdot H$ corresponding to an exactly triangular at-rest pressure distribution.

190. The resulting vertical shear force, F_v, acting on section B-B is zero for all three analyses. This is due to the lack of differential settlements from one side of B-B to the other.

191. The vertical shear stress coefficient (K_v) at this section is zero, since F_v is zero. The value of K_v was calculated using the following equation

$$K_v = \frac{F_v}{0.5 \cdot \gamma_{backfill} \cdot H^2} \qquad (17)$$

192. The mobilized angle of friction, δ_m, is also zero at section B-B. δ_m is given by

$$\tan(\delta_m) = \frac{F_v}{F_h} \qquad (18)$$

Forces on the wall

193. The forces on the monolith are summarized in Table 6. The resultant shear force along the base of the monolith (T) increases with increasing value of Poisson's ratio. For horizontal equilibrium, T must be equal to the lateral force applied to the monolith by the backfill and, thus, increases with increasing value of Poisson's ratio.

194. The resultant normal force (N) acting on the base is the same for the three analyses. However, the location of the resultant approaches the toe (x_n approaches zero) as the value of Poisson's ratio increases. This reflects

the greater magnitude of the lateral force applied to the wall, as the value of Poisson's ratio is increased.

195. In Table 6, x_n^* is the location of the resultant normal force for those elements remaining in compression, while x_n is the location of the resultant force considering all of the interface elements along the base of the monolith. The accuracy of the results of the analysis can be gaged by comparing these two values; ideally, if the results contained no numerical inaccuracies, these two values would be identical. For both runs, 13a and 14a, each pair of values are very nearly equal (they differ by less than 3 in.), indicating that the development of a crack between the monolith and its foundation was accurately modeled. For run 15a there is a slightly larger difference between these values, indicating that the analysis was somewhat less accurate. This is not surprising, since a negative value for x_n indicates the monolith was unstable. It may also be noted that only a fraction of one interface element, located adjacent to the toe, remains in compression during the last stage of loading in analysis 15a. As discussed in Part IV, a single element is not sufficient to model the behavior accurately.

196. The normalized effective base contact area, B_e/B, decreases with lateral load and, thus, with increasing values of Poisson's ratio. As the value of Poisson's ratio assigned to the backfill increases from 0.15, the computed value of B_e/B decreases from 0.45 to 0.25 for $\upsilon = 0.30$ and ultimately to about 0.09 for $\upsilon = 0.38$.

197. As the value of Poisson's ratio increases and the effective base contact area decreases, the maximum compressive stress developed within the toe region of the monolith increases. As the Poisson's ratio of the backfill is increased, the computed maximum compressive stress increases from 40,000 to more than 165,000 psf. As discussed in paragraph 195, due to the incipient instability of the monolith in run 15a, the compressive stress approaches infinity as the structure rotates on its toe during overturning.

198. The mobilized friction angle, δ_{bm}, along the base increases with increasing lateral force and, thus, with increasing value of Poisson's ratio. For the three analyses, δ_{bm} increases from 25 to 29 deg, and ultimately 32 deg.

199. The lateral movement of the monolith also increases with increasing value of Poisson's ratio, due to the larger applied lateral forces. The normalized lateral deformation at the crest of the monolith (u_x/H) increases from 0.000063 for $\upsilon = 0.15$, to 0.000134 for $\upsilon = 0.30$, and to 0.000325 for

$\upsilon = 0.38$. Although the deformation of the wall increases with the applied lateral force, the computed displacements are not sufficient to develop active pressures within the soil backfill, even for the case in which a state of limiting equilibrium of the wall is incipient. Terzaghi (1934) showed that the active condition on a rough wall was reached for a value of $u_x/H = 0.0014$ for a dense sand, and a value of $u_x/H = 0.0084$ for loose sand. The largest displacements calculated in these analyses ($u_x/H = 0.000325$) was only about 25 percent as large as the displacement needed to develop active pressure in dense sand.

Forces on section C-C

200. Section C-C corresponds to the interface between the concrete monolith and the soil backfill. The magnitude and distribution of the resulting stresses reflect the value of K_o for the backfill, the settlement of the backfill as it is placed, and the effects of the movements of the wall during backfilling.

201. The resultant shear, or downdrag, force, F_s , decreases slightly with increasing Poisson's ratio of the backfill. The value of F_s is 25,000 lb/ft for $\upsilon = 0.15$ and about 22,000 lb/ft for $\upsilon = 0.38$. This is due to the fact that as the value of Poisson's ratio increases, the backfill settles less during placement.

202. The normal force, F_n , increases with increasing values of Poisson's ratio. This corresponds to the larger value of K_o characteristic of backfill with large Poisson's ratio. For all three analyses, this force acts at a distance of 14 ft above the heel, as measured along the interface. This distance corresponds to 35 percent of the interface length (L).

203. The mobilized friction angle, δ_m , along section C-C decreases with increasing Poisson's ratio. For the three analyses, δ_m decreased from 25 deg for $\upsilon = 0.15$ to 19 deg for $\upsilon = 0.30$ and ultimately to 17 deg for $\upsilon = 0.38$.

Forces on section A-A

204. Section A-A is a vertical plane, within the soil backfill, passing through the heel of the wall. Because of its close proximity to the wall, the forces on this plane are affected by the soil-structure interaction.

205. The resulting vertical shear force, F_v , acting on section A-A is nearly constant for all three analyses and is, thus, nearly independent of the value of Poisson's ratio assigned to the backfill. The fact that this force is independent of Poisson's ratio is due to counteracting influences.

206. Since F_v has a stabilizing influence on the wall, its magnitude is very significant. Further study of the factors that affect its magnitude is needed to determine under what conditions it may be relied on as a stabilizing influence on the wall. The vertical shear stress coefficient, K_v, at this section also has a nearly constant magnitude, varying from 0.13 to 0.14 for the three analyses.

207. The magnitude of the resulting lateral force (F_h) acting on section A-A increases with the value of Poisson's ratio assigned to the backfill. As the value of Poisson's ratio of the backfill increases, the value of K_h increases from 0.45 for $\upsilon = 0.15$, to 0.55 for $\upsilon = 0.30$, and to 0.62 for $\upsilon = 0.38$. When the lateral earth pressure coefficient for section A-A (K_h) is divided by K_o, the resulting values range from 0.85 to 0.88 for the three cases analyzed.

208. It is interesting to compare the values of K_h for plane A-A with the values of K_a and K_o for the soil. A convenient means of making this comparison is the earth pressure index (EPI), which is defined as

$$EPI = \frac{K_o - K_h}{K_o - K_a} \tag{19}$$

This value of EPI varies from zero to unity when $K_h = K_o$ and $K_h = K_a$, respectively. Thus, a value of $EPI = 0$ represents conditions where there is no effect of wall movement on the earth pressure. A value of $EPI = 1.0$ represents conditions where the wall movement effect has reached its maximum, reducing the earth pressure to its active value. The values of EPI for the three cases analyzed are quite close, ranging from 0.20 to 0.22. This indicates that approximately the same level of soil-structure interaction occurred in all three analyses. This is consistent with the small lateral displacements of the monolith, when compared to those required to develop active earth pressures.

209. The resultant lateral force, F_h, acts at the same normalized height above the heel of the wall, $0.36 \cdot H$, in the three cases. Thus, the resultant normal force on plane A-A acts at nearly the same height as on plane B-B, where the earth pressure is not influenced by soil-structure interaction.

210. The mobilized angle of friction, δ_m, for section A-A decreases as Poisson's ratio increases. There is a decrease in δ_m from 17 deg for $\upsilon = 0.15$, to 14 deg for $\upsilon = 0.30$, and ultimately to 12 deg for $\upsilon = 0.38$.

This is due to the fact that F_h increases with increasing value of Poisson's ratio, while F_v remains essentially constant.

Conclusions on the effect of Poisson's ratio of the backfill

211. The value of Poisson's ratio assigned to the backfill influences the magnitudes of the resultant forces acting on the wall and several of the parameters which characterize its stability. As the magnitude of Poisson's ratio increases, the lateral force applied by the backfill increases, tending to destabilize the wall. The shear force on the back of the wall decreases slightly with increasing value of Poisson's ratio, but the shear force on the vertical plane through the heel of the wall remains essentially constant. The degree of soil-structure interaction, as measured by the EPI, was essentially the same for all three cases.

Effect of Unit Weight of the Backfill

212. One analysis was performed to determine the effect of changing the unit weight of the backfill. The analysis (run 16a as shown in Table 6) was performed using the finite element mesh shown in Figure 51. All of the parameters were the same as the base case (run 13a), except that the unit weight of the backfill was reduced from 135 to 120 pcf.

Forces on section B-B

213. The magnitude of the resultant lateral force, F_h, acting on section B-B was found to be proportional to the unit weight assigned to the backfill. As in Table 6, when the unit weight was decreased from 135 to 120 pcf (11 percent) the calculated value of F_h also decreased by 11 percent. The value of the lateral earth pressure coefficient, K_h, which for section B-B corresponds to K_o, was 0.51 for both analyses. The calculated lateral force acts at the same normalized height (0.35·H) for both analyses. The shear force on section B-B was zero in both analyses, and K_v and δ_m were also equal to zero.

Forces on the wall

214. The magnitude of the resultant shear force, T, on the base of the wall changed in proportion to the unit weight of the backfill. For horizontal equilibrium, the lateral force applied by the backfill must be equal to T, and the magnitudes of both forces are thus influenced in exactly the same way.

215. The magnitude of the normal force, N, on the base of the wall decreased as the unit weight assigned to the backfill decreased. The magnitude of this change is about 3.6 percent, only about one-third as large as the percentage change in the shear force on the base. The difference stems from the fact that a large portion of N is due to the weight of the wall, the same in runs 13a and 16a. Because the magnitude of N decreases by a smaller percentage than the magnitude of the horizontal load on the wall, the value of x_n (the distance from the toe to N) increases.

216. The normalized effective base contact area, B_e/B, is larger for the analysis using the lower unit weight backfill by about the same proportion as the change in the backfill density. When the backfill density was decreased by 11 percent, the value of B_e/B increased by the same percentage. Also, as the effective base contact area increases, the maximum compressive stress developed at the toe decreases in the same proportion.

217. The mobilized friction angle on the base, δ_{mb}, decreased from 24.5 to 22.8 deg (by 10 percent) as the density was decreased from 135 to 120 pcf (by 11 percent).

218. The lateral deformation at the crest of the monolith, u_x, decreased from $0.000063 \cdot H$ for $\gamma = 135$ pcf to $0.000053 \cdot H$ for $\gamma = 120$ pcf. Thus, an 11-percent reduction in density resulted in a 16-percent reduction in horizontal movement.

Forces on section C-C

219. The magnitudes of the shear and normal forces, F_s and F_n, acting on section C-C changed in the same proportion as the change in backfill density. The normal forces act at the same point along the interface, reflecting the same normalized stress distributions. The mobilized friction angle for section C-C is the same (24.6 deg) for the two analyses.

Forces on section A-A

220. The magnitude of the vertical shear force, F_v, varies in proportion to the density of the backfill. The vertical shear stress coefficient, K_v, is equal to 0.14 for both analyses, since the value of F_v changes in proportion to the change in density.

221. The lateral force, F_h, acting on section A-A is proportional to the backfill density, all other things being equal. The lateral earth pressure coefficient, K_h, was equal to 0.45 for run analyses 13a and 16a, since the value of F_h varies in proportion to the unit weight of the backfill. Also, the ratio of K_h/K_o was the same for both analyses ($K_h/K_o = 0.88$), as

was the earth pressure index (EPI = 0.21). The normalized lateral stress distribution was also the same, with the resultant lateral force acting at a height of $0.37 \cdot H$ in both cases. Similarly, the mobilized angle of friction was the same (δ_m = 17 deg for both analyses).

Conclusions on the effect
of the density of the backfill

222. As the magnitude of the unit weight decreases, the lateral thrust applied by the backfill decreases, resulting in greater stability of the wall. The magnitudes of the shear forces, F_s on section C-C and F_v on section A-A, decreased as the magnitude of the backfill unit weight decreased. However, the vertical shear stress coefficient, K_v, for section A-A was equal to 0.14 for both values of unit weight.

Effect of Soil Backfill in Front of the Toe of the Wall

223. The finite element meshes used in evaluating the effect of toe fill are shown in Figures 51 and 52. Both meshes represent a monolith 40 ft in height with a 16-ft-wide base. The mesh in Figure 52 differs from that in Figure 51 by the addition of 17.8 ft of fill at the toe of the monolith. The standard set of material properties were used in both analyses. The results for the two analyses (runs 13a and 17a) are summarized in Table 6.

Forces on section B-B

224. Since both analyses were assigned the same backfill material parameters, the magnitude and distribution of the resultant forces acting on section B-B are the same. This is due to the fact that the results for this section are solely dependent upon the properties of the backfill. The lateral earth pressure coefficient, K_h, which for section B-B is equal to K_o, was equal to 0.51, as mentioned in paragraph 213.

Forces on the wall

225. The response of the wall is summarized in Table 6 using the resultant normal and shear forces acting on the base and the lateral movement of the crest. Due to the presence of the toe fill in the second analysis, the base interface is no longer required to provide the entire resistance to the forces exerted on the wall by the backfill. The magnitude of the resultant shear force, T, was 24 percent smaller when the toe fill was present. The distribution of the shear stress along the base was similar, but its magnitude was smaller, as shown in Figure 54.

226. The magnitude of the resultant normal force, N, increased by 3 percent as a result of the downward shear force exerted on the front of the wall by the toe fill. The distributions of the normal stresses along the base are similar for the two cases, as shown in Figure 54. The resultant normal force acts at a larger distance from the toe when the toe fill is present.

227. The effective base contact area, B_e/B, was slightly larger, 0.5 compared to 0.45, with the toe fill, and the maximum compressive stress decreased by 16 percent. The mobilized friction angle along the base (δ_{bm}) decreased from 24.5 to 18.6 deg as a result of the toe fill. The normalized lateral deformation at the crest of the monolith, u_x/H, was reduced by about 21 percent (from 0.000063 to 0.000050) by the toe fill.

Forces on section C-C

228. The magnitude of the shear and normal forces, F_s and F_n, on section C-C were the same for the two analyses. This appears to be due to the fact that the backfill properties were the same and the lateral deformations of the wall were nearly the same in both cases. The normal forces act at the same location along the interface, reflecting the same distribution of normal stresses. The mobilized friction angle for section C-C was 24.5 deg for run 17a (with toe fill) as compared to 24.6 deg for run 13a (Table 6).

Forces on section A-A

229. The vertical and lateral forces, F_v and F_h, on section A-A are very nearly the same for both analyses. In Figure 55, the distributions of normal and shear stresses for section A-A are the same for both cases. The lateral stresses are considerably higher than those corresponding to an active condition. The mobilized angle of friction is the same for the two analyses (δ_m = 17 deg). Figure 55 shows the distribution of mobilized angle of friction with depth. Its value ranges from 0 deg at the surface of the backfill to a maximum value of 25 deg near the foundation.

Forces on section H-H

230. Like section B-B, the stresses developed along vertical section H-H are independent of the movement of the wall. The lateral earth pressure coefficient, K_h, at this section corresponds to the at-rest earth pressure coefficient, K_o, and is equal to 0.6. The reason for the differences between the K_o values for sections B-B and H-H is that fewer lifts were used in placing the toe fill. When each lift is placed, the stresses in the new lift correspond to $K_o = 1.0$. As more lifts are placed, the average value of K_o gradually decreases from $K_o = 1.0$ to a lower value. Thus the

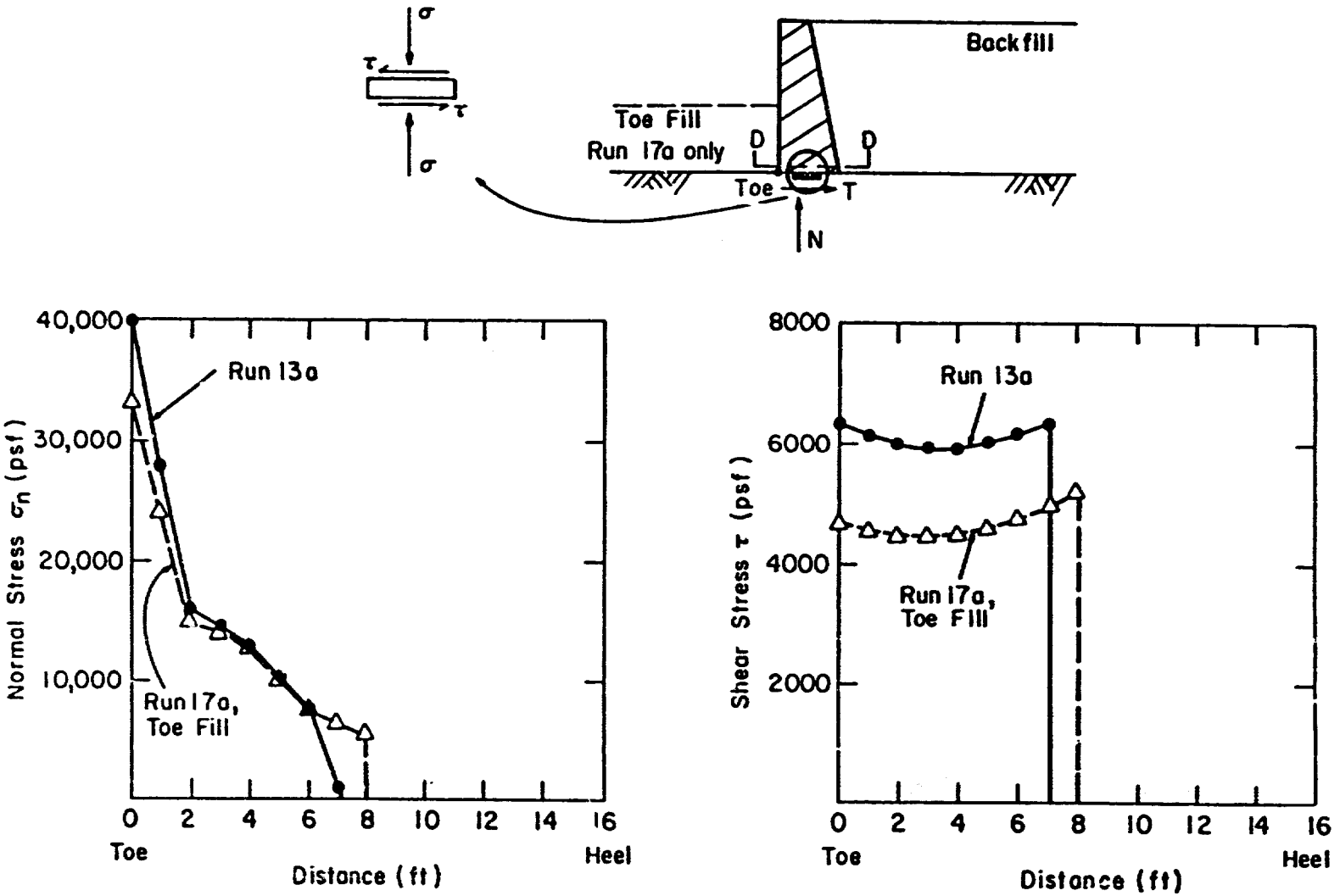

Figure 54. Stress distributions along the base of a structure with and without toe fill

average value of K_o decreases as the number of layers increases. The value of K_o thus decreases with depth. This is reflected in the normalized depth at which the resultant lateral force acts.

231. The fact that K_o varies with depth in the backfill and the toe fill complicates the distribution of stresses somewhat. However, the analytical procedures that give rise to these stress conditions were considered to be necessary for the following reasons:

a. Clough and Woodward (1967) showed that calculation of reasonable stresses in fills placed in layers is only possible if each layer has negligible stiffness when placed, so that it does not "bridge over" uneven displacements in the underlying layer. Thus to meet this criterion, newly placed elements were assigned very small values of Young's modulus. Because the values of bulk modulus are not reduced, however, the newly placed elements have the properties similar to those of a dense liquid, with $K_o = 1.0$.

b. Usually, because $K_o = 1.0$ is considered not representative of the properties of real soils, the horizontal stresses in newly placed layers are assigned the smaller values of K_o input by the user. In the present analyses, however, this could not be done. If the horizontal stresses in the newly placed layers had been reassigned arbitrarily, the correspondence between element stresses and nodal point forces would have been lost, and precise evaluations of the results as explained previously would not have been possible.

232. As a matter of fact, however, it is not unreasonable that values of K_o decrease with depth in compacted fills. Compaction induces higher lateral stresses near the surface of the fills, and the value of K_o therefore decreases with depth in the top 5 to 15 ft of the fill (Duncan and Seed 1986).

Forces on section E-E

233. Section E-E is a vertical plane that passes through the toe of the monolith and corresponds to the interface between the toe fill and the wall. The magnitude of the vertical shear stress coefficient, K_v, is equal to 0.16 for plane E-E, and the lateral earth pressure coefficient, K_h, is equal to 0.55. The ratio of the lateral earth pressure coefficient for section E-E divided by the at-rest earth pressure coefficient, K_o, is equal to 0.92. The mobilized angle of friction has approximately the same value, 16 deg, as for section A-A.

Conclusions on the effect of toe fill

234. Toe fill has a stabilizing influence on the wall. The forces exerted on the back of the wall (planes C-C and A-A) are changed very little

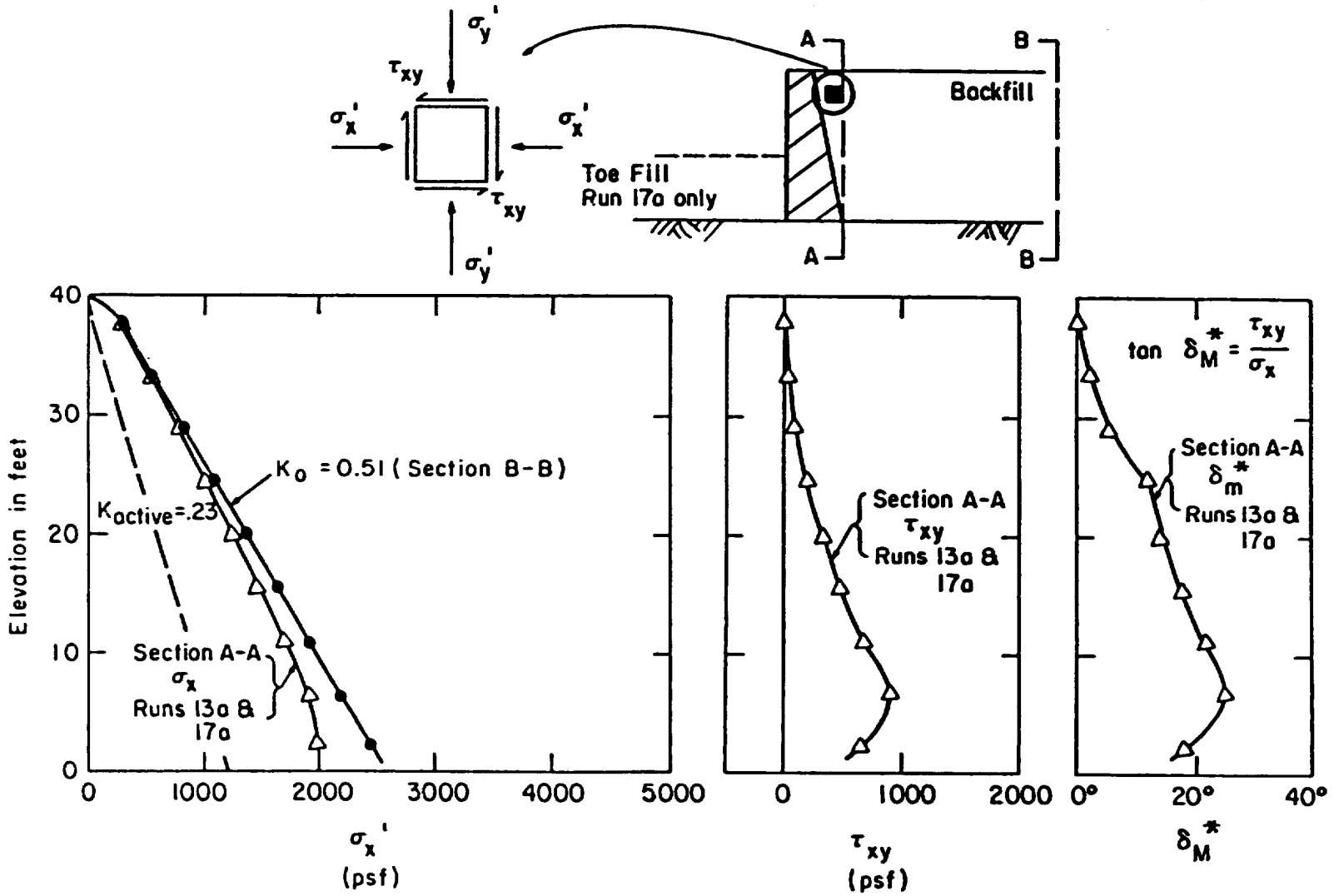

Figure 55. Distributions of stress and mobilized angle of friction on section A-A with and without toe fill

by the toe fill. However, as a result of the forces exerted on the wall by the toe fill, the forces on the base of the wall are changed significantly, and the stability of the wall is improved.

Effect of Wall Deflections

235. The forces exerted on the wall by the backfill are influenced by two types of movement that occur during placement of the backfill. The first is settlement of the fill under the weight of overlying layers. Although this movement is not large, it results in a downward shear load on the back of the wall. The second type of movement that affects the forces on the wall is deflection of the wall itself due to the backfill loads. As the wall deflects from the backfill, the backfill loads decrease. Also, to the extent that the back of the wall may rotate upward in relation to the backfill as the wall deflects laterally, the wall movements may tend to increase the shear force acting on the back of the wall. In the previous analyses these effects were always coupled. Run 18a was analyzed to uncouple these effects. In run 18a, no movement of the wall was permitted, thus eliminating this aspect of soil-structure interaction.

236. The results for the fixed wall analysis (run 18a) are summarized in Table 6. These results can be compared to those of runs 13a and 17a, in which the wall was free to displace, to determine the effects of wall movements.

237. It may be seen that the magnitudes of the forces acting on sections C-C and A-A are the same with and without wall movement. This is also true for the forces developed along section E-E. The vertical shear stress coefficient K_v, for section A-A is equal to 0.14 and for section E-E is equal to 0.16.

238. It is interesting to note that the ratio of K_h/K_o for section A-A is 0.9 rather than 1.0, as might have been expected. This indicates that the compliance in the interface elements along the back of the wall is more important than the movement of the wall itself in controlling the magnitudes of the earth pressures exerted on the wall by the backfill. A similar result is observed for section E-E.

The Effect of Shear Stiffness of the Interface Between the Monolith and its Foundation

239. One analysis was performed to determine the influence of changing the shear stiffness of the interface between the base of the monolith and its foundation. The analysis (run 19a) was performed using the finite element mesh shown in Figure 52, and this includes toe fill. All of the parameters were the same as for the base run 17a with toe fill except that the shear stiffness for the interface between the monolith and its foundation (K_s) was reduced from 10,000 to 10 pci. The results are summarized in Table 6.

Forces on section B-B

240. The magnitudes of the resultant lateral forces, F_h, acting on section B-B are the same for runs 17a and 19a, due to the fact that the soil properties were the same. The lateral earth pressure coefficient, K_h, corresponds to K_o and is equal to 0.51, as discussed previously.

Forces on the wall

241. The magnitude of the resultant shear force, T, on the base of the wall decreased when the base interface shear stiffness was reduced. T decreased from 37,300 lb for run 17a to 5,500 lb for run 19a, an 85-percent reduction. Figure 56 shows that the distribution of the shear stress is considerably different for the two runs.

242. The magnitudes of the resultant normal forces, N, for the two runs differ by only 2 percent. Figure 56 shows that the distributions of the normal stresses along the base were similar. The value of x_n (the distance from the toe to N) increased from 2.8 ft for run 17a to 4.1 ft for run 19a (a 47-percent increase).

243. The effective base contact area, B_e/B, increased from 0.5 to 0.75 (a 50-percent increase), and the maximum compressive stress decreased by 34 percent. The mobilized friction angle along the base, δ_{bm}, decreased from 19 to 3 deg. The lateral deformation at the crest, u_x/H, increased twelve fold (from 0.000050 to 0.000607). These results indicate that when the magnitude of the shear stiffness for the interface at the base of the wall is reduced, there is a tendency for sliding along the base, rather than rotation about the toe. The larger movement mobilizes greater stabilizing forces within the toe fill.

Forces on section C-C

244. In run 19a, the magnitude of the resultant shear force, F_s, on

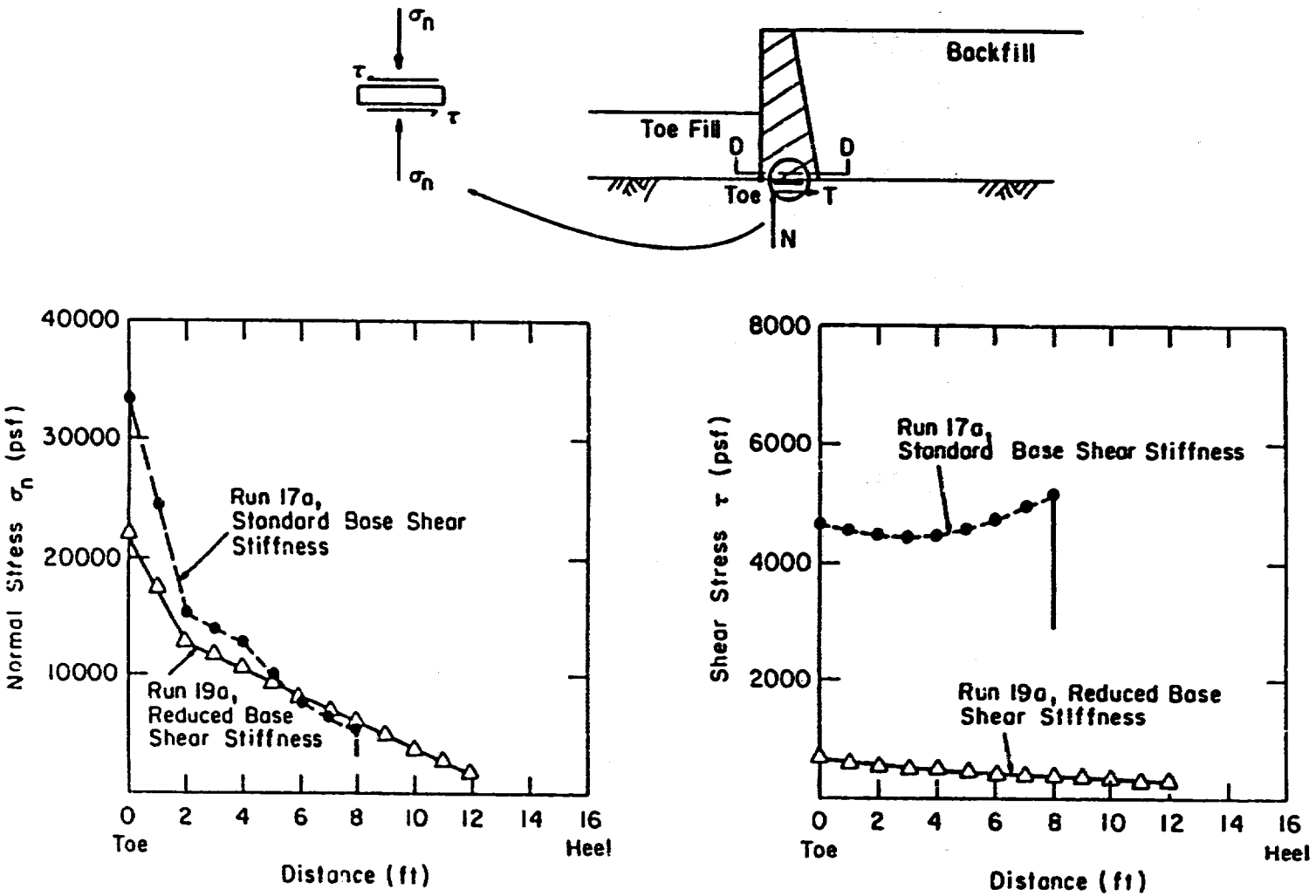

Figure 56. Stress distributions along the base for the standard and reduced base shear stiffness analyses

section C-C increased by 8 percent and the normal force (F_n) decreased by 23 percent, as compared to the results for run 17a. The point of action of the normal force (as measured from the heel) increased from $0.37 \cdot L$ to $0.42 \cdot L$, and δ_m increased from 24.5 to 32.4 deg (32 percent).

Forces on section A-A

245. The vertical resultant force, F_v, acting on section A-A differs by less than 1 percent, and the vertical shear stress coefficient, K_v, equals 0.14 for both runs 17a and 19a. Figure 57 shows that the distribution of shear stress is about the same. The lateral resultant force, F_h, decreased by 26 percent as the lateral movement of the wall increased. The lateral earth pressure coefficient, K_h, decreased from 0.45 for run 17a to 0.34 for run 19a and remained greater than K_a (0.23). The increased lateral wall movements (run 19a) result in lower lateral earth pressures, as shown in Figure 57. The larger displacements were sufficient to develop an active state of stress within soil element 150, located adjacent to the heel of the wall.

246. Two stress paths for element 150 are shown in Figure 58; one resulting from the backfilling in the fixed wall analysis (run 18a), and the second for the backfilling analysis in which a reduced base shear stiffness was assigned (run 19a). These stress paths are loci of points describing the states of stress on the plane of maximum shear, in terms of p (the average of the major and minor principal stresses) and q (the maximum shear stress). The stress path in the fixed wall analysis was almost linear and did not approach the failure envelope. However, in run 19a the wall moved away from the backfill sufficiently to develop an active state of stress in soil element 150. The computed ultimate stresses slightly exceed those defining the failure envelope because of the finite load increments used in the analysis.

247. K_h/K_o for section A-A decreased from 0.88 for run 17a to 0.67 for run 19a (a 24-percent decrease). The EPI increased from 0.21 to 0.61, reflecting the increased soil-structure effect of interaction with larger movement. The mobilized angle of friction on plane A-A increased from 16.8 to 22.2 deg (32 percent). The distribution of δ_m ranges from 0 deg at the surface of the backfill, to more than 39 deg near the foundation, as shown in Figure 57.

Forces on sections H-H and E-E

248. The lateral earth pressure coefficient, K_h, for section H-H is

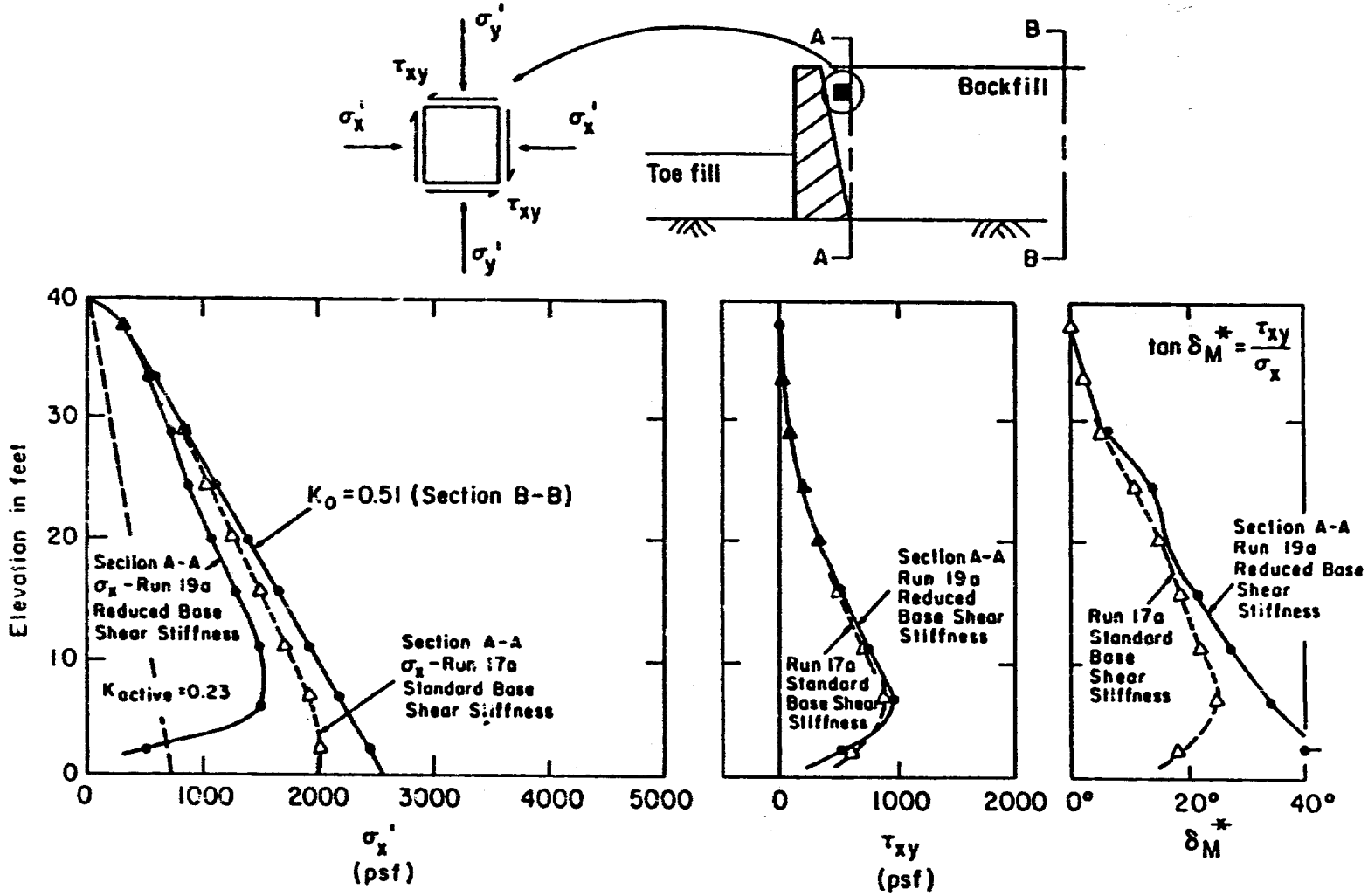

Figure 57. Distributions of stress and mobilized angle of friction on section A-A for the standard and reduced base shear stiffness analysis

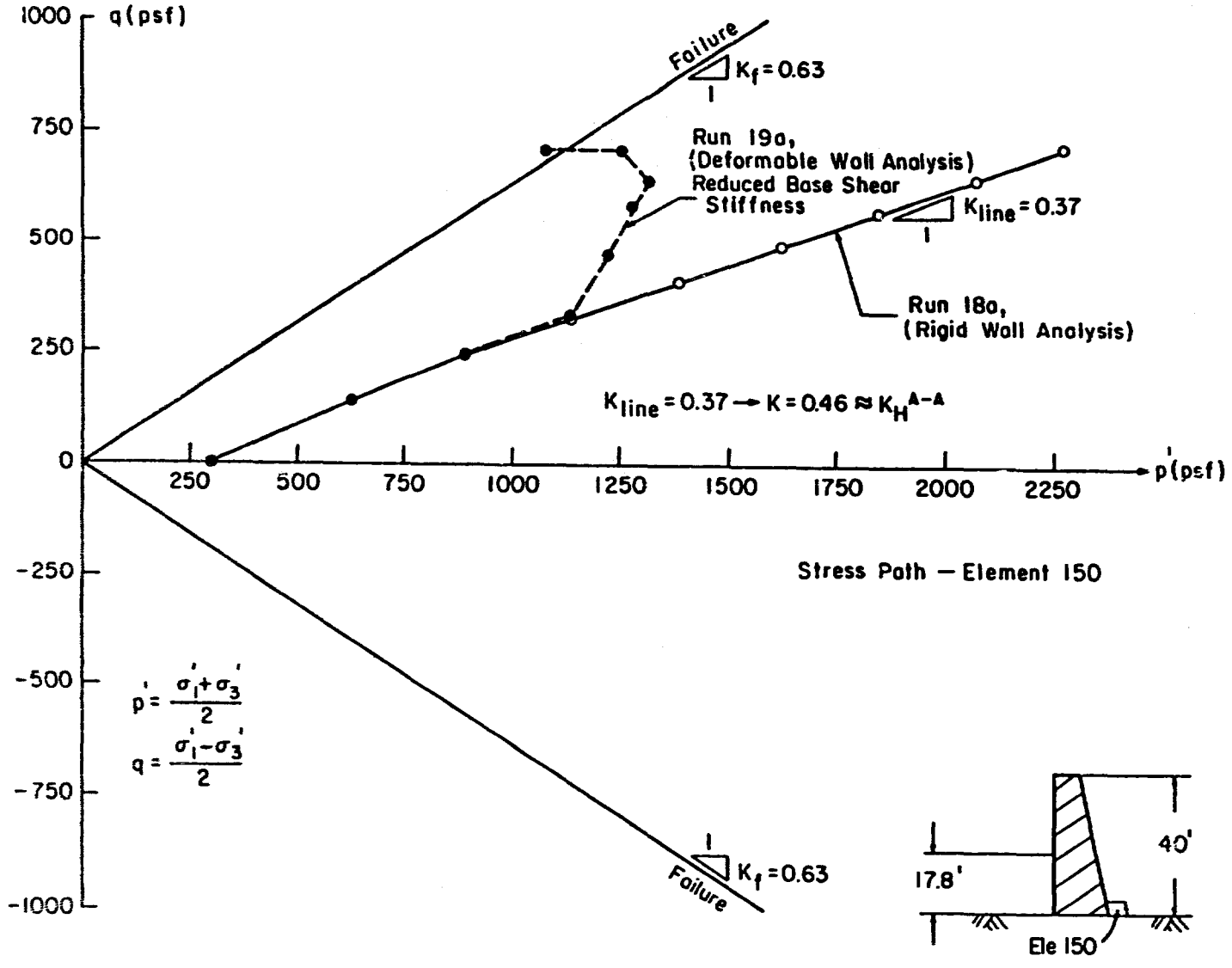

Figure 58. Stress paths for soil element 150, adjacent to the heel of the wall

0.6, and is equal to K_o , the same as for run 17a. Section H-H is sufficiently far from the wall so that the earth pressures at this section were not affected by the wall movement.

249. The shear force, F_v , on section E-E acts downward and was equal to 3,342 psf for run 17a. For the fixed wall analysis of run 18a, it was almost the same, 3,490 lb/ft. For run 19a, the value of F_v was smaller (1,479 lb/ft), and it still acted downward. The vertical shear stress coefficient, K_v , decreased from a value of 0.16 for runs 17a and 18a to 0.07 for run 19a (56 percent).

250. The relationship between the wall displacements and F_v is shown in Figure 59. F_v attained its maximum value after placement of the fourth, and final, soil layer in front of the wall for the three cases. As backfilling continued behind the wall, F_v was constant for the first two analyses because the wall movements were zero (run 18a) or very small (run 17a). In run 19a, F_v decreased in magnitude as the wall displaced toward the toe fill during placement of the fifth and subsequent lifts of backfill behind the wall. This resulted from the plowing action as the wall moved toward the toe fill and the tendency to develop an upward shear force on the wall as the soil moved upward along the front face of the wall.

251. The magnitude of the lateral force, F_h , is also related to the wall displacements shown in Figure 59. The value of F_h increased about threefold, from a value equal to 11,711 lb for run 17a, to 11,311 lb for run 18a, to 30,930 lb for run 19a. The amount of movement was not sufficient to develop the maximum passive force. The value of K_h increased from 0.55 to 1.45 and the value of K_h/K_o increased from 0.92 to 2.41. The mobilized angle of wall friction decreased from 16 to 3 deg.

252. The stress paths for soil elements 81 and 84 (adjacent to the wall) are shown in Figure 60 for run 19a. The stress path for element 81 located near the surface of the toe fill is inclined slightly toward the failure envelope and might have reached it with greater wall movement. The stress path for element 84, which is nearer the foundation, has two distinct segments. The first part of the stress path reflects the effect of backfilling in front of the wall. The second part reflects the effect of filling behind the wall and is parallel to the stress path for element 81.

Forces, earth pressure
coefficients, and wall displacements

253. The relationship between the magnitudes of the forces acting on

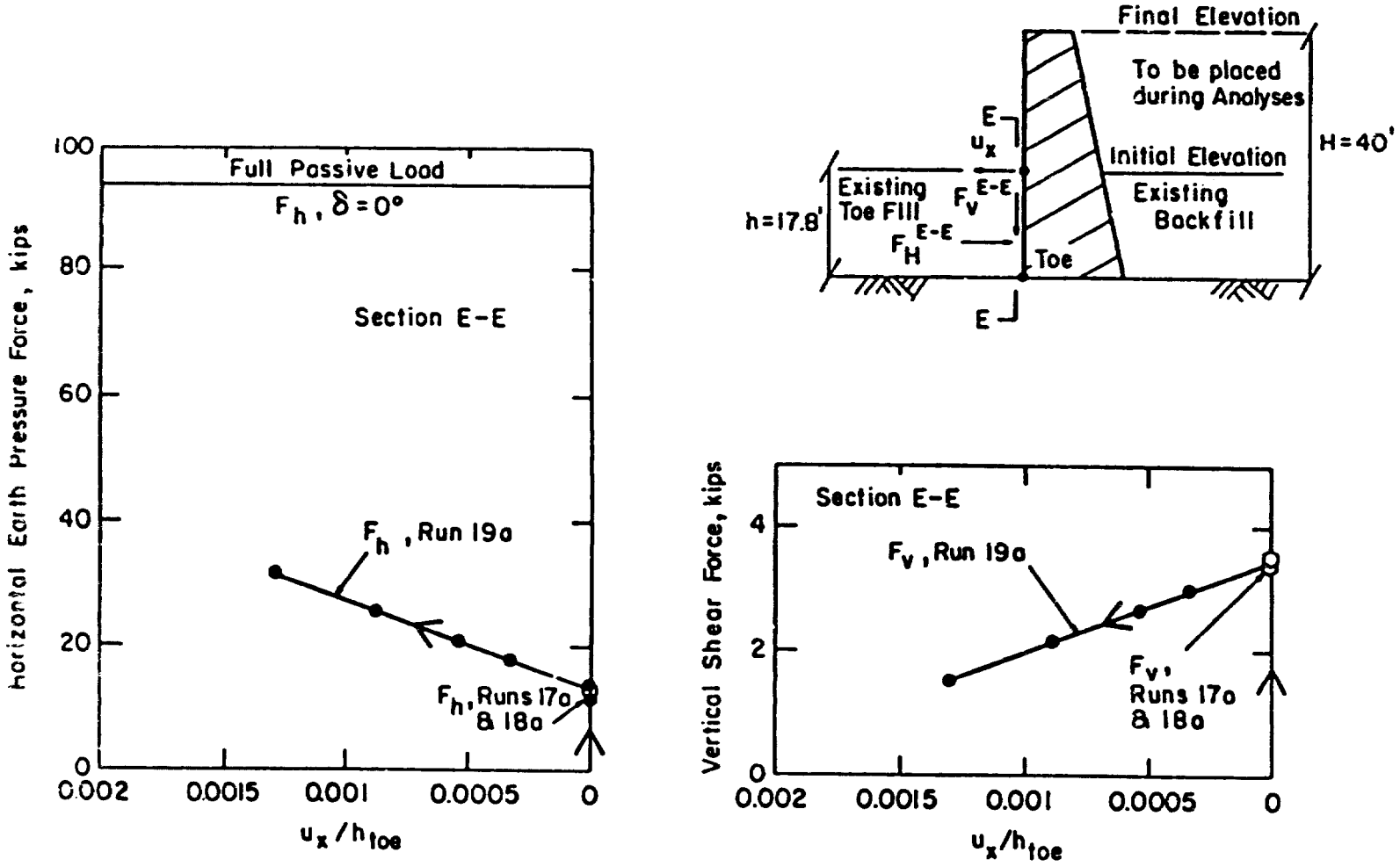

Figure 59. Development of lateral and vertical forces on section E-E

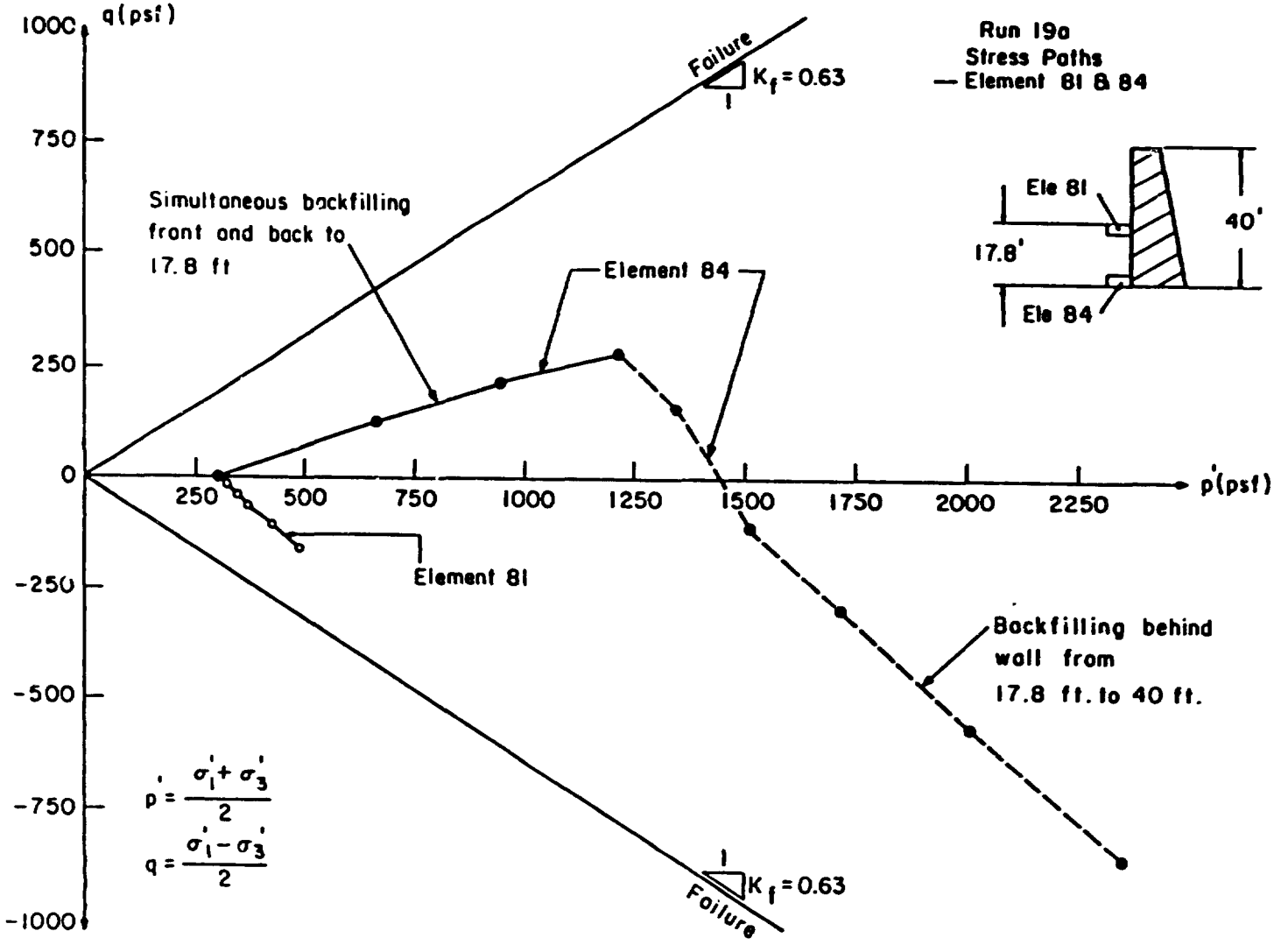

Figure 60. Stress paths for soil elements 81 and 84, adjacent to the toe of the wall

the wall and its displacement is shown in Figure 61 (runs 17a and 19a). Since the wall movements were directed away from the backfill and toward the toe fill, the magnitude of F_h on section A-A decreased and the magnitude of F_h on section E-E increased. The contribution of T to the horizontal equilibrium of the wall decreased as wall movements increased, because the toe fill provided greater resistance to the force exerted by the backfill, and the force exerted by the backfill was smaller. The wall displacement for run 19a was not large enough to develop an active state behind the wall nor a passive state in front of the wall.

254. Figure 62 shows the variations in the values of lateral earth pressure coefficients, K_h, in front of and behind the wall with wall displacements. K_h is plotted versus the lateral displacements at the crest of the wall, u_{x1}/H, for section A-A, while K_h for section E-E is plotted versus the lateral displacements of the front of the wall at the surface of the toe fill u_{x2}/h_{toe}. The results show that F_h decreases on the back of the wall and increases on the front of the wall as the displacement of the wall increases.

Conclusions on the effect of the shear stiffness of the interface between the wall and its foundation

255. The magnitude of the shear stiffness assigned to the interface between the wall and its foundation influences the wall movements and the magnitude of the forces acting on the wall. A reduction in the shear stiffness of the base interface resulted in increased displacements of the wall, decreased value of F_h on section A-A, increased value of F_h on section E-E, and decreased value of T. The magnitude and direction of F_v on section E-E is dependent upon the magnitude of the wall movements. The vertical shear stress coefficient for section A-A (K_v) is essentially constant, equal to 0.14 for the three analyses (runs 17a, 18a, and 19a). The EPI increased from 0.21 (runs 17a and 18a) to 0.61 (run 19a), reflecting the greater soil-structure interaction when the wall displacements are larger.

Comparison of Results of Conventional Equilibrium and Finite Element Analyses

256. The CEA of the structures discussed previously were performed for the purpose of comparing the results with the results of FEA. Analyses were

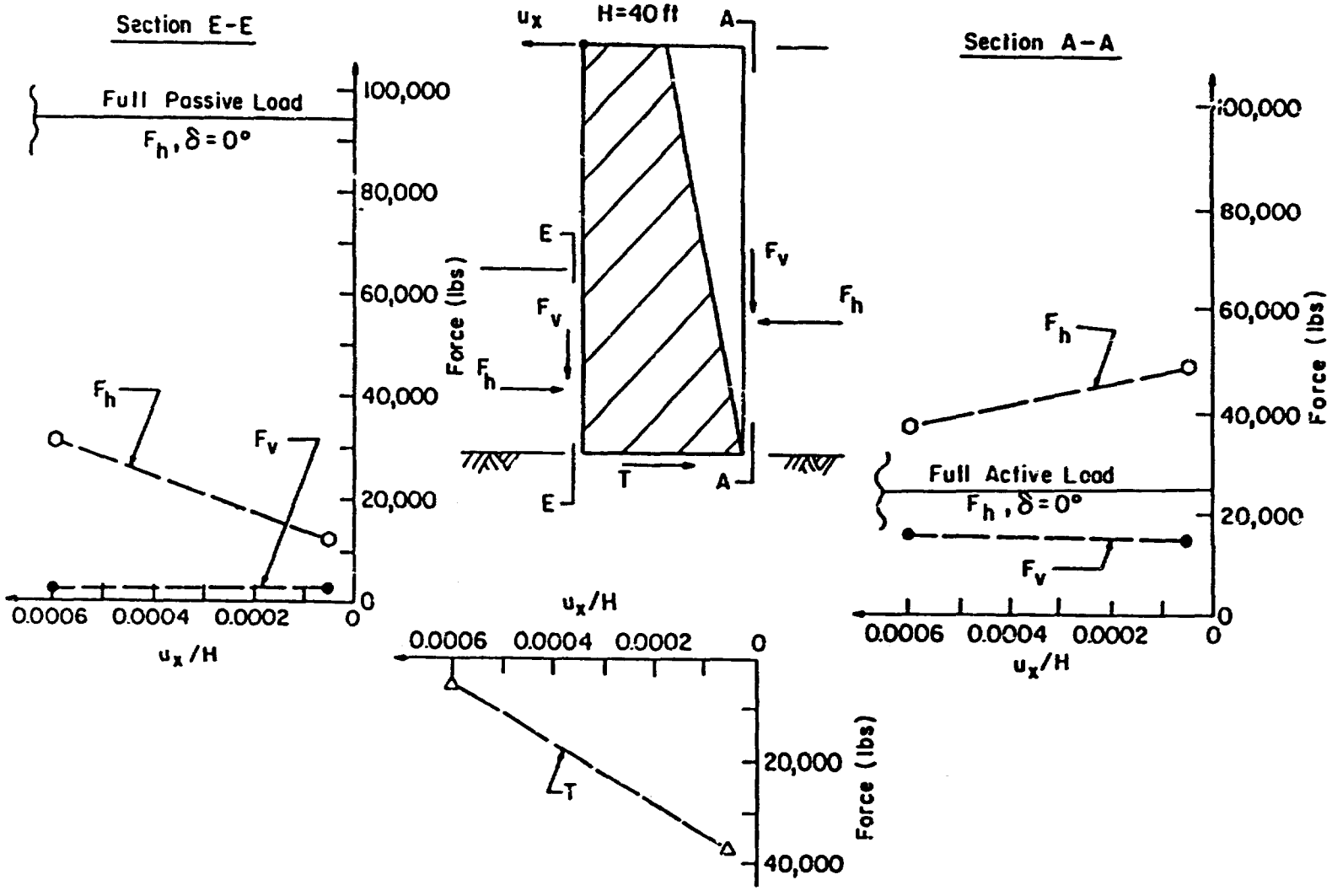

Figure 61. Forces acting on the wall versus normalized lateral displacements of the wall

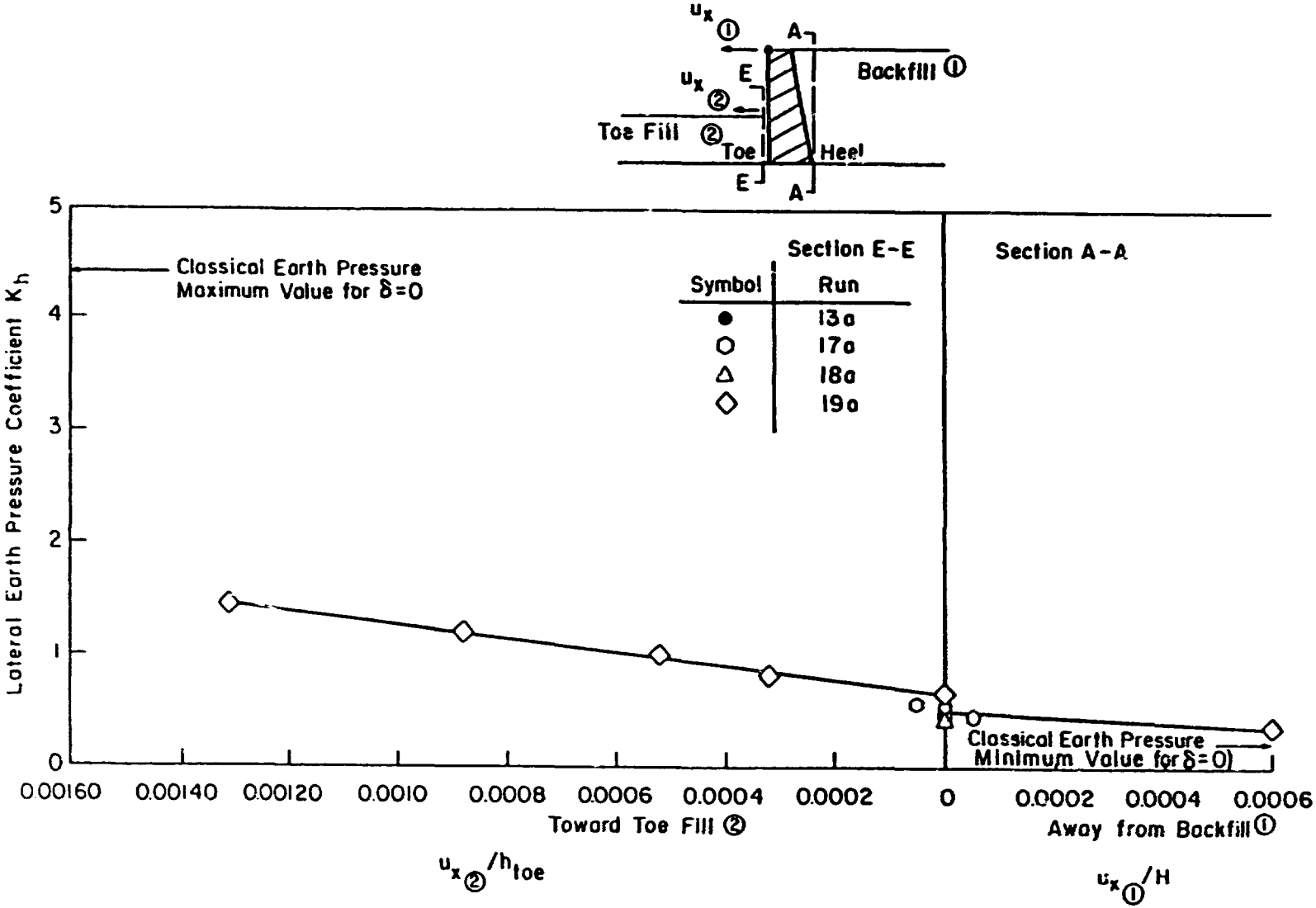

Figure 62. Lateral earth pressure coefficients versus normalized lateral wall displacements

performed for structures with and without toe fills. The results are summarized in Table 7.

257. The CEA differed from the FEA in two important ways:

a. In the CEA, the at-rest earth pressure force, corresponding to $K_o = 0.51$, was applied to plane A-A, the vertical plane through the heel of the wall. In the FEA, the force on plane A-A was smaller, because of the wall movement from right to left as the backfill was placed. For the finite element analyses, K_h was 0.45.

b. In the CEA, no vertical shear force was applied on plane A-A. In the FEA, a downward shear force developed on plane A-A as the backfill settled under its own weight. The value of K_v for plane A-A was thus equal to zero for the CEA, whereas $K_v = 0.14$ for the FEA.

258. As a result of these differences in loading, the FEA resulted in a smaller shear force and a larger normal force on the base of the structure. These differences had a considerable effect on the value of the factor of safety against sliding and the ratio of moments about the toe (RM). The value of RM was calculated using the following equation:

$$RM = \frac{\text{Sum of stabilizing moments about the toe}}{\text{Sum of overturning moments about the toe}} \quad (20)$$

259. Using the CEA forces on the base of the structure, the mobilized base friction angle of 30.5 deg was equal to the assumed angle of sliding resistance for the interface. The factor of safety against sliding calculated using CEA is, thus, 1.00. Using the FEA forces, however, the mobilized friction angle is only 24.6 deg, corresponding to a factor of safety against sliding equal to 1.29.

260. Using the CEA forces, x_n was equal to 0.02 ft, RM was equal to 1.0, and B_e/B was equal to 0.3 percent. On this basis therefore, it would be concluded that the wall was on the verge of instability. Using the FEA forces, however, the value of x_n was 2.14 ft, RM was 1.32, and B_e/B was 45 percent. Thus, while the wall does not satisfy current criteria for new walls, it is clearly stable.

261. There is also a considerable difference between the values of maximum bearing pressure at the toe calculated using the two analysis procedures: The CEA results indicate that the effective base contact area is very small, with the wall nearly balanced on its toe. The calculated value of q_{max} was 3,700,000 psf (25,700 psi), a value that would surely result in

Table 7

Comparisons Between the Results Using the Conventional Equilibrium Analysis and the Finite Element Analysis for Three Structures

Method of Analysis	H ft	B/H	h_{toe} ft	h_{toe}/H	K_o Section B-B	K_o Section H-H	Monolith W_C lb	Monolith X_{WC} ft	Backfill Wedge W_S lb	Backfill Wedge X_{WS} ft	Base of Monolith T lb	Base of Monolith N lb	Base of Monolith X_n ft	Base of Monolith B_e/B
CEA	40	0.4	--	--	0.51	--	72,000	6.22	21,600	2.67	55,080	93,600	0.017	0.003
FEA Run 13a									20,520	2.88	48,922	107,408	2.14	0.45
CEA	40	0.4	18	0.45	0.51	0.6	72,000	6.22	21,600	2.67	42,248	93,600	0.83	0.16
FEA Run 17a									20,534	2.84	37,299	110,671	2.81	0.50
CEA	40	0.4	18	0.45	0.51	0.6	72,000	6.22	21,600	2.67	42,248	93,600	0.83	0.16
FEA Run 19a									19,934	5.63	5,475	108,276	4.14	0.75

Note: CEA = Conventional equilibrium analysis; FEA = Finite element analysis; -- indicates no toe fill, thus no values

(Continued)

Table 7 (Concluded)

Method of Analysis	Base of Monolith		Section A-A			Section E-E			Factor of Safety Against Sliding	Ratio of Moments About the Toe
	q_{max} psf	δ_{bm} deg	F_v lb	F_h lb	h_{Fh} ft	F_v lb	F_h lb	h_{Fh} ft		
CEA	3.7×10^6	30.5	0	55,080	13.3	--	--	--	1.0	1.0
FEA Run 13a	4.0×10^4	24.6	14,888	48,922	14.7	--	--	--	1.29	1.32
CEA	7.5×10^4	24.3	0	55,080	13.3	0	12,832	5.9	1.30	1.11
FEA Run 17a	3.3×10^4	18.6	14,795	49,008	14.7	3,342	11,713	6.6	1.75	1.43
CEA	7.5×10^4	24.3	0	55,080	13.3	0	12,882	5.9	1.30	1.11
FEA Run 19a	2.2×10^4	2.9	14,863	36,405	16.8	1,479	30,930	5.4	11.6	1.73

crushing of the concrete. The FEA results, however, indicate that nearly one-half of the base is in contact with the underlying rock. The calculated value of q_{max} in this case is 40,000 psf (278 psi), a weight that could be carried by the concrete without distress.

262. Thus, the differences between the results of the CEA and the FEA are very significant. Primarily because the CEA includes no shear force on the vertical plane through the heel of the wall, the CEA results indicate that the wall is on the verge of failure in sliding and in overturning and is beyond failure in regard to the stress on the concrete at the toe of the wall. The FEA results, however, indicate the factor of safety against sliding and the ratio of moments about the toe in the neighborhood of 1.3, about one-half of the base still in compression and clearly tolerable compressive stresses at the toe of the wall.

263. Similar analyses were done for a wall with toe fill, and the results were compared with the results of FEA runs 17a and 19a, as shown in Table 7. In the conventional analyses, the at-rest forces were applied to both the back and the front of the wall. The values of K_o used were the same as found from the FEA, $K_o = 0.51$ for the backfill and $K_o = 0.6$ for the toe fill. No vertical shear forces were applied in the CEA. However, as discussed previously, shear forces on the vertical planes through the heel and the toe were found to develop in the FEA, and these have a significant effect on the behavior of the wall.

264. The CEA results are compared to the FEA results for the case of a stiff base interface and small wall movement (run 17a) and for the case of a very much less stiff base interface (run 19a) in Table 7.

265. In run 17a, where the base interface is stiff and the wall movements are small, the toe fill force is very close to the at-rest value. In run 19a, where the base interface is not as stiff, the wall moves sufficiently from the right to the left to develop an appreciable amount of passive resistance on the toe. The toe force in this case is about 2.5 times the at-rest force.

266. As can be seen in Table 7, the force exerted by the toe fill can have a significant influence on the stability of the wall. The results of the CEA, including a toe force, are appreciably different from the results of the CEA with no toe force:

a. The factor of safety against sliding increases from 1.0 to 1.3 through inclusion of a toe force.

b. The ratio of moments about the toe increases from 1.0 to 1.1.

c. The effective base contact area increases from 0.3 to 16.0 percent.

d. The compressive stress at the toe decreases from 3,700,000 psf (25,700 psi) to 75,000 psf (521 psi).

267. The FEA results indicate even greater stability and smaller compressive stresses at the toe, since they include vertical shear forces on the toe and heel of the wall. In the case where the base interface is stiff and the wall movements are small (run 17a), the FEA results indicate a factor of safety against sliding equal to 1.75, RM equal to 1.43, an effective base contact area of 50 percent, and a maximum compressive stress of 33,000 psf (229 psi).

268. In the case where the base interface was much less stiff (run 19a), the FEA results indicate a factor of safety against sliding equal to 11.6, RM equal to 1.73, an effective base contact area of 75 percent, and a maximum compressive stress of only 22,000 psf (153 psi). These differences are due to a toe force only 2.5 times as large as the at-rest pressure of the toe fill, corresponding to a movement of the wall of only 0.3 in. from right to left.

269. It is clear from these comparisons that CEA of wall stability are very conservative, due to the fact that they ignore possible vertical shear forces at the heel and toe of the wall, and that they often ignore or greatly discount resisting forces from toe fills. The FEA discussed in this part indicate that appreciable vertical shear loads develop with negligible wall movement, and that appreciable toe resisting forces develop with wall movements less than 1 in.

PART VII: SUMMARY AND RECOMMENDATIONS

270. The program of research described in this report is still in progress, particularly concerning the material described in Part VI. Some of the conclusions reached thus far are therefore considered to be tentative and subject to modifications as the studies continue.

Summary of Objectives

271. This study focuses on two main objectives: (a) developing new finite element procedures for analysis of gravity retaining walls founded on rock to allow insight into the wall behavior under varying degrees of loading and stability conditions; and (b) evaluating the accuracy and reliability of CEA of these structures. Because of several simplifying assumptions made in the conventional analyses that neglect the true process of soil-structure interaction, improvements in the present procedures are needed, and it is likely that the improvements will lead to more realistic and less conservative predictions of response. The latter assertion is supported by the fact that some existing gravity walls under Corps of Engineers jurisdiction (e.g., navigation lock walls) do not satisfy current stability criteria, while at the same time they do not exhibit signs of distress or substandard performance. The studies are divided into two phases--the first phase, completed herein, and the second phase (Ebeling, Duncan, and Clough 1990). The first phase defined the analytical requirements for this category of structure and resulted in the development of new finite element procedures, while the second phase explored the effects of a number of variables on the stability of the wall.

272. The characteristics of Corps of Engineers' retaining structures at three locks (Emsworth, Montgomery, and Troy) were examined to determine what range of wall characteristics should be considered in the analytic studies. A number of dimensionless parameters were established, and it was shown that the conventional criteria of mobilized base friction angle and percentage of effective base contact area are uniquely related to these dimensionless ratios. The hypothetical structures studied in the FEA cover essentially the same range of these dimensionless parameters as do the walls at Emsworth,

Montgomery, and Troy locks, all founded on rock.

273. Two approaches were used in the FEA. The first studies were performed using the following load analysis procedures. The structures were subjected to predetermined earth and water loads that were increased gradually in magnitude. Later studies were performed using backfill placement analysis procedures, in which the placement of backfill behind the walls was simulated, layer by layer.

274. The FEA performed during this study posed difficulties as a result of the fact that portions of the interface between the structure and its foundation are in a condition of incipient instability. Maintaining solution stability and allowing for yielding and stress transfer along the material interfaces required development of refined analysis techniques. Of the three analytical procedures developed, the alpha method proved to be the most accurate and cost effective. This method eliminated the overshoot of the tension and shear stress forces on the interface between the base of the wall and its foundation where a gap developed.

275. In the second phase (Ebeling, Duncan, and Clough 1990), the influence of seven geometric, material, and loading parameters on the response of retaining structures to following loads were studied. The FEA used the alpha method, allowing for the separation of a monolith from its rock foundation. The analysis results show that as expected, smaller base widths and application of uplift forces lessen the stability of the monolith. Also, it is found that for most practical problems, it is not important to incorporate the effect of incremental modeling of the construction of the structure on the initial base stress distribution. Analyses of material parameter effects show that the stiffness of the rock foundation and the interfaces have a selective effect on the behavior of the system in the following load analyses. In addition to the influence of particular parameters, other conclusions can also be drawn:

a. Values of mobilized base friction angles calculated by FEA are in precise agreement with values calculated using CEA procedures.

b. Values of percentage effective base contact area calculated by FEA are somewhat larger than those calculated using CEA.

c. The maximum values of contact pressure between the base of the structure and the foundation calculated by the FEA are somewhat higher than those calculated using CEA.

d. While certain of the parameters showed no significant influence on the results of the following load analyses, this does not necessarily extrapolate to backfill placement analyses. In particular, this applies to base-foundation interface properties.

276. A second phase of parametric studies (Ebeling, Duncan, and Clough 1990) was performed with the loads resulting from simulation of placement of fill behind the wall. The backfill placement analyses are believed to be the most realistic that can be performed using the finite element method. The magnitude of the forces acting on the wall depends on the relative movement of the soil and the wall and requires no assumptions with regard to the applied earth loads. Increases in the values of Poisson's ratio or the unit weight of the soil in turn increase the magnitude of the lateral force applied on the wall, tending to destabilize the wall. As expected, the presence of toe fill has a stabilizing influence on the wall. The level of influence the toe fill has on the stability of the wall depends upon the deformation of the wall.

277. The displacements of the wall have a significant influence on the distribution of both stabilizing and destabilizing forces exerted on the wall by the fill and on the base of the wall. In general, as the wall moves away from the backfill, the lateral forces behind the wall decrease and the lateral forces in front of the wall increase. Calculations indicate that the magnitude of the wall displacements required to develop significant changes in the magnitude of the forces acting on the wall are less than 1 in. for a 40-ft-high wall, less than those required to develop active pressures behind the wall and much less than those required to develop passive pressures in front of the wall.

278. Increased wall displacements may be achieved in many ways, including variances in the magnitudes of the material properties of the backfill and the magnitude of the base-to-foundation interface stiffnesses.

279. A stabilizing force, observed in the results of the finite element computations and not considered in conventional procedures, is a downdrag force on the face of the wall. This force results from the settlement of the soil fill under its own weight and serves to counter the overturning moment, increase the normal force acting on the base, reduce the angle of mobilized base friction, and increase the effective base contact area. The shear force acting on a vertical plane within the backfill and passing through the heel of

the wall has been conveniently described in terms of a vertical shear stress coefficient, K_v . The limited number of calculations found the value of K_v to be within the narrow range of 0.13 to 0.14. However, further studies are required to determine the factors that influence the magnitude of this coefficient. The value and direction of the stabilizing shear force and K_v on the front (toe side) of the wall depend on the deformation of the wall, due to soil- structure interaction considerations.

280. Comparisons between the results of backfill placement analyses and CEA of retaining structures indicate that the conventional analysis is very conservative. This is due to two factors;

a. The conventional analyses ignore possible vertical shear forces at the heel and the toe of the wall.

b. The resisting forces from the toe fill are often ignored or greatly discounted.

Important Unanswered Questions

281. At this stage of the investigation, a number of important questions remain unanswered.

a. Can vertical shear loads on the wall faces be relied upon as permanent contributors to the stability of gravity retaining walls? While it is clearly reasonable that they should develop during backfilling, the FEA used to study their occurrence and magnitude are not capable of showing whether they will persist under field conditions.

b. How does the behavior of gravity retaining walls on soil foundations differ from the behavior of gravity retaining walls on rock? Both would be treated the same in CEA. However, soil foundations are typically more compressible than rock, and the interface between the soil foundation and the overlying structure is not bonded. Both of these characteristics will lead to more structure movement relative to the backfill, and, hence, more redistribution of the earth pressures than in the case of a structure founded on rock.

c. Is it possible that the tendency for overturning of a retaining structure is preempted by sliding after the structure-foundation bond is broken, with sliding leading to reductions of pressure behind the wall and increases in the pressures in front of the wall resulting in stabilizing of the structure? This effect is implied in some of the latest results of our study, and it is thought that it can be modeled more fully in future analyses.

d. Are the currently used methods of applying factors of safety in the design of retaining walls consistent with the fundamentals of the soil-structure interaction process? It appears that there are both explicit and hidden factors of safety in the present procedures, and that improvements on this technique can be found to define a true factor of safety.

Recommendations

282. It is recommended that the questions discussed in paragraph 281 be addressed in subsequent series of second phase analyses (Ebeling, Duncan, and Clough 1990). The studies would include:

a. Data regarding the persistence of shear loads on retaining walls will be reviewed to develop a basis for assessing the permanence and reliability of shear loads as contributors to wall stability. It is expected that the data can be obtained from field instrumentation and large-scale model tests. It is hoped to find the means to reassess the instrumentation at Port Allen and Old River Locks, since in both cases the instrumentation data following construction showed downdrag forces to exist.

b. FEA will be conducted to investigate the influence of the stiffness of the backfill on the magnitude of the shear force acting on the back of the wall and variations (if any) in the magnitude of the vertical shear stress coefficient, K_v .

c. A backfill placement analysis will be conducted to consider the effects of water pressures on the wall and backfill.

d. FEA will be performed to study the behavior of gravity retaining walls founded on soils. The foundation soil will be modeled as a nonlinear medium, the interface elements will be used between the foundation, and the base of the wall will be treated to allow relative movements.

e. An analysis will be attempted to allow for slippage of the gravity retaining structure after the structure has initially tipped enough to break the foundation bond. This should allow a better understanding of those problems where stability is marginal.

f. An assessment will be made of the methods used for inclusion of factor of safety in conventional design analyses. If appropriate, recommendations will be made for improvements in this process.

g. A procedure will be developed to allow simplified determination of the downdrag force on the back of the wall so that, wherever appropriate, it can be included in conventional analyses.

REFERENCES

American Society for Testing and Materials. 1970. "Moisture Density Relations of Soils Using 5.5 lb (2.5 kg) Hammer and 12 in. (304.8 mm) Drop," ASTM D-698-70, 1790 Book of ASTM Standards, Philadelphia, PA.

Benson, C. P., Brandon, T. L., Clough, G. W., and Duncan, J. M. 1987. "Literature Review of Rock Properties for Analysis of Navigation Structures Founded on Rock," Interim report prepared for US Army Corps of Engineers, Virginia Polytechnic Institute and State University, Blacksburg, VA.

Clough, G. W., and Duncan, J. M. 1969 (Sep). "Finite Element Analyses of Port Allen and Old River Docks," Contract Report S-69-6, US Army Engineer Waterways Experiment Station, Vicksburg, MS.

_____. 1971 (Dec). "Finite Element Analyses of Retaining Wall Behavior," Journal, Soil Mechanics and Foundation Division, American Society of Civil Engineers, Vol 97, No. SM12, pp 1657-1673.

Clough, R. W., and Woodward, R. J., III. 1967 (Jul). "Analysis of Embankment Stresses and Deformations," Journal, Soil Mechanics and Foundation Division, American Society of Civil Engineers, Vol 93, No. SM4, pp 529-549.

Duncan, J. M., and Chang, C. Y. 1970 (Sep). "Nonlinear Analysis of Stress and Strain in Soils," Journal, Soil Mechanics and Foundation Division, American Society of Civil Engineers, Vol 96, No. SM5, pp 1629-1653.

Duncan, J. M., and Seed, R. B. 1986 (Jan). "Compaction-Induced Earth Pressures under K_0-Conditions," Journal, Geotechnical Engineering, American Society of Civil Engineers, Vol 112, No. 1, pp 1-22.

Dunlop, P., Duncan, J. M., and Seed, H. B. 1968 (May). "Finite Element Analyses of Slopes in Soil," US Army Engineer Waterways Experiment Station, Vicksburg, MS.

Ebeling, R. M , Duncan, J. M., and Clough, G. W. 1990 (Oct). "Methods of Evaluating the Stability and Safety of Earth Retaining Structures Founded on Rock, Phase 2 Study," Technical Report (ITL-90-7), US Army Engineer Waterways Experiment Station, Vicksburg, MS.

Headquarters, Department of the Army. 1989. "Retaining and Flood Walls," Engineer Manual 1110-2-2502, Washington, DC.

Kulhawy, F. 1974. "Analysis of a High Gravity Retaining Wall," Proceedings of American Society of Civil Engineers Conference on Analysis and Design in Geotechnical Engineering, University of Texas, Austin, Vol 1, pp 159-172.

Meyerhof, G. G. 1953. "The Bearing Capacity of Foundation Under Inclined and Eccentric Loads," 3rd International Conference of Soil Mechanics and Foundation Engineering, American Society of Civil Engineers, Vol 1, pp 440-445.

Pace, C. E. 1976. "Engineering Condition Survey and Structural Investigation of Emsworth Locks and Dam, Ohio River," Miscellaneous Paper C-76-8, US Army Engineer Waterways Experiment Station, Vicksburg, MS.

Pace, C. E., and Peatross, J. T. 1977. "Engineering Condition Survey and Structural Investigation of Montgomery Locks and Dam, Ohio River," Miscellaneous Paper C-77-2, US Army Engineer Waterways Experiment Station, Vicksburg, MS.

Pace, C. E., Campbell, R., and Wong, S. 1981. "Engineering Condition Survey and Evaluation of Troy Lock and Dam, Hudson River," Miscellaneous Paper C-78-6, US Army Engineer Waterways Experiment Station, Vicksburg, MS.

Peterson, M. S., Kulhawy, F. H., Nucci, C. R., and Wasil, B. A. 1976. "Stress-Deformation Behavior of Soil-Concrete Interfaces," Contract Report B-49 to Niagara Mohawk Power Corporation, Syracuse, NY.

Terzaghi, K. 1934 (Feb). "Large Retaining Wall Tests. I. Pressure of Dry Sand," Engineering News Record, Vol III, pp 136-140.

Zienkiewicz, O. C. 1977. The Finite Element Method, McGraw-Hill, New York.

APPENDIX A: CROSS SECTIONS THROUGH CORPS OF ENGINEERS MONOLITHS

1. This appendix contains cross sections through the Emsworth, Montgomery, and Troy lock monoliths showing load cases 1 through 39. The load cases for each cross section are tabulated in Table A1, and the cross sections are shown in Figures A1 through A19.

Table A1

Load Cases 1 through 39 of Emsworth, Montgomery and Troy Lock Monoliths

Case	Lock	Station	Loading*
1	Emsworth	L-3	I
2		L-19	H
3		L-37	NC, H
4		L-37	MC
5		L-52	NC, I
6		L-52	NC, H
7		L-52	MC
8		L-68	I
9		L-68	NC, H
10		M-8	NC, H, I
11		M-8	MC
12		M-22	NC, H, I
13		M-22	MC, I
14		R-4	NC, I
15		R-17	NC, H, W
16		R-17	MC, W
17		R-24	NC, I
18		R-24	MC
19		R-32	NC, I
20	Montgomery	L-19	NC, H
21		L-19	MC
22		L-25	NC
23		L-25	MC
24		M-7	NC, H, I
25		M-7	MC, I
26		M-13	NC, H, I
27		M-13	MC, I
28		R-13	NC, H, I
29		R-13	MC, I
30		R-15	NC, H, I
31		R-15	MC, H
32		R-20	NC, I
33		R-20	MC
34	Troy	L-5	NC
35		L-5	MC
36		L-12	NC
37		L-12	MC
38		L-20	NC
39		L-20	MC

* I = ice loading; H = hawser pull; NC = normal condition; MC = maintenance condition; W = wind loading.

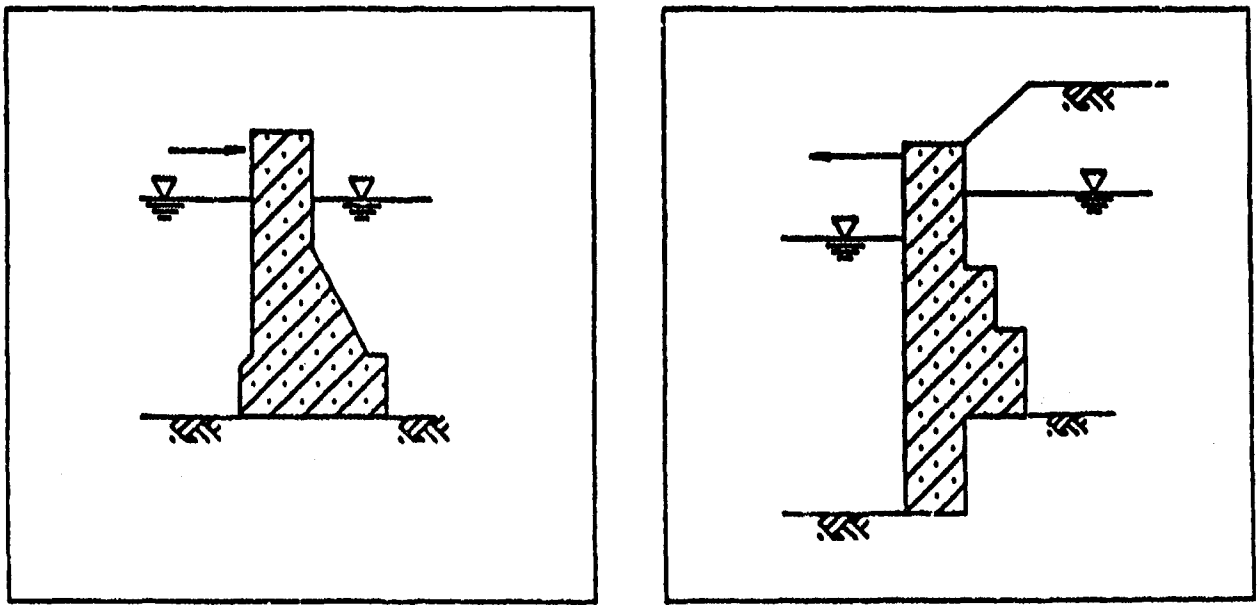

Case 1 Case 2

Figure A1. Cross sections through Emsworth L-3 and L-19, cases 1 and 2

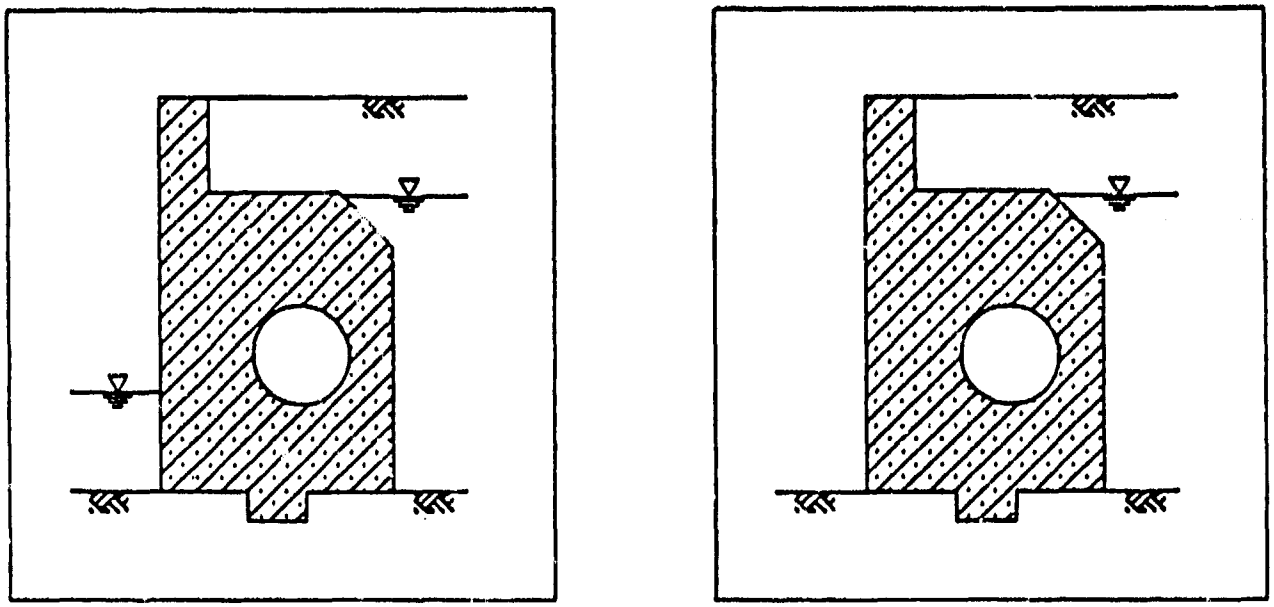

Case 3 Case 4

Figure A2. Cross sections through Emsworth L-37, cases 3 and 4

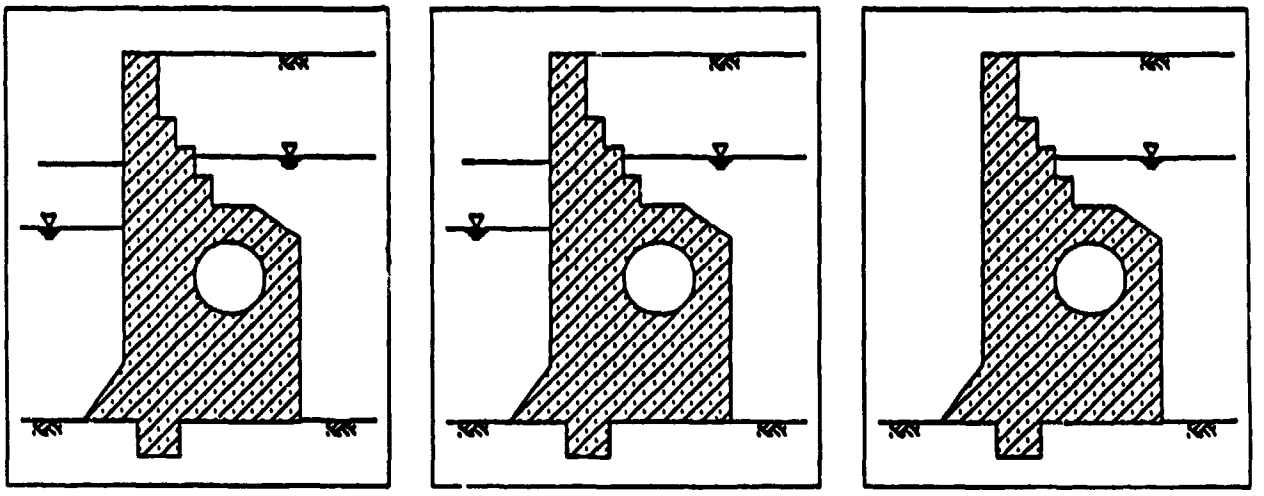

Figure A3. Cross sections through Emsworth L-52, cases 5, 6, and 7

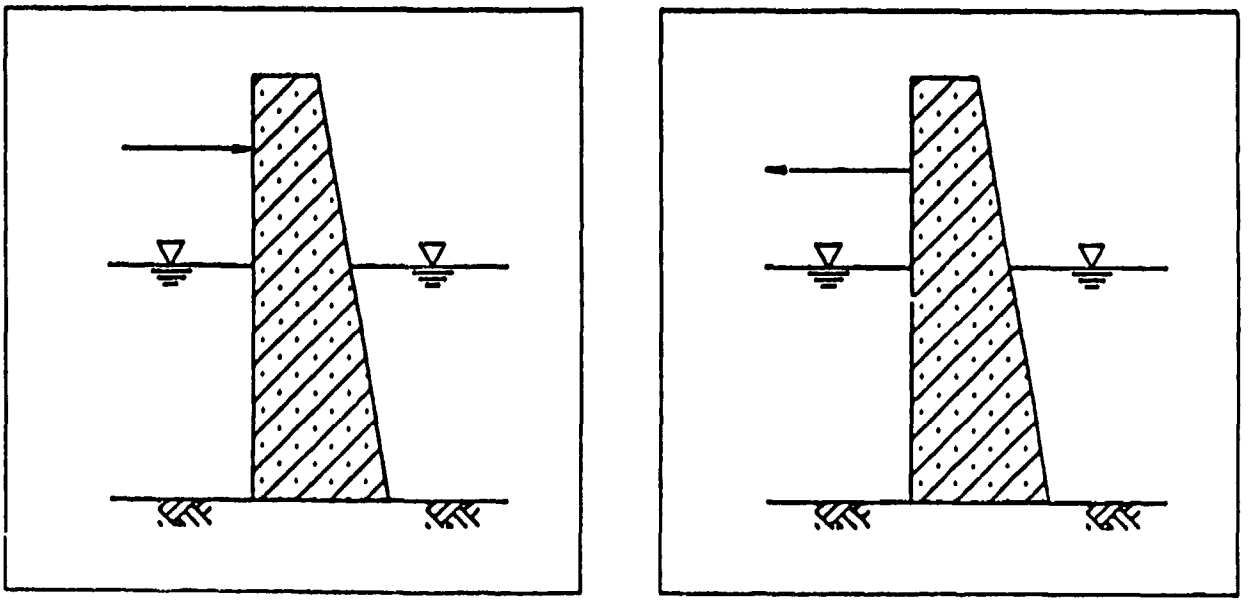

Figure A4. Cross sections through Emsworth L-68, cases 8 and 9

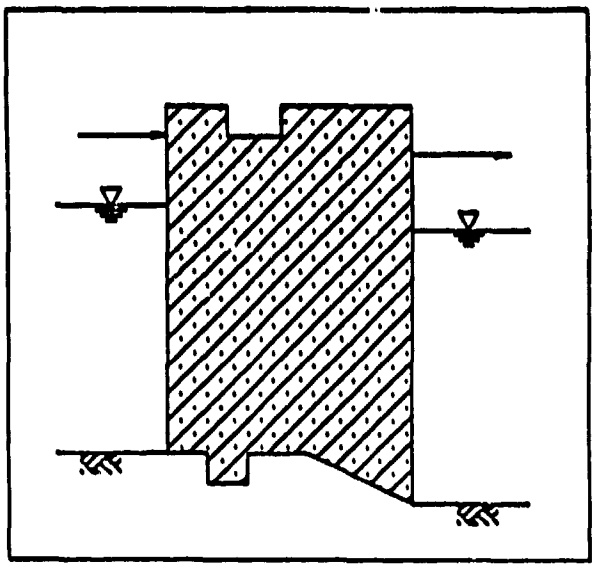

Case 10

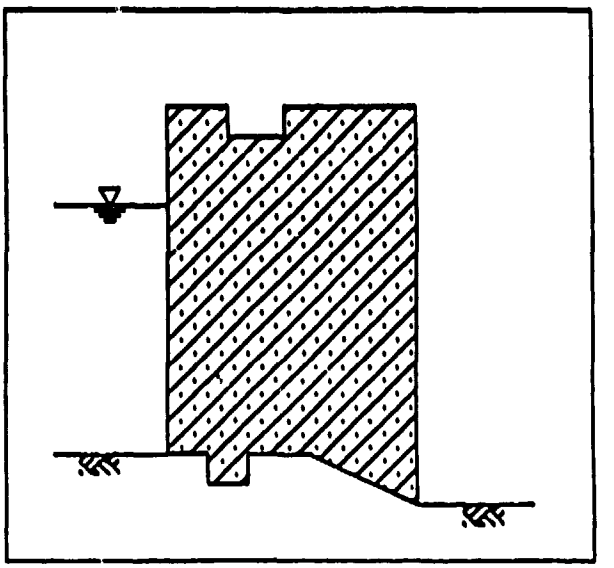

Case 11

Figure A5. Cross sections through Emsworth M-8, cases 10 and 11

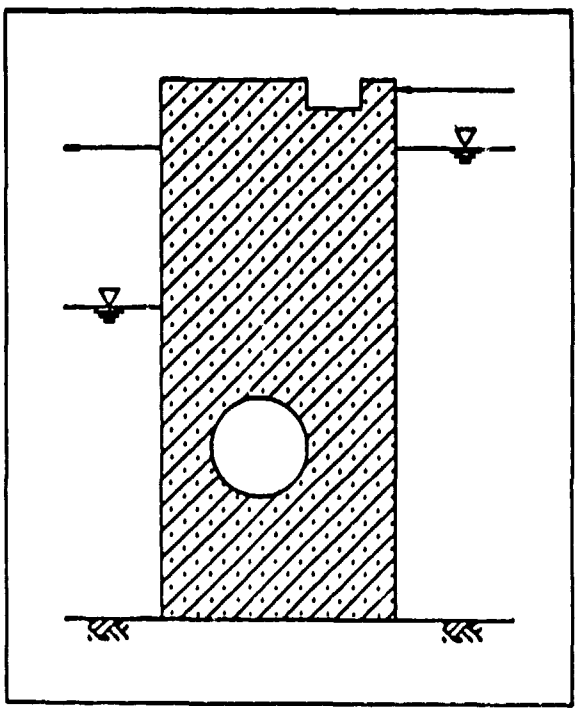

Case 12

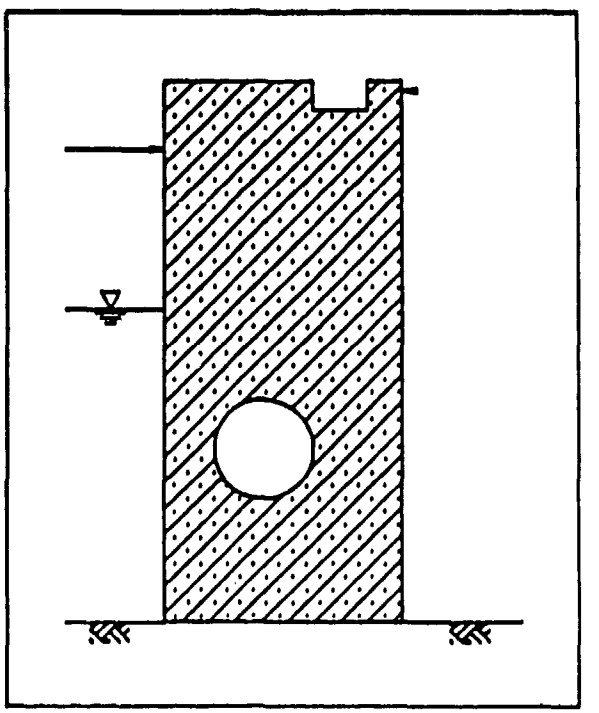

Case 13

Figure A6. Cross sections through Emsworth M-22, cases 12 and 13

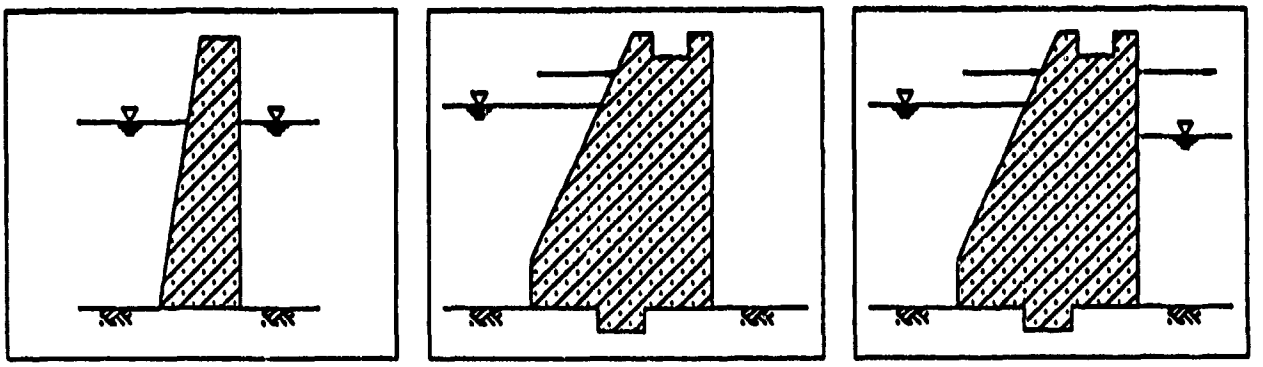

Case 14 Case 15 Case 16

Figure A7. Cross sections through Emsworth R-4 and R-17, cases 14, 15, and 16

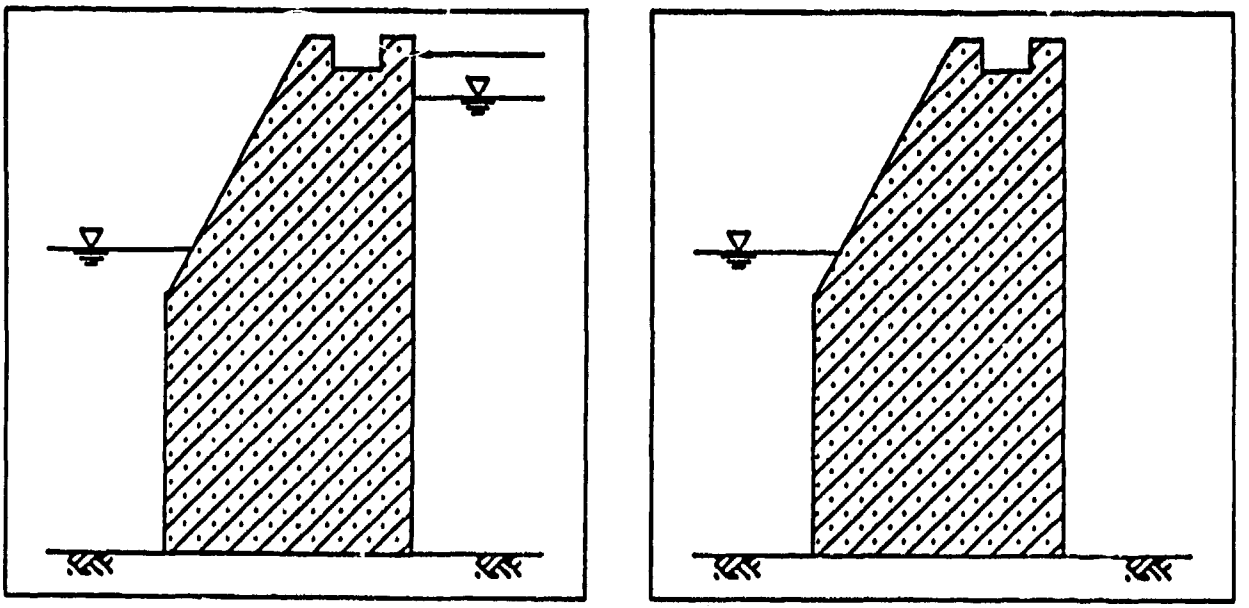

Case 17 Case 18

Figure A8. Cross sections through Emsworth R-24, cases 17 and 18

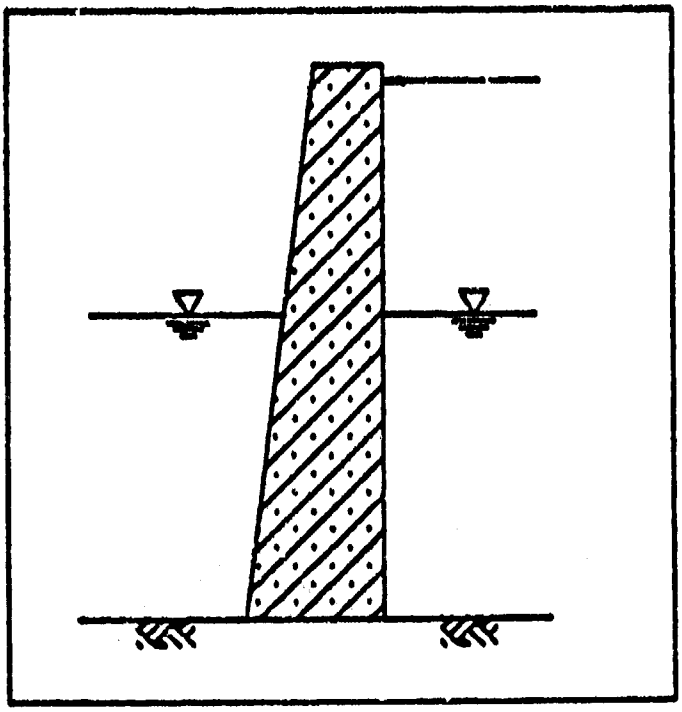

Case 19

Figure A9. Cross section through Emsworth R-32, case 19

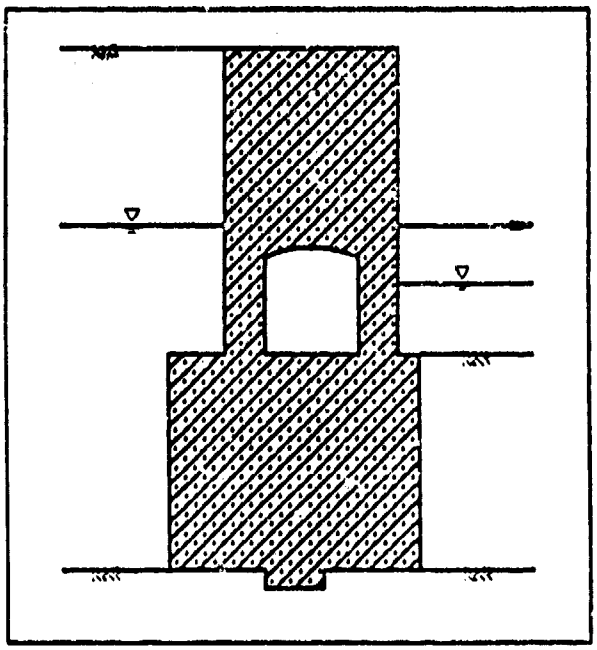

Case 20

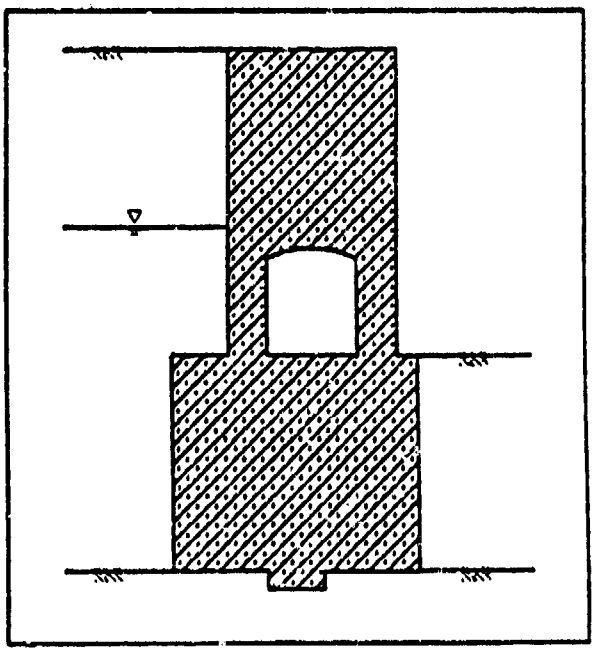

Case 21

Figure A10. Cross sections through Montgomery L-19, cases 20 and 21

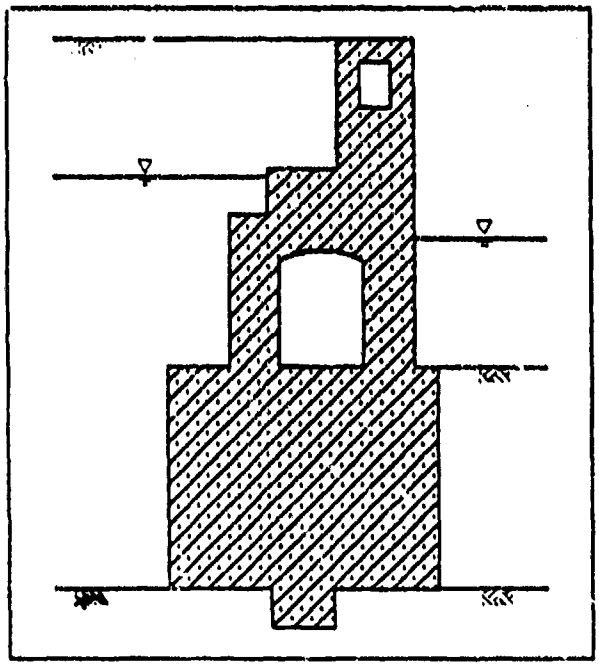

Case 22

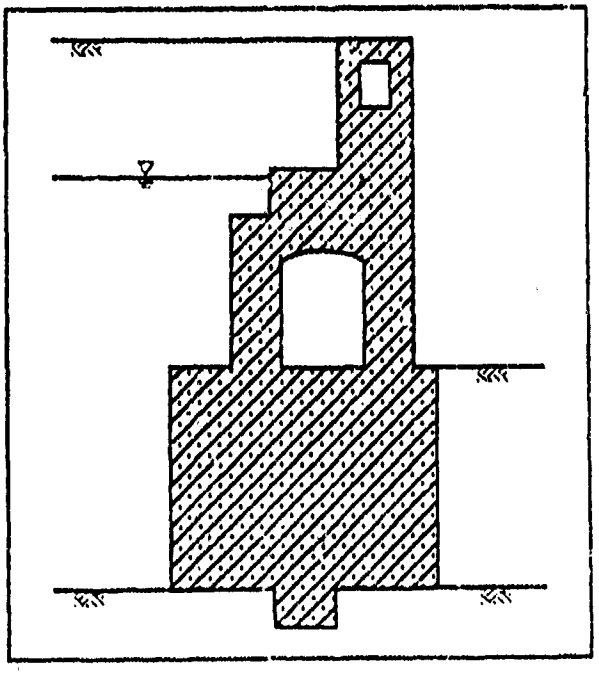

Case 23

Figure A11. Cross sections through Montgomery L-25, cases 22 and 23

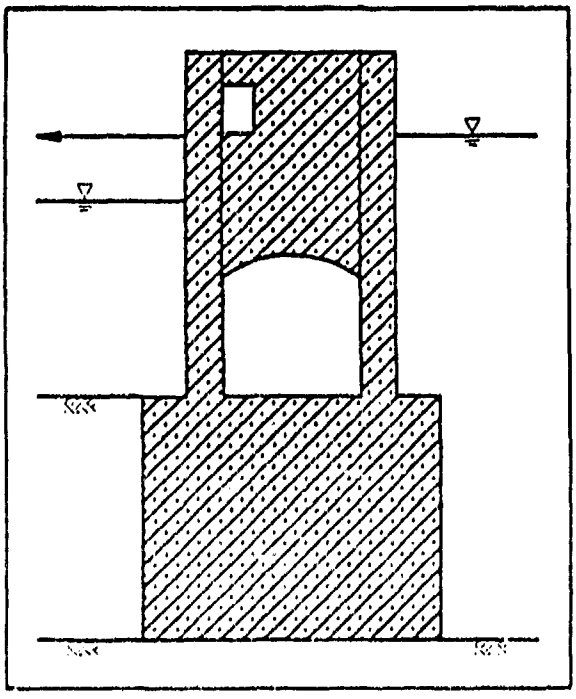

Case 24

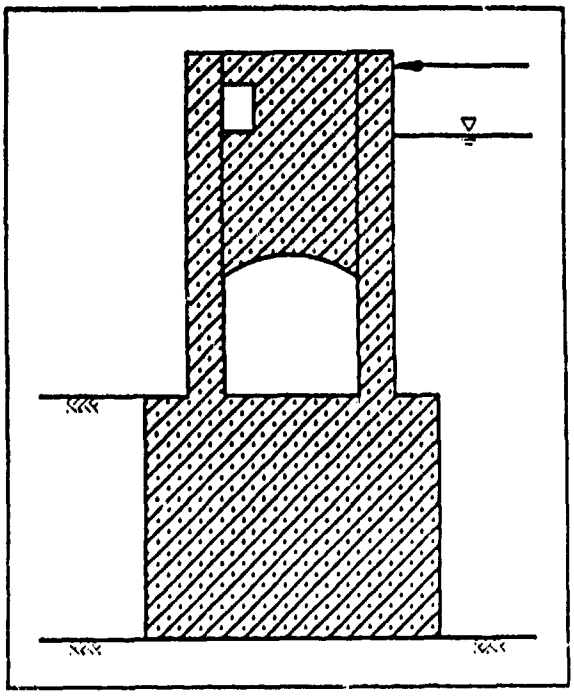

Case 25

Figure A12. Cross sections through Montgomery M-7, cases 24 and 25

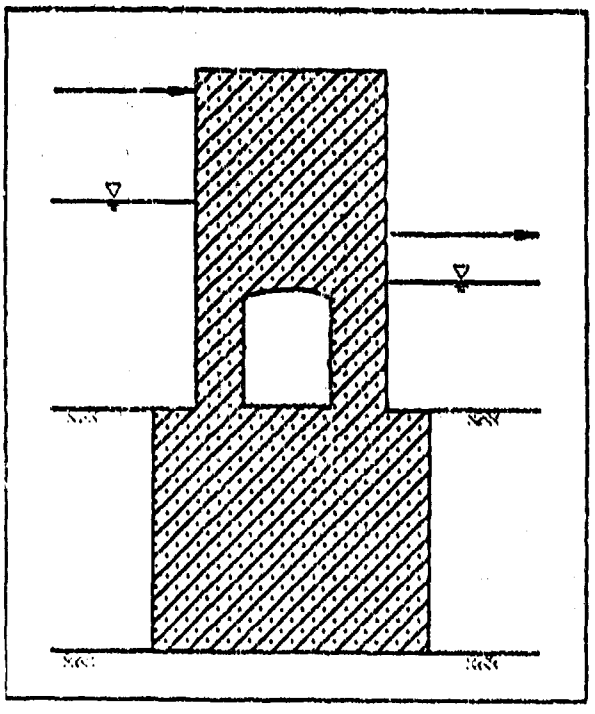

Case 26

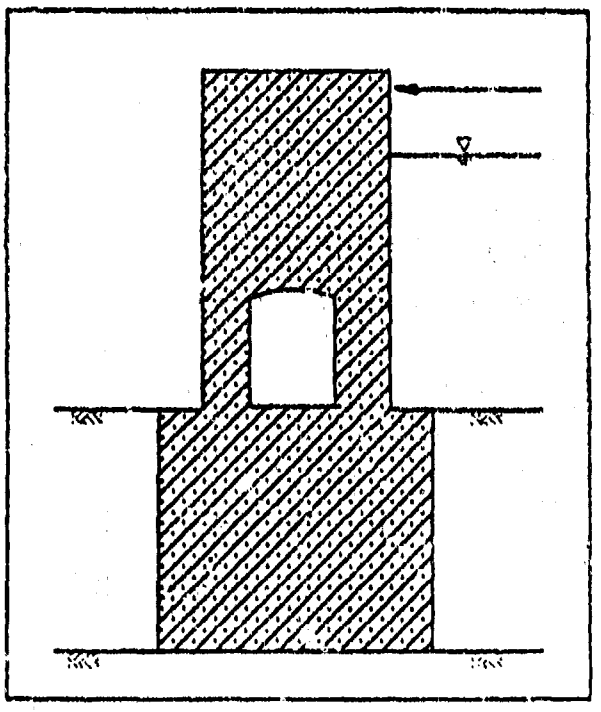

Case 27

Figure A13. Cross sections through Montgomery M-13, cases 26 and 27

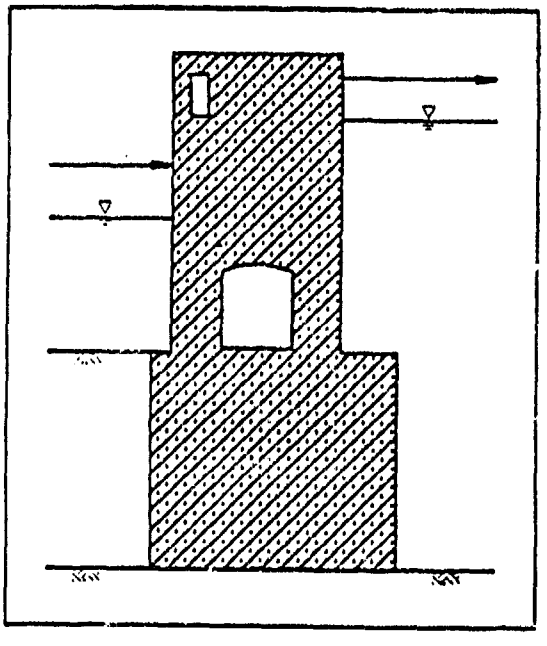

Case 28

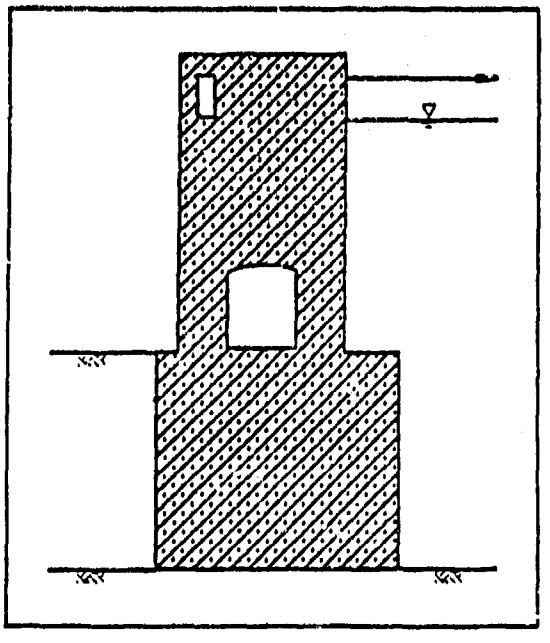

Case 29

Figure A14. Cross sections through Montgomery R-13, cases 28 and 29

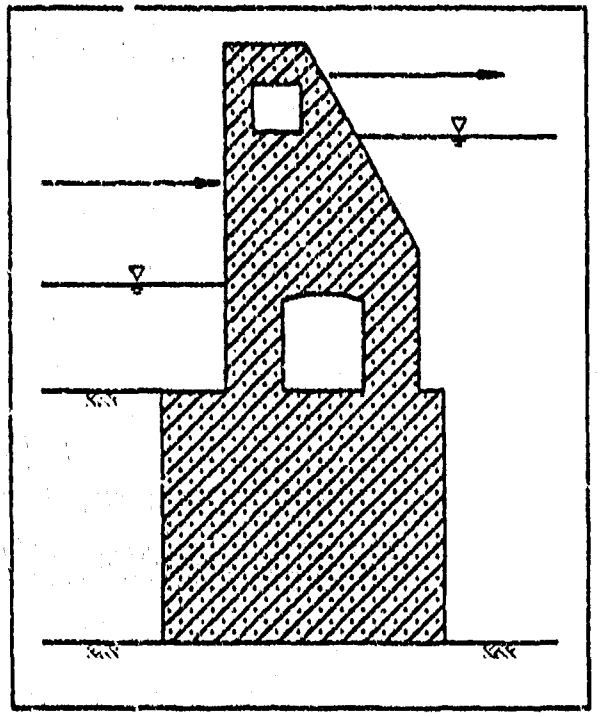

Case 30

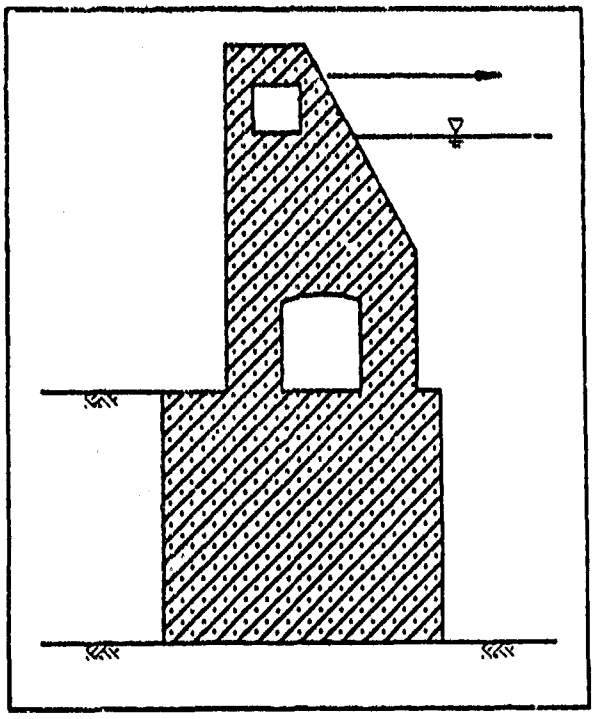

Case 31

Figure A15. Cross sections through Montgomery R-15, cases 30 and 31

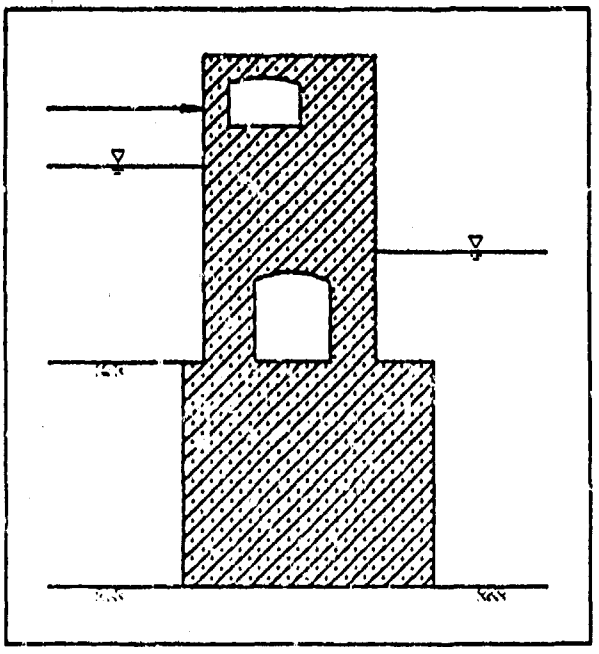

Case 32

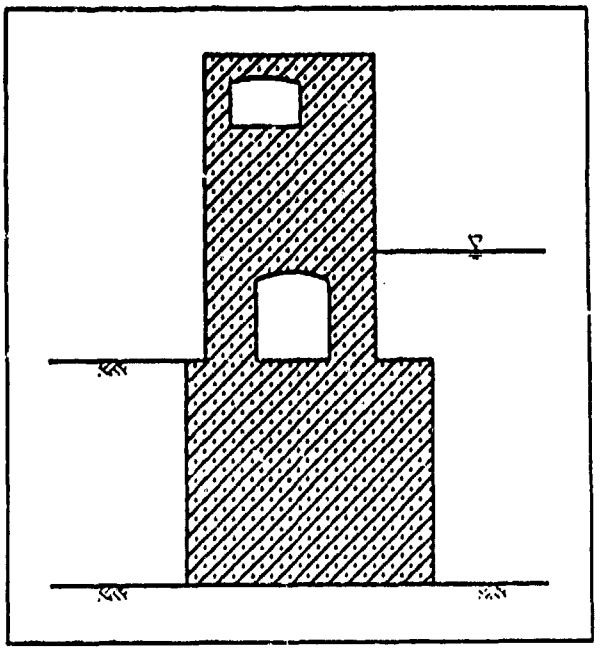

Case 33

Figure A16. Cross sections through Montgomery R-20, cases 32 and 33

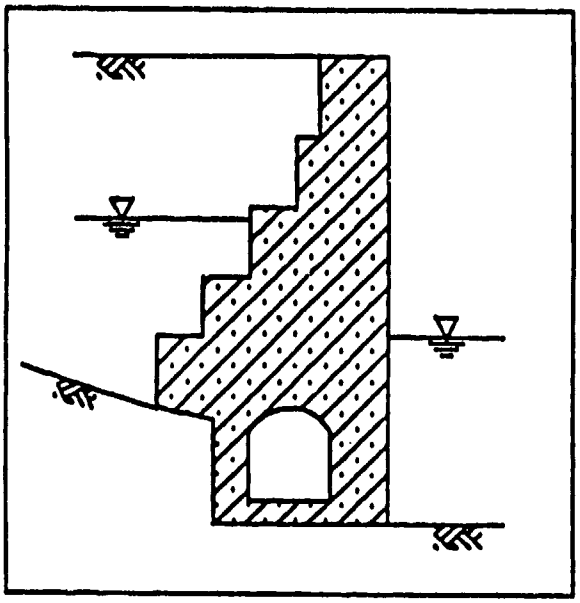

Case 34

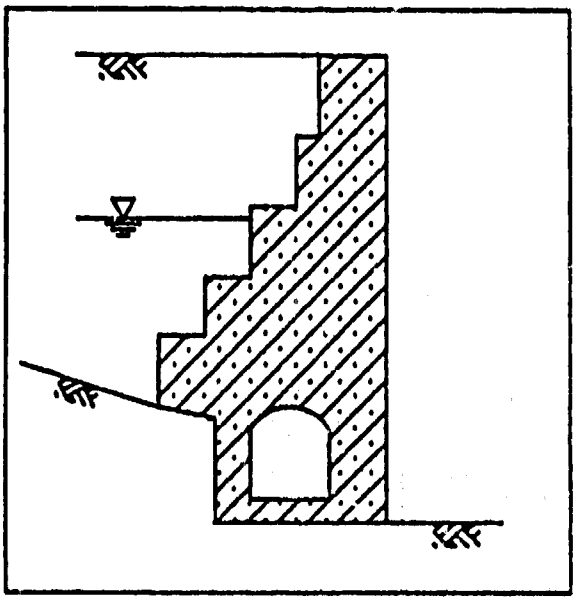

Case 35

Figure A17. Cross sections through Troy L-5, cases 34 and 35

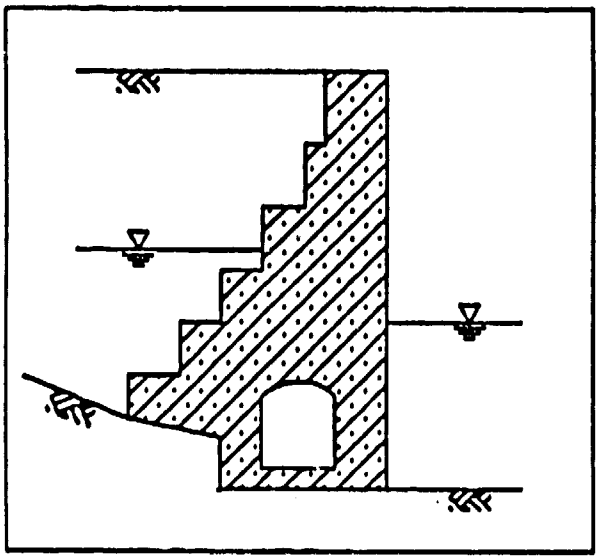

Case 36

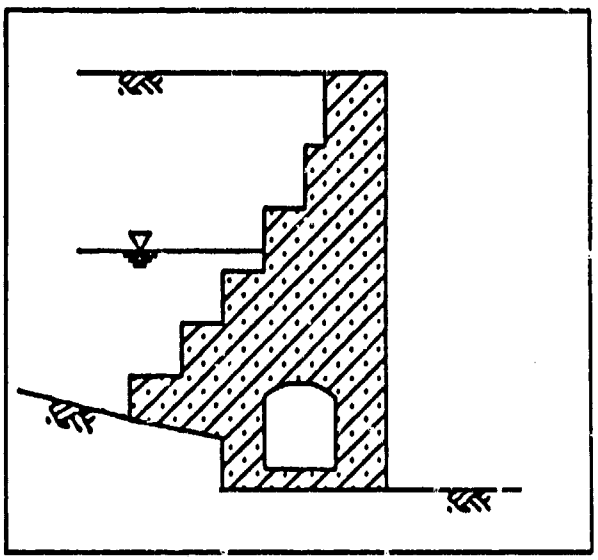

Case 37

Figure A18. Cross sections through Troy L-12, cases 36 and 37

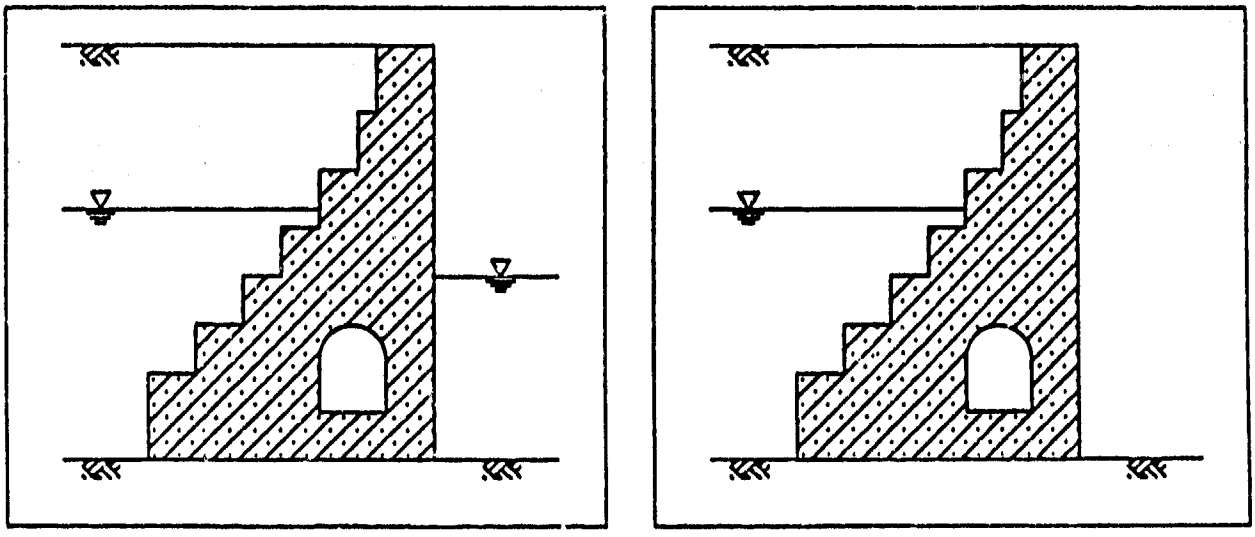

Case 38 Case 39

Figure A19. Cross sections through Troy L-20, cases 38 and 39

APPENDIX B: THEORETICAL CONSIDERATIONS OF THE EFFECTS OF SCALE

1. In this appendix, relationships are developed that describe the effect of the scale of the structure upon the computed results. They are valid for a specific class of bodies described in Part V of the main text. The relationships are based upon equilibrium and energy considerations, as well as constitutive equations. They quantify the influence of scale on these factors; the stress and strain developed within the body, the work performed by the applied forces, the energy stored within the body, and the displacements resulting from the applied forces.

Review of Energy Considerations

2. The first law of thermodynamics gives rise to the specific internal energy relationship, which for elastic bodies under isothermal conditions consists only of stored elastic strain energy. The strain energy density, U_o , is given as

$$U_o = \int_0^{\epsilon_{ij}} \sigma_{ij} \, d \, \epsilon_{ij} \tag{B1}$$

where

ϵ_{ij} = strain tensor

σ_{ij} = stress tensor

U_o represents the mechanical energy stored in the body per unit volume through development of the stresses σ_{ij} and the corresponding strains ϵ_{ij} . Integrating the strain energy density, U_o , over the volume, v , of the body results in the strain energy of the body, U :

$$U = \iiint_v U_o \, dv \tag{B2}$$

3. The work performed on the body, W, by the applied forces equals the product of force, F, and displacement in the direction of the force, u:

$$W = F \cdot u \tag{B3}$$

Consideration of the conservation of energy requires that the stored strain energy of the body is equal to the work performed on the body;

$$dU = dW \tag{B4}$$

Stress and Strain Developed Within the Body

4. A discussion on the influence of the scale factor on the geometry and applied loads is presented in Part IV of the main text. It is apparent that the magnitude of the applied load varies in proportion to the scale factor. Further, since the normalized geometry, normalized pressure distribution, and region of application of load are the same for both structures, the differences in the incremental stress changes throughout the body are also proportional to the scale factor. This is exemplified by considering a point within the body that is adjacent to the region of the boundary pressure. Any changes in the magnitude of the applied pressure distribution will result in changes of equal magnitude within the body.

5. In each incremental analysis, linear elastic material behavior is assigned for all regions of the body. According to Hooke's law, the factors that affect stress will also affect strain. Thus, the difference in the incremental strains are also proportional to the scale factor.

Work Performed and Energy Stored

6. The elastic strain energy density is given by Equation B1. At every point in the body, it is a function of the change in stress and strain. Since each of these terms are proportional to the scale factor between the meshes, the strain energy density will vary with the square of this factor.

7. The strain energy stored within the entire body is given in Equation B2 as the integral of the strain energy density within the entire volume.

Since the height and width of the meshes are proportional to the scale factor, the area per unit thickness varies with the square of this factor. Thus, the strain energy will vary with the scale factor to the fourth power.

8. Based upon the conservation of energy principle, the work performed upon the body equals the strain energy stored within the body. Since the strain energy varies with the scale factor to the fourth power, the work performed on the body also obeys the same relationship.

Displacements Within the Body

9. The influence of the scale of the structure upon the computed displacements is evaluated by considering a single point located at the boundary upon which the applied forces are prescribed varies. As noted, each of the applied forces varies with the square of the scale factor. Also, in the previous section it was determined that the work performed by these forces vary with the scale factor to the fourth power. Since superposition theory is valid for this category of problem, this relationship also holds for the individual forces. Therefore, by Equation B3 the displacements will vary with the square of the scale factor.